

Mapping Suitability for Managed Aquifer Recharge in the Albuquerque Basin

Daniel J. Koning, Colin T. Cikoski, Alex J. Rinehart, and Andy P. Jochems

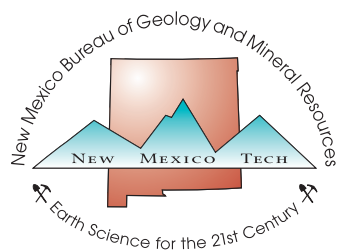
Open-File Report 605
August 2019



Mapping Suitability for Managed Aquifer Recharge in the Albuquerque Basin

Daniel J. Koning, Colin T. Cikoski,
Alex J. Rinehart, and Andy P. Jochems

Open-File Report 605
July, 2019

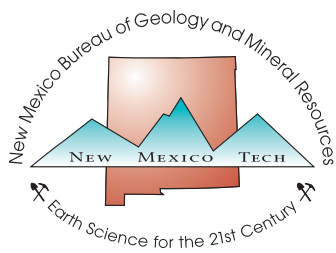


New Mexico Bureau of Geology and Mineral Resources
A Research Division of New Mexico Institute of Mining and Technology

PROJECT FUNDING

The Albuquerque Bernalillo County Water Utility Authority funded this project for the New Mexico Bureau of Geology and Mineral Resources.

The views and conclusions are those of the authors and should not be interpreted as necessarily representing the official policies, either expressed or implied, of the State of New Mexico.



New Mexico Bureau of Geology and Mineral Resources
A Research Division of New Mexico Institute of Mining and Technology

Socorro, NM 87801-4750
(575) 835-5490
www.geoinfo.nmt.edu

CONTENTS

Executive Summary	1
I. Introduction	3
II. Previous Work	5
III. Study Area	7
IV. Background	10
Geologic setting	10
Ceja Formation	10
Axial-river facies of the Sierra Ladrones Formation	13
Eastern piedmont facies of the Sierra Ladrones Formation	13
Post-Santa Fe Group deposits	13
Hydrogeologic setting	14
MAR projects in the Albuquerque metropolitan area	14
Bear Canyon Arroyo Recharge Project	14
Drinking water treatment plant	15
V. Approach	23
Data compilation and initial work	23
Hydrostratigraphic units	23
Units for hydrocompaction assessment	23
Hydraulic properties of saturated-zone deposits	25
Hydraulic properties of unsaturated sediment	25
Potentiometric surface and depth-to-groundwater	27
Subsurface geologic model	27
Wireline log analyses	32
VI. Mapping Managed Aquifer Recharge Suitability	35
Weighted Overlay Analyses	35
Exclusionary (unsuitable) buffers	35
Estimating susceptibility to soil hydrocompaction	35
VII. Methods	41
Suitability for deep-injection recharge	41
Geologic criteria	41
Summation of geologic unit scores	41
Adverse groundwater mounding	43
Hydraulic properties	44
Water and well infrastructure	44
Suitability for shallow-based recharge	44
Surface characteristics	44
Soil saturated hydraulic conductivity	45
Soil drainage class	45
Summation of soil map unit component scores	46
Surface slope	46
Adverse groundwater mounding	46
Deep-geology considerations	50
Percolation time	50
Proportion of clay layers	50
Soil-hydrocompaction susceptibility map	50
VIII. Results	53
Subsurface lithologic interpretations	53
MAR using deep injection	53
Geologic criteria	53
Allowable injection rates	54
Hydraulic properties	54
Infrastructure properties	54

MAR using shallow-based recharge	55
Surface characteristics.....	55
Adverse groundwater mounding.....	56
Deep-geology considerations.....	56
Mapped suitability for shallow-based recharge.....	56
Mapped susceptibility to soil hydrocompaction.....	57
IX. Discussion.....	78
Deep-injection recharge.....	78
Shallow-based recharge.....	78
Soil hydrocompaction.....	79
Limitations.....	79
Acknowledgments.....	80
References.....	81
Tables	
1. Hydrostratigraphic units.....	24
2. Statistics of horizontal hydraulic conductivity per hydrostratigraphic unit.....	24
3. Infiltration rates calculated for surficial units.....	26
4. Vertical hydraulic conductivity.....	26
5. Results of well wireline log analyses.....	34
Figures	
1. Location of the northern Albuquerque Basin.....	8
2. Location of the study area.....	9
3. Geologic map of the Calabacillas sub-basin.....	11
4. Structure of the Albuquerque Basin.....	12
5. Block diagram of the structure of the Calabacillas sub-basin.....	15
6. Cross section of the stratigraphy and structure in the central part of the study area.....	16
7. Cross sections illustrating the lithostratigraphy of the Santa Fe Group and overlying units.....	17
8. Paleocurrent directions, Santa Fe Group.....	18
9. Axial-river facies of the Sierra Ladrones Formation.....	19
10. Eastern piedmont facies of the Sierra Ladrones Formation.....	20
11. Map of potentiometric surface.....	21
12. Block diagram of subsurface geology relative to MAR projects in the study area.....	22
13. Box and whisker plot of hydraulic conductivity.....	25
14. Map of depth-to-groundwater.....	28
15. Structural contour maps of the Sierra Ladrones Formation.....	29
A. Axial-river facies.....	29
B. Piedmont facies.....	30
16. 3D subsurface geologic model of the Santa Fe Group.....	31
17. Method for determining lithologic texture.....	33
18. Weighted overlay method.....	36
19. Workflow of rating criteria for MAR suitability.....	38
20. Exclusionary buffers.....	39
A. Deep-injection recharge.....	39
B. Shallow-based recharge.....	40
21. Flow chart for scoring criteria for deep-injection MAR.....	42
22. Method for determining storage- zone thickness.....	43
23. Lithologic textures of hydrostratigraphic units.....	47
24. Flow chart for scoring criteria for shallow-based MAR.....	48
25. Histogram of saturated vertical hydraulic conductivity for soil map unit components.....	49
26. Histogram of drainage classes for soil map unit components.....	49
27. Map of ratings for transmissivity.....	59
28. Map of ratings for storage-zone thickness.....	60
29. Map of ratings for allowable injection rate.....	61
30. Map of ratings for potentiometric- surface gradient.....	62
31. Map of ratings for distance to non-ABCWUA well density.....	63
32. Map of ratings for distance to ABCWUA well density.....	64

33. Map of ratings for distance to San Juan-Chama treated water pipelines	65
34. Histogram of ratings for deep-injection MAR.....	66
35. Map of final suitability ratings for deep-injection MAR.....	67
36. Map of ratings for soil vertical hydraulic conductivity.....	68
37. Map of ratings for soil drainage class.....	69
38. Map of ratings for surface slope	70
39. Map of ratings for depth-to-groundwater	71
40. Map of ratings for percolation time.....	72
41. Map of ratings for clay abundance	73
42. Areas previously hypothesized to be favorable for MAR (from Hawley, 1996).....	74
43. Histogram of ratings for shallow-based MAR.....	75
44. Map of final suitability ratings for shallow-based MAR.....	76
45. Summary of soil-hydrocompaction susceptibility	77
A. Soil taxonomic order.....	77
B. Soil taxonomic suborder.....	77
C. Soil taxonomic great group.....	77
D. Soil texture	77
E. Depth-to-groundwater	77
F. Geologic units.....	77

Appendices

1. Well data for the Albuquerque metropolitan area
2. Hydraulic conductivity data from pump tests
3. Structure contour maps of the 10 hydrostratigraphic units
4. 3D views of units in geologic model and model data
5. Well wireline log analyses of lithologic textures and plots of storage-zone thicknesses of hydrostratigraphic units
6. GIS data and Python scripts for MAR suitability
7. Soil-hydrocompaction susceptibility of geologic units
8. GIS data and Python scripts for soil-hydrocompaction susceptibility

Plates

1. Suitability for managed aquifer recharge (MAR) via deep-injection
2. Suitability for managed aquifer recharge (MAR) via shallow-based methods
3. Final estimate of susceptibility to soil hydrocompaction
4. Layers used in estimation of soil-hydrocompaction susceptibility

EXECUTIVE SUMMARY

The suitability for managed aquifer recharge (MAR) in the eastern Albuquerque metropolitan area was mapped using weighted overlay analyses. The study area extends from the Rio Grande eastward to the Sandia Mountains and from Sandia Pueblo southward to ~1 mi (~2 km) south of Tijeras Arroyo. This area is under the jurisdiction of the Albuquerque Bernalillo County Water Utility Authority (ABCWUA), which will likely be the main user of this map. The subsurface stratigraphy of the Santa Fe Group (about 1 to 3 Ma) consists of Rio Grande axial-river sediment that interingers westward with deposits of the Rio Puerco distributive fan system and eastward with piedmont sediment eroded from the Sandia Mountains. The Santa Fe Group is overlain by up to ~50 m of weakly consolidated middle to upper Quaternary sediment that includes piedmont alluvium, Rio Grande terrace deposits, and incised-valley fill. Long-term pumping of groundwater by the city has created a large, trough-like depression of the water table centered under the study area, leaving up to 500 ft (150 m) of unsaturated, relatively permeable sediment that can potentially be used to store excess surface water—which is allotted to the ABCWUA from the San Juan-Chama Drinking Water Project—for future use.

We produced two maps for MAR suitability, each with a grid cell resolution of 100 x 100 m: one showing the suitability for deep-injection recharge (i.e., pumping water directly into the saturated zone) and the other for shallow recharge (by infiltration or vadose-zone injection). Exclusionary buffers were *a priori* assigned to the Rio Grande floodplain (due to potential for injected water to reach the river or induce swamping) and for known groundwater-contamination sites. For the deep-injection MAR suitability map, an exclusionary buffer zone was also drawn along major faults. These exclusionary buffers were *a priori* deemed unsuitable. Initial steps included: (1) description of outcrops to qualitatively assess the permeability characteristics of lithologic units that continue into the subsurface beneath the study area as potential aquifers; (2) compilation of hydraulic data from pump and infiltration tests; (3) drawing structural contours of 10 geologic (hydrostratigraphic) units under the study area; (4) assessment of the proportion of sand, clayey sand, and clay layers for each unit (by interpreting wireline logs of 17 deep water wells); and (5) construction of a 3D geologic model using Esri ArcGIS tools to perform analyses of stacked geologic units.

For the weighted overlay analyses, we considered several criteria that could impact MAR. For deep-injection recharge, these included: transmissivity; the 50th percentile of the cumulative distribution of storage-zone thickness (i.e., of the total thickness of permeable beds between clay layers); allowable injection rates; potentiometric-surface gradient; density of ABCWUA and non-ABCWUA wells; and distance to existing San Juan-Chama treated water pipelines. For shallow-based recharge, criteria include: soil characteristics [hydraulic conductivity and drainage class from Natural Resources Conservation Service (NRCS) soil maps]; surface slope; depth-to-groundwater; percolation time of surface water to reach the water table; and the

proportion of clay layers. Each criterion was subdivided into classes (binned), which were ranked from 0 to 2 based on their impact to MAR (2 being most favorable, and 0 being least). For criteria that vary among geologic units (e.g., transmissivity and storage-zone thickness), the score for each unit was weighted with respect to its relative thickness within the 1,500 ft in the zone of interest, summed, then normalized to between 0 and 2 in each grid cell location to produce a single score. All criteria in each cell were then weighted (using best-judgment by the authors and staff of the ABCWUA), summed, and normalized (to 0–2) to produce an overall rating. We compared the final values to previous maps of known or predicted MAR-suitable sites and subsequently used a histogram analysis to translate the scores to qualitative MAR-suitability ratings.

If water is spread on the ground for the purposes of shallow recharge, soil hydrocompaction (also called “collapsible soils”) are a valid concern in the Albuquerque area. Consequently, we produced a complementary map identifying the susceptibility of regions within the study area to soil hydrocompaction. This map was also made using weighted overlay analyses of various factors commonly correlated to hydrocompaction susceptibility. These factors included: soil type based on taxonomy from order to the great group; soil texture from Soil Survey Staff (2014) sources; depth-to-groundwater derived from the water-elevation contours presented in this report; and geologic units as mapped by Connell (2008).

The resulting MAR maps depict three color-coded suitability bins—low suitability, moderate suitability, and high suitability—as well as exclusionary zones. For deep-injection recharge, the high-suitability areas trend north-south in two areas: between I-25 and Moon Street and near Tramway Boulevard south of Montgomery Boulevard. Low-suitability areas lie under the Rio Grande floodplain (corresponding to an exclusion zone) and near Eubank and Juan Tabo Boulevards north of Candelaria Road. For shallow-based recharge, the central part of the study area exhibits high suitability, which also extends northwest past I-25 to the Rio Grande floodplain. Low-suitability areas include: north and south of the lower reach of Tijeras Arroyo; most of the Rio Grande floodplain south of Ranchito Road; and a north-south swath between Moon Street and Tramway Boulevard. The eastern low-suitability zone in both maps corresponds to a subsurface geologic unit of relatively low permeability (the distal-piedmont facies and where it interfingers with axial-river deposits). Highly suitable areas in both maps commonly correspond to thick axial-river deposits of the Rio Grande and the sandy medial-proximal piedmont facies.

The soil hydrocompaction map indicates high to extreme susceptibility for much of the area north of I-40 (especially near I-25 north of Comanche Road), along the eastern part of the Rio Grande floodplain (west of I-40 around Edith Boulevard), and in the bottom of Tijeras Arroyo. Site-specific geotechnical studies are recommended if groundwater spreading is to be conducted in areas noted here as highly or extremely susceptible to hydrocompaction.

I. INTRODUCTION

Managed aquifer recharge (MAR) is the intentional recharge and storage of water in an aquifer; this water can be subsequently recovered for civil use (e.g., municipal water supply) or for environmental benefit (e.g., maintaining sufficient groundwater to supply springs or wetlands). It is an appealing method for handling municipal water resources for a number of reasons. First, storing water underground (below the root zone) means the water is not lost to evaporation or transpiration. Second, infiltration of water through the vadose zone can remove some undesirable contaminants. Third, storage of water in an aquifer can be more cost-effective and practical than above-ground storage impoundments. For example, a standard municipal water storage tank holds ~77 acre-feet (~25 million gallons). At a MAR project in the Bear Canyon Arroyo in Albuquerque, however, 413 acre-feet of water percolated to the water table in two months (Daniel B. Stephens and Associates, 2010)—equating to five storage tanks.

The City of Albuquerque, New Mexico, is ideally located for MAR, both in regard to water supply and hydrogeology. The City is increasingly reliant on surface water from the Rio Grande [i.e., its share of the San Juan-Chama Drinking Water (diversion) Project], which is extracted from the river and combined with local groundwater. This water is delivered to the San Juan-Chama Drinking Water Treatment Plant (SJCDWTP), where suspended sediment is removed, ozone and chlorine added to kill bacteria, and impurities removed via filtration through sand and carbon (www.water-technology.net/projects/san_juan/). When supply exceeds usage, it is desirable to store the San Juan-Chama water for future use. Underlying much of Albuquerque are aquifers consisting of relatively permeable sediment, including deposits of the early Rio Grande and medial-proximal piedmont deposits associated with the Sandia Mountains. Because of sustained groundwater pumping by the City over the past several

decades, the unsaturated-zone thicknesses in these and other sediment types are hundreds of feet thick. Thus, there is a large volume of unsaturated sediment that can potentially store water.

Cognizant of the benefits of storing excess water underground, the Albuquerque Bernalillo County Water Utility Authority (ABCWUA) funded the New Mexico Bureau of Geology and Mineral Resources (NMBGMR) to map the spatial differences in suitability for conducting MAR. The NMBGMR completed three maps. The first shows the suitability for conducting artificial recharge to the saturated zone via deep-injection wells. The second shows the suitability for MAR via near-surface methods, such as vadose-zone injection wells, infiltration galleries, infiltration ponds, or arroyo-bottom infiltration. Both maps apply exclusionary buffer zones that *a priori* identify undesirable areas, including groundwater-contamination sites, the Rio Grande floodplain, and fault zones that may act as groundwater barriers in the deeper saturated zone. The floodplain is excluded because the infiltrated water could negatively impact the shallow water table and potentially reverse gradients toward the river (causing the water to go into the river instead of being stored). These two maps were made using Esri ArcGIS tools that performed a summation and normalization of weighted-ranked criteria, which is equivalent to ArcGIS weighted overlay analyses. A third map predicts the susceptibility of different areas to soil hydrocompaction, which is when subsidence results from the saturation of previously unsaturated, surficial sediment—an obvious concern for some near-surface recharge methods.

After a brief introduction of past MAR studies and the hydrogeology of the Albuquerque area, we expound on the procedures used in this study to assess suitability for MAR and susceptibility to soil hydrocompaction. Discussion follows regarding how these maps can be used for MAR projects.



At the Bear Canyon Arroyo Recharge Project in Albuquerque, New Mexico, arroyo-bottom infiltration MAR has been intermittently conducted along ~3,000 feet (~910 meters) of the arroyo between Wyoming Boulevard and the Arroyo del Oso Golf Course.

Photograph from the Albuquerque Bernalillo County Water Utility Authority
(<http://www.abcwua.org/education/23b/Recharge.html>)

III. PREVIOUS WORK

As mentioned above for the current Bear Canyon Arroyo MAR project, storing water underground can be a practical and effective way to manage water resources. Interest in underground water storage began in the middle 1900s (Mitchelson and Muckel, 1937; Babcock and Cushing, 1942; Meinzer, 1946; Beeby-Thompson, 1950; Buchen, 1955; Todd, 1959). The term coined for this practice is “managed aquifer recharge” (MAR, as defined above). Water for recharge comes from a variety of sources, and several methods can be used to recharge aquifers, including: deep- or shallow-injection wells; infiltration structures (ponds, basins, galleries, trenches); and natural seepage from arroyo bottoms or floodplains. MAR using wells to inject or extract water into or from aquifers is called aquifer storage and recovery, respectively—abbreviated as ASR (Pyne, 1995).

Mapping of areas suitable for artificial recharge is enhanced by using Geographic Information System (GIS) techniques. Researchers commonly use relevant software to execute Multi-Criteria Decision Analysis (MCDA) via weighted overlay of thematic layers (Chowdhury et al., 2009; Ganapuram et al., 2009; Dar et al., 2010; Rahman et al., 2012; Agarwal et al., 2013; Nasiri et al., 2013; Singh et al., 2013; Mahmoud et al., 2014; Senenayake et al., 2016; Yeh et al., 2016; Ahani Amineh et al., 2017). An Analytical Hierarchy Process (following Saaty, 1977, 1980, 1987, 1990, 2008) in the weighting scheme has been frequently used in the past decade (e.g., Chowdhury et al., 2009; Rahman et al., 2012; Nasiri et al., 2013; Sing et al., 2013; Ahani Amineh et al., 2017). Another method for assigning weights is computation of the principal eigenvector of a pairwise comparison matrix to produce a best-fit set of weights (e.g., Mahmoud et al., 2014). Groundwater flow and transport models have also been applied to map artificial recharge suitability (Lowry and Anderson, 2006; Ward et al., 2009; Smith and Pollock, 2012).

Our study was heavily influenced by the approaches, classification methods, and ranking values used in previous studies. Gibson et al. (2018) mapped the suitability of ASR in the state of Washington using two methods: a site scoring system

and an analytical method. In the site scoring system, three subcategories were assigned (hydrogeologic properties, operational considerations, and regulatory influences), each with their own set of scored criteria (0 for least favorable, 2 for most favorable). The metrics for criteria in each subcategory were summed and divided by the total possible value, resulting in a total percentage of ASR suitability. The analytical method used a water well suitability index that applied the Cooper-Jacob (1946) approximation to the Theis (1935) equation in order to characterize the hydraulic properties of aquifers.

Brown (2005) and Brown et al. (2005) developed an ASR-site selection suitability index for the Everglades. After a preliminary site-selection procedure, the following criteria were applied to site polygons: aquifer transmissivity; water quality; ecologic suitability; well density; road density; distance to power lines; and operational flexibility. Classification and scoring of criteria were accomplished by evaluation of 50 other ASR site studies in addition to Brown’s (2005) own ASR simulation modeling. Raw scores for each site were multiplied by a weighting factor (1 to 4) developed by the consensus-driven approach of an interagency team. The weighted scores were then normalized from 0 to 1 and plotted to create a color-coded ASR suitability index map.

Our scoring for shallow-recharge suitability was particularly influenced by Fisher et al. (2017), who employed both weighted overlay analyses and process-based, numerical modeling to identify locations suitable for stormwater-sourced, infiltration-based MAR for several topographic basins in California. Their criteria included both surficial and, where data were available, subsurface characteristics. Russo et al. (2015) performed a similar, albeit more narrowly spatially focused, study for the Pajaro Valley groundwater basin in California and provided additional weighting-factor considerations. We also found the weighted overlay suitability assessments by Chowdhury et al. (2009) and Mahmoud et al. (2014) useful in determining which criteria, scoring, and weighting systems to apply.

Hydrocompactive soils (also called “collapsible soils”) are surficial sediment with high porosity (>20%) that consolidate when simultaneously wetted and loaded (Beckwith and Hansen, 1989; National Research Council, 1999). Several conditions are conducive to this process. Collapsible soils have moderate to high clay content with clay minerals in a framework-supporting role (Li et al., 2016). This texture may result from rapid deposition of poorly sorted sediment, generally either eolian (wind-blown) or alluvial (laid down by streams) (Rogers, 1995). The soil must remain minimally saturated to maintain this uncompacted texture; thus, hydrocompactive soils are typically restricted to arid regions. In New Mexico and other arid regions of the southwestern U.S., most modern hydrocompactive soils formed from material deposited during the Holocene and latest Pleistocene (0 to ~15,000 years ago) (Beckwith and Hansen, 1989; Rogers, 1995; Momeni et al., 2012). An intermittently wetter climate earlier in the Pleistocene, combined with time-dependent consolidation and pedogenesis (soil-forming) processes, resulted in compaction of older sediment that may have originally qualified as hydrocompactive (Johnpeer et al., 1985; Beckwith and Hansen, 1989).

Hydrocompactive soils pose a notable hazard for much of New Mexico (Rinehart et al., 2017). Collapsible soils caused millions to tens of millions of dollars of damage during the 1990s (National Research Council, 1999). Furthermore, such incidents may be underreported because of adverse legal ramifications (J. Hawley, personal commun., 2017).

Although some of the seminal research on hydrocompactive soils was done in New Mexico (Johnpeer et al., 1985), few detailed assessments followed. Rinehart et al. (2017) mapped collapsible soil susceptibility for the entire state at a reconnaissance level (scale of 1:750,000), using correlations based on those of Lutteneger and Saber (1988) and Momeni et al. (2012). Their method did not incorporate geotechnical observations (such as blow counts or density measurements), however, as done by Williams and Rollins (1991), Jorgenson (1998), and Momeni et al. (2012). This suggests that regional maps by Rinehart et al. (2017) highlight areas of concern but may lack data adequate to identify site-specific hazards.

III. STUDY AREA

The study area lies in the northern Albuquerque Basin, which is one of many tectonic basins in the north-south trending Rio Grande rift (Fig. 1). Figure 2 shows the study area relative to topography and the Albuquerque street network. The western boundary corresponds to the Rio Grande, and the northern boundary coincides with the southern edge of Sandia Pueblo lands (~1 mi north of Tramway Boulevard). The base of the Sandia Mountains demarcates the eastern boundary. Away from the Rio Grande floodplain, the southern boundary trends northeast, parallel to Tijeras Arroyo located 0.6–2.0 mi (0.9–3.2 km) to the north.

Hydrogeologic units considered potentially viable for various MAR projects are present within the first 1,500 ft (457 m) below the land surface and include strata of the Santa Fe Group and post-Santa Fe Group sediment. Therefore, the cumulative thickness of weakly to moderately consolidated sediment scored herein for MAR suitability is a corresponding ~1,500 ft. The 3D geologic model used in this study (discussed later) extends to a constant subsurface elevation of 3,500 ft (1,067 m) above sea level, which is also about ~1,500 ft (457 m) below the lowest surface elevation in the area.

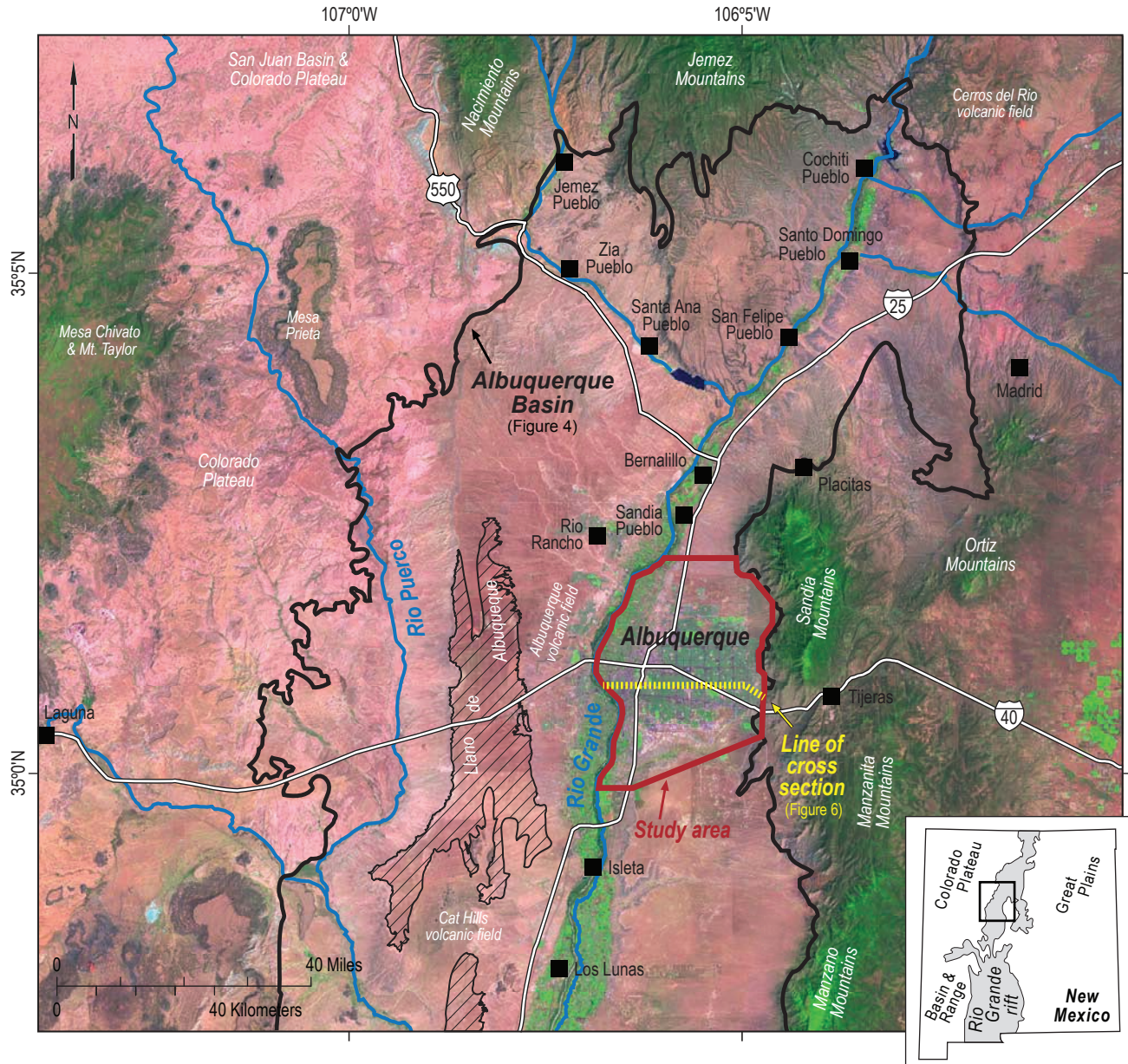


Figure 1. Location of the northern Albuquerque Basin and the City of Albuquerque in north-central New Mexico. Thick black line delineates the basin boundary. Hatched pattern denotes a geomorphic surface called the Llano de Albuquerque (see Connell et al., 2013). Study area defined by red outline.

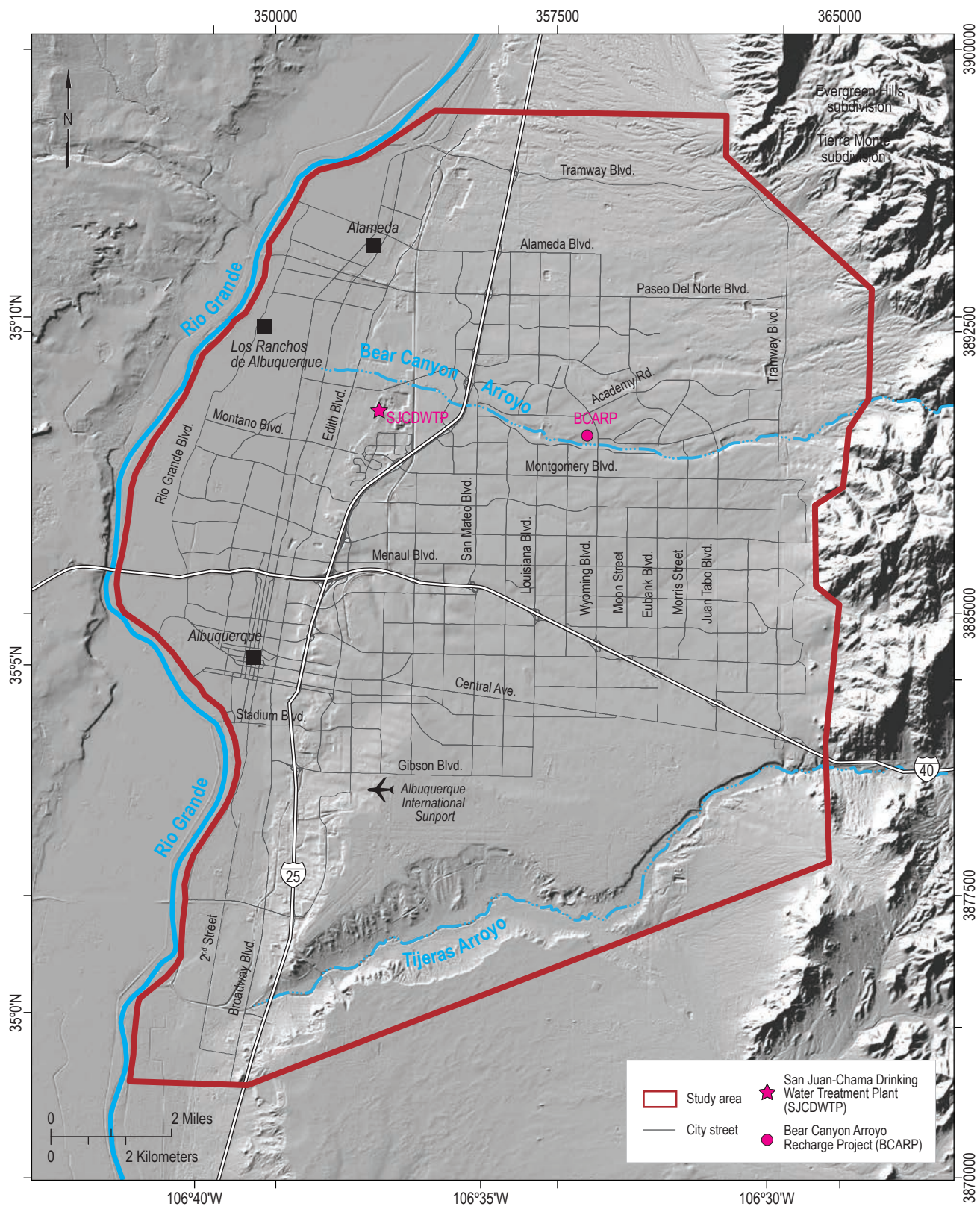


Figure 2. The study area in Albuquerque. Locations of the San Juan-Chama Drinking Water Treatment Plant (SJCDWTP) and Bear Canyon Arroyo Recharge Project (BCARP) are shown.

IV. BACKGROUND

Geologic Setting

The study area lies in the Calabacillas sub-basin of the Albuquerque Basin, an extensional feature located in the central part of the Rio Grande rift (Fig. 1). Figure 3 illustrates the geology of the Calabacillas sub-basin and surrounding areas. The Calabacillas sub-basin is a relatively deep feature west of the Sandia Mountains (Fig. 4). By depicting the subsurface elevation of the base of basin fill (i.e., rift-related sediment), Figure 4 shows the overall structure of the Albuquerque Basin. The overall structure of the sub-basin was inferred from inverse-gravity modeling, calibrated with well data and seismic reflection (Grauch and Connell, 2013). The model shows that this sub-basin is asymmetric, with basin fill progressively thickening to the east towards a series of large-displacement, west-side-down normal faults located between I-25 and the Sandia Mountains (Figs. 5–6). These faults are, from west to east, the Coronado-Alameda, Eubank Boulevard, Ranchito, and Sandia faults (including the West and East Embudo strands of the Sandia fault). The base of the basin fill is estimated to be ~3 mi (~5 km) deep on the immediate west side of the Coronado-Alameda fault (Grauch and Connell, 2013).

The Santa Fe Group (~28–1 Ma) is the clastic basin fill associated with the Rio Grande rift (Spiegel and Baldwin, 1963; Galusha and Blick, 1971; Lipman and Mehnert, 1975; Kelly, 1977; Mack et al., 1993, 1998, 2002; Connell, 2008a; Connell et al., 2013; Koning et al., 2013). In the Calabacillas sub-basin, the eastward-thickening Santa Fe Group is subdivided into lower, middle, and upper parts (Connell, 2008b) (Appendix 1). The upper Santa Fe Group is of focus in this study (Fig. 5), as is a unit called the “middle” Santa Fe Group (MSF) in the Well_point feature class of Connell (2008b). The MSF is included with undivided Santa Fe Group on the cross sections of Connell (2008b). The lead author suspects MSF in these well data is actually part of the upper Santa Fe Group but designates it as geologic (hydrostratigraphic) unit Tsm to maintain consistency with Connell (2008b). Where exposed to the northwest of Albuquerque and Rio Rancho, the

upper Santa Fe Group overlies a prominent unconformity, but the contact may become conformable to the east under Albuquerque. This unconformable contact has been called the Rincones surface (Connell, 2008a; Connell et al., 2013). Where exposed to the west and northwest of Albuquerque, basal sediment of the upper Santa Fe Group was deposited between ~4 and 2.5 Ma (Connell et al., 2013), although its maximum age likely increases eastward in the subsurface. The top of the Santa Fe Group is ~1.5 Ma on the Llano de Albuquerque (Fig. 1), but it is 1.0–0.7 Ma in the study area due to asymmetric basin subsidence (Connell et al., 2013).

The upper Santa Fe Group comprises interfingering sedimentary packages associated with distinct paleo-drainage systems (Figs. 7–8). Upper Santa Fe Group deposits associated with a large alluvial fan system of the early Rio Puerco are part of the Ceja Formation (Connell, 2008a, 2008b). To the east, axial-river facies of the early Rio Grande and piedmont facies derived from the Sandia Mountains are part of the Sierra Ladrones Formation (Machette, 1978; Connell, 2008a) (Figs. 7–8). Axial-river facies deposited by the early Rio Grande predominantly consist of interfingering sand (including paleo-channel fills) and finer-grained floodplain sediment. Piedmont facies refer to ephemeral stream sediment deposited on sloping paleo-land surfaces that extended from highlands to the basin floor (in this case, the early Rio Grande).

Ceja Formation

An early version of the Rio Puerco flowed south-southeastward into the western Albuquerque Basin, where the river deposited an oblong fan elongated in a north-south direction (note that such a fan is included in a distributive fluvial system, abbreviated as DFS, Weismann et al., 2011). Channels on the alluvial fan near the study area were directed toward the southeast (Fig. 8), probably veering to the south as they entered the basin floor. The channels would have bifurcated toward the southeast, becoming progressively smaller downstream of each bifurcation, based on modern examples of DFS.

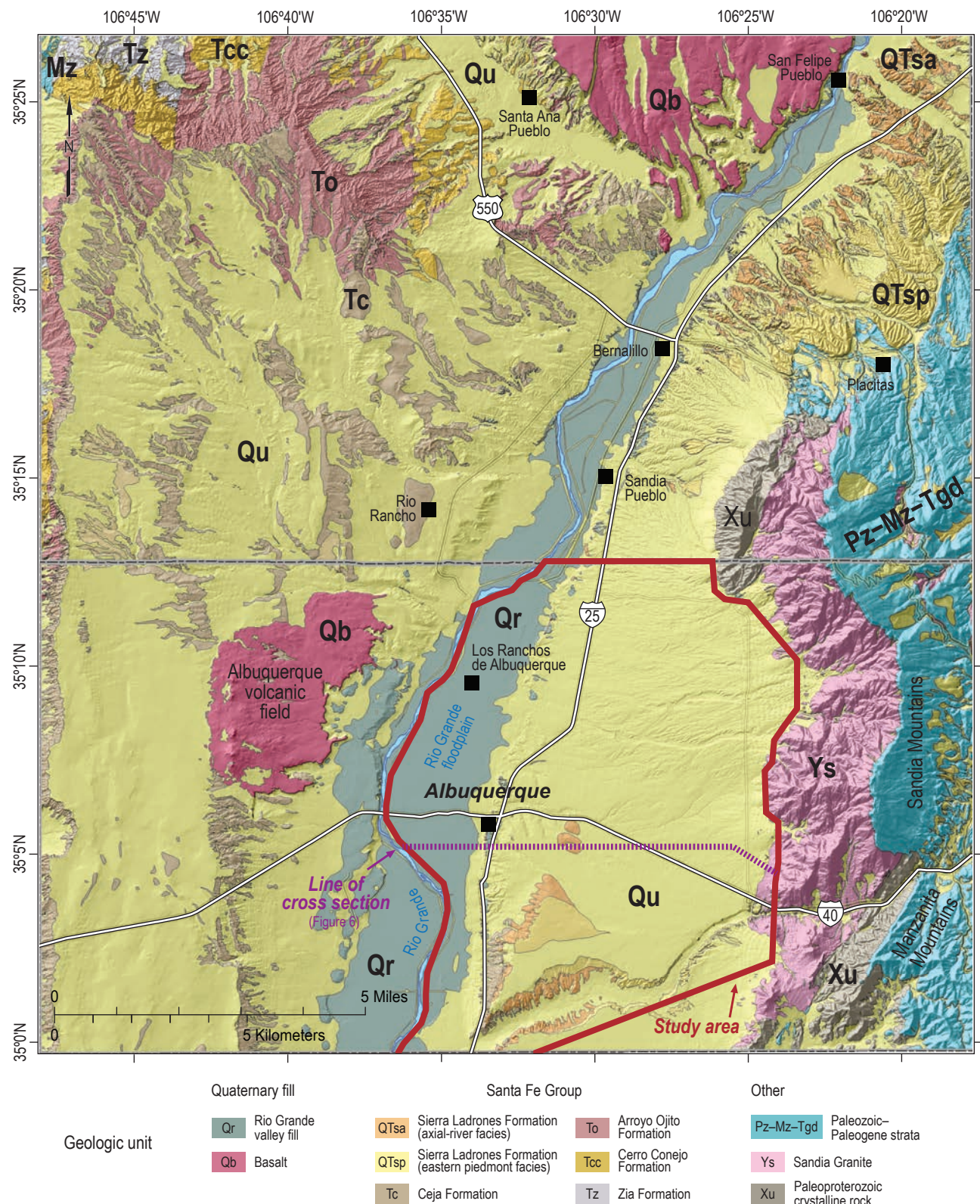


Figure 3. Simplified geologic map of the Calabacillas sub-basin and the southern Santo Domingo sub-basin (see Fig. 4). Figure courtesy of Sean Connell, formerly of the New Mexico Bureau of Geology and Mineral Resources. Undifferentiated Paleozoic–Paleogene strata (blue) includes the Galisteo and Diamond Tail formations (Tgd). See Connell (2008a) for more detail on older units of the Santa Fe Group (Arroyo Ojito, Cerro Conejo, and Zia formations).

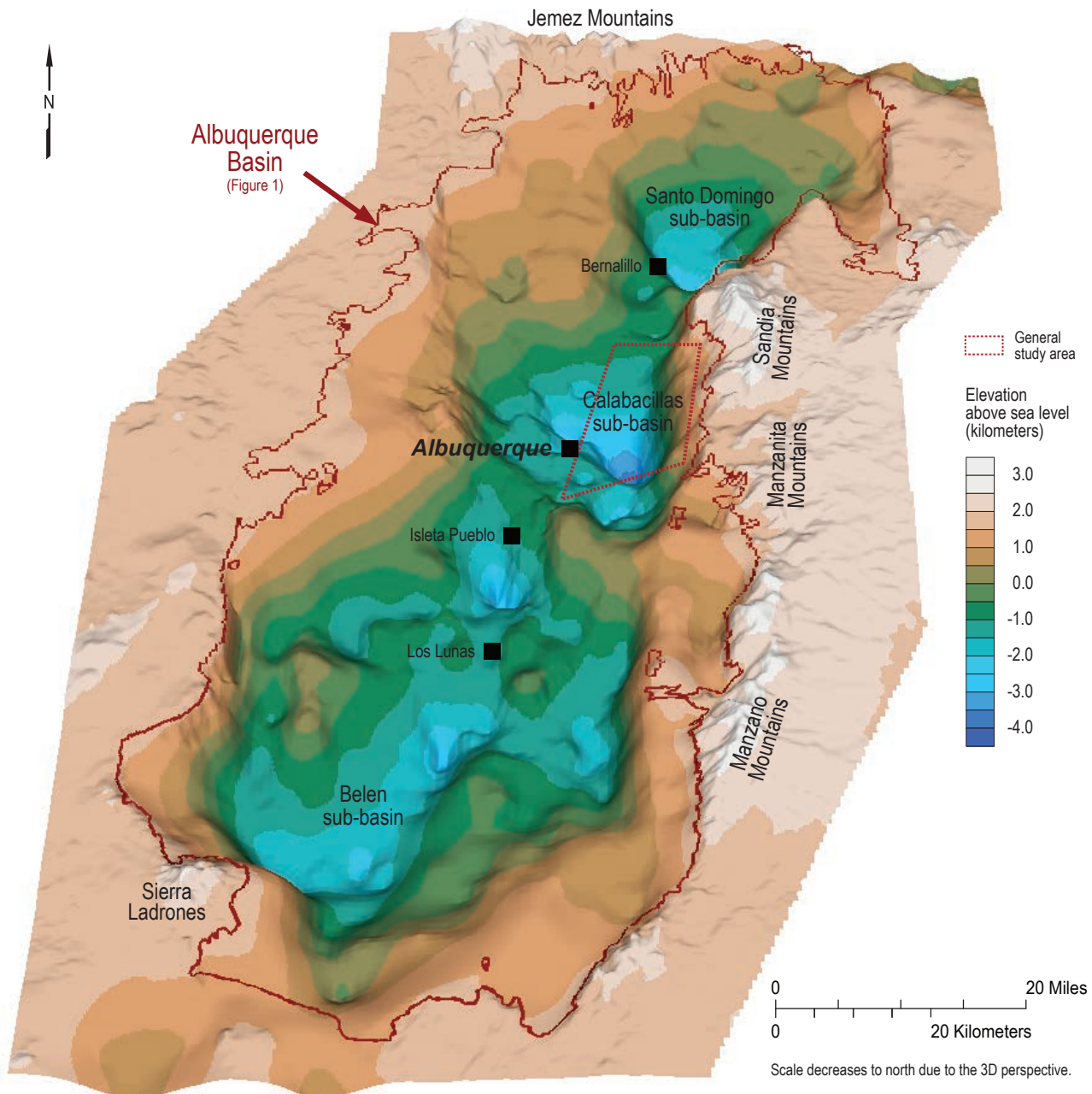


Figure 4. Structure of the Albuquerque Basin (modified from Grauch and Connell, 2013). It models the basal elevation of rift-fill sediment of the Santa Fe Group, thereby conceptually illustrating the basin geometry with the sediment removed. The depiction was created by calibrating a gravity-inversion model with information from geologic maps, boreholes, and geophysical studies (e.g., seismic-reflection, aeromagnetic, and magnetotelluric data). The study area lies in the eastern part of the Calabacillas sub-basin.

channels. In addition, similar to other large fan deposits in the Rio Grande rift (e.g., lithosome S of the Tesuque Formation, Koning et al., 2004, and Koning and Read, 2010), the gross sediment texture of the Rio Puerco alluvial fan would be expected to fine to the east-southeast.

Deposits associated with the early Rio Puerco DFS are assigned to the Ceja Formation (Kelly, 1977; Connell, 2008a). It ranges in age range from ~6 to 1.5 Ma (Connell et al., 2013, their fig. 22). The Ceja Formation can be subdivided into two member-rank units in the study area, both of which interfinger with the axial-river facies of the Sierra Ladrones Formation (QTsa) (Connell, 2008a, 2008b) (Fig. 7).

The Rio Puerco Member (QTcr) is notably coarser grained than the underlying Atrisco Member (Tca). Where exposed west of the study area, the former consists of tan to pale-brown to light yellowish-brown gravelly sand, sandy gravel, and fine- to coarse-grained sand. Gravel includes mafic to intermediate volcanic rock with subordinate chert, red granite, and sedimentary (mostly sandstone) clasts (Connell, 2008a, 2008b). In contrast, data from downhole wireline well logs indicate substantially more fine-grained material is present near where the Rio Puerco Member interfingers with the axial facies of the Rio Grande (discussed below).

The Atrisco Member comprises pink to yellowish-brown to reddish-yellow sand, mud, and minor pebbly sand (Connell, 2008b). Well data indicate that the predominant texture is sand, clayey-silty sand, and silt-clay. The Atrisco Member probably represents distalmost alluvial-fan deposits or sedimentation on a wide basin floor between the early Rio Grande and the toe of the Rio Puerco fan (DFS).

Axial-river facies of the Sierra Ladrones Formation

The axial-river facies of the Sierra Ladrones Formation (QTsa) consists of sand interbedded with subordinate sandy gravel, gravelly sand, and fine-grained beds (with clay, silt, and very fine- to fine-grained sand) associated with an early, through-flowing Rio Grande. Sand is typically light gray to tan, cross stratified, and present in layers >20 ft (>6 m) thick. Bodies of finer material tend to be thinner than the sandy bodies. Gravels consist of rounded volcanic rocks (mostly intermediate with lesser mafics), quartzite, granite, gneiss, Paleozoic and Mesozoic sedimentary clasts, and chert. The upper ~230 ft (~70 m) contains rhyolitic pumiceous gravel sourced from the Jemez Mountains (Connell, 2008b) (Fig. 1). Photos of the axial facies are shown in

Figure 9. The axial-river facies is as young as 1 to 0.8 Ma at Tijeras Arroyo (Connell et al., 2013, their fig. 9), but its maximum age is uncertain.

Eastern piedmont facies of the Sierra Ladrones Formation

Located east of the axial facies, the piedmont facies of the Sierra Ladrones Formation consists of gravel, sand, and clayey-silty sand derived from the western front of the Sandia Mountains. It has a similar age range as the axial-river facies (QTsa). Colors range from tan to yellowish brown and reddish brown. The eastern piedmont facies coarsens towards the Sandia Mountains, as observed near Placitas (Fig. 10). Adjacent to and interfingered with the axial facies is a fine-grained distal-piedmont facies (Fig. 7).

The distal-piedmont facies and the interfingering zone comprise a transitional unit labeled QTst, whereas the medial-proximal piedmont facies is labeled QTsp. Within this transitional zone, extending laterally into both the axial and distal-piedmont facies, are beds of calcium carbonate variably mixed with sand (Figs. 9E–9F). These beds are up to 1 ft (30 cm) thick and laterally extensive (for over several hundred feet, 100–250 m). They formed by evaporation of shallow groundwater near the lowest part of the valley floor (Mack et al., 2000) and can be barriers to percolating vadose water. Figure 10 shows the finer-grained distal-piedmont facies and the coarser-grained medial-proximal piedmont facies of the Sierra Ladrones Formation. Note that up to ~300 ft (~100 m) of the eastern piedmont deposits prograded over the axial sediment west of the Ranchito fault (Fig. 6).

Post-Santa Fe Group deposits

Deposition of the Santa Fe Group in the study area ended between 1.0 and 0.8 Ma, when the Rio Grande began to incise after millions of years of net aggradation (Connell et al., 2013). Gravel, sand, and clayey-silty sand continued to accumulate on most of the eastern piedmont, either on top of the Santa Fe Group or within incised valleys inset against the Santa Fe Group (Figs. 6–7). These deposits are light reddish brown, reddish yellow, or yellowish brown and up to 170 ft (51 m) thick (Connell, 2008b). Time periods of local geomorphic stability, probably in conjunction with localized incision, resulted in paleosol formation, typically characterized by argillic or cambic soil horizon(s) overlying calcic soil horizon(s). Net incision between

0.8 and 0.1 Ma created a series of geomorphic piedmont surfaces. These surfaces commonly feature well-developed topsoils containing calcic horizons having stage II+ to stage IV pedogenic carbonate morphology (Connell, 2008b; carbonate morphology stages are described in Gile et al., 1966, 1981). We refer to this collection of middle to upper Pleistocene piedmont alluvium as “older piedmont alluvium” (Qao, Fig. 6).

Valley fill underlying modern drainages (that flow into the Rio Grande) lacks well-developed paleosols, has weakly developed topsoils (stages I-II pedogenic carbonate morphology), and comprises gravel, sand, and clayey-silty sand (Connell, 2008b). We refer to these Holocene-age, relatively coarse-grained deposits as “younger alluvium” (Qaya_{cs}, Figs. 6–7).

Middle to upper Pleistocene-age terraces flank both sides of the Rio Grande (Qtr, Figs. 6–7). Associated terrace deposits range in thickness from 10 to 170 ft (3 to 52 m) (Connell et al., 2007). The deposits have sandy gravel at their base, which is overlain by more poorly sorted, finer-grained sediment containing sand, pebbles, silt-clay, and very fine- to fine-grained sand (Connell et al., 2007).

The Rio Grande incised during the latest Pleistocene and then backfilled during the latest Pleistocene through the Holocene (Connell et al., 2007). This geologically young backfill is 50–95 ft (15–29 m) thick and includes fine- to coarse-grained sand along with subordinate gravel, fine-grained sand, silt, and clay (Qaya_{fp}, Figs. 6–7). Alluvium under the valley floor of the modern Rio Grande (Qaya_{fp}) likely contains more clay-silt beds than tributary backfill (Qaya_{cs}), due to deposition on a relatively large floodplain.

Hydrogeologic Setting

Map contours of the potentiometric surface (described below) indicate that groundwater flows away from the Rio Grande towards a north-south elongated, trough-like low centered between San Mateo and Eubank Boulevards (Powell and McKean, 2014) (Fig. 11). In the study area, depth-to-groundwater ranges in depth from 1 to 850 ft (0.3 to 259 m) below ground surface (bgs), but it is restricted to 1–140 ft (0.3–12 m) bgs under the Rio Grande floodplain. Otherwise, depths of 300–850 ft (91–259 m) bgs typify most of the study area, largely underlying the west-sloping piedmont. There, the axial facies (QTsa) is the primary aquifer used by the ABCWUA. In it, groundwater flows

through interconnected sand bodies; clay beds (deposited on past floodplains) form local aquitards. The potentiometric surface can locally vary [by as much as 25 ft (8 m) or more] from the water table due to confined-aquifer conditions at depth (Powell and McKean, 2014)—although the potentiometric surface and the water table are of relatively close elevations when considered at scales commensurate of this study. Vertical hydraulic gradients are mostly oriented down to the west and up to the east, except at the mountain front where they are difficult to generalize (Bexfield and Anderholm, 2002).

MAR Projects in the Albuquerque Metropolitan Area

Two MAR projects are currently underway in the ABCWUA jurisdiction, an arroyo-bottom infiltration project at the Bear Canyon Arroyo and both deep-injection and vadose-zone recharge at the San Juan-Chama Drinking Water Treatment Plant (SJCDWTP). Figure 12 is a schematic illustration of these MAR projects relative to the subsurface geology and surface geomorphology of the study area.

Bear Canyon Arroyo Recharge Project

MAR arroyo-bottom infiltration has been intermittently conducted along a ~3,000 ft (~910 m) length of Bear Canyon Arroyo between Wyoming Boulevard and the Arroyo del Oso Golf Course since November, 2014, following two periods of recharge in 2008 and 2009 that operated under a demonstration project permit (D. Agnew, written commun., May 9, 2019). Two demonstration discharge-infiltration runs were conducted to monitor the effectiveness of recharge (Daniel B. Stephens and Associates, 2010). The first was between February 6, 2008, and April 2, 2008, and involved 423 acre-ft (141 million gallons) of water. The second took place between December 11, 2008, and March 31, 2009, and involved 737 acre-feet (240 million gallons) of water. The water supply was from a tank that stores excess water treated for irrigation purposes. In 2007, three deep-monitoring wells [556–580 ft (169–177 m) bgs] and four shallower vadose-zone wells [50–150 ft (15–46 m) bgs] were installed along the same reach of Bear Canyon Arroyo. The purpose was to measure groundwater levels and the moisture content of vadose zones in order to evaluate the efficacy of the arroyo-bottom recharge (Daniel B. Stephens and Associates, 2009). Vadose-zone wells

were equipped with temperature sensors, heat dissipation sensors, and neutron logging devices to determine lateral migration and percolation rates. The demonstration tests at Bear Canyon Arroyo showed that >95% of the water percolated from the surface into the saturated zone (Daniel B. Stephens and Associates, 2010).

Drinking water treatment plant

Two types of injection wells were drilled in proximity to the San Juan-Chama Drinking Water Treatment Plant (SJCDWTP) in 2017 (Daniel B. Stephens and Associates, 2018). The first well is 1,237 ft (377 m) deep and designed for deep injection of treated San Juan-Chama water into the saturated zone of the upper Santa Fe Group. The saturated zone resides in 770 ft (235 m) of axial-river deposits (sand plus subordinate silt-clay and gravel) that overlie the finer-grained Atrisco Member of the Ceja Formation. The well penetrated 320 ft (98 m) of the Atrisco Member, which consists of interbedded clay, silt, and sand. Above the axial-river deposits of the upper Santa Fe Group lies 140 ft (43 m) of Rio Grande terrace alluvium (middle to upper Pleistocene), of which only the basal 5–10 ft (2–3 m) is saturated. Zone tests of the axial sediment indicated horizontal

hydraulic conductivity (Khoriz) of 88 ft/d and total dissolved solids (TDS) of 252 mg/L at depths of 820 to 840 ft (Daniel B. Stephens and Associates, 2018). The aquifer in the Atrisco Member is lower quality, in which Khoriz from two zone tests (depths of 925–935 ft and 1,125–1,135 ft) averaged 5–7 ft/d with TDS of 327–342 mg/L (Daniel B. Stephens and Associates, 2018). The recommended maximum operating rate was 3,000 gallons per minute (gpm) (Daniel B. Stephens and Associates, 2018). The planned injection rate of this well is ~2,500 gpm (D. Agnew, personal commun., 2019). Depth-to-groundwater is ~135 ft bgs and steadily rising at ~3 ft (1 m) per year (Daniel B. Stephens and Associates, 2018).

Additionally, during August of 2017, a 32-in diameter vadose-zone well was drilled ~200 ft (61 m) to the north of the deep-injection well, reaching 139 ft bgs. The sediment in this well correlates with terrace deposits of the Rio Grande (Qtr, Figs. 6–7) and consists of sand plus minor silt. A step infiltration test conducted for 10 hours indicated saturated Khoriz of 13 ft/d. In this test, there were six 100-minute steps beginning with an injection rate of 100 gpm and progressing to 350 gpm. At the maximum injection rate of 363 gpm, there was ~45 ft (14 m) of a raised groundwater column in the well casing (Daniel B. Stephens and Associates, 2018).

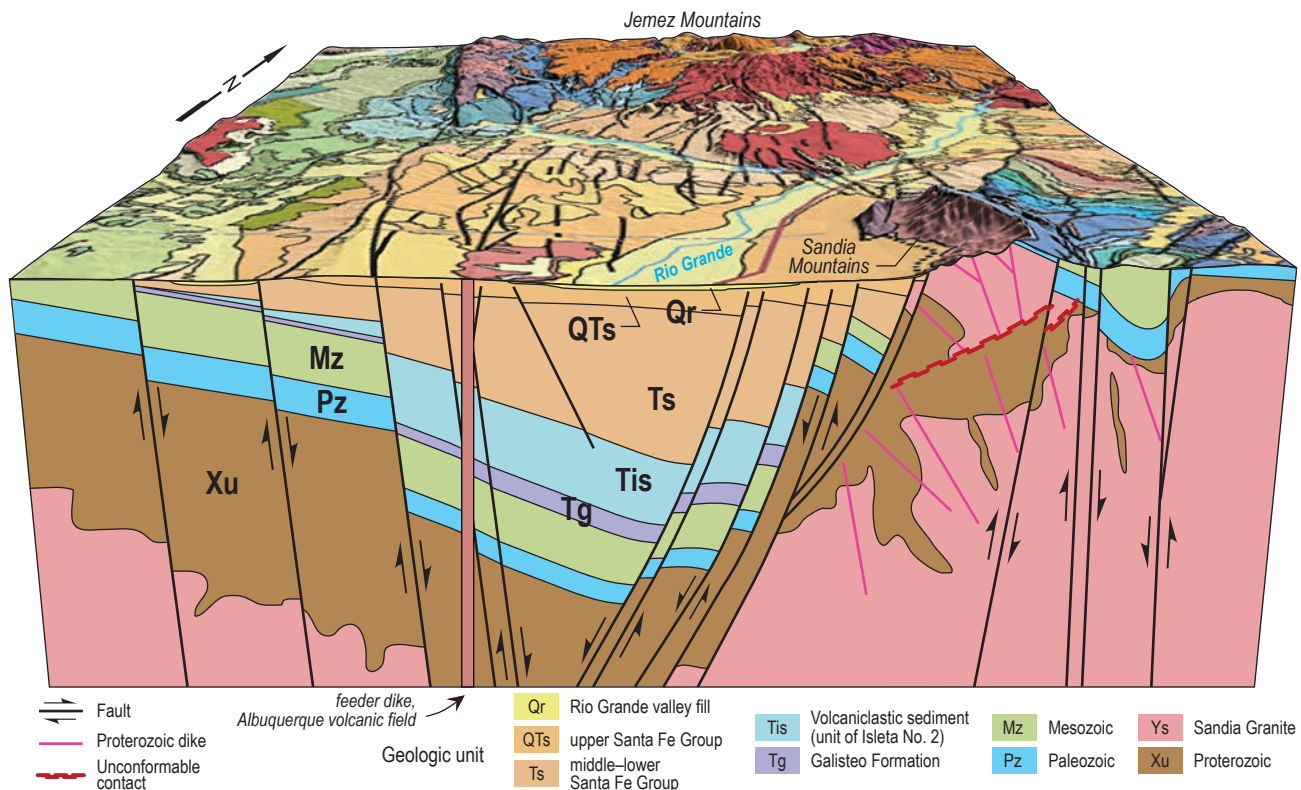


Figure 5. Schematic block diagram of the general structure of the Calabacillas sub-basin. The upper Santa Fe Group (QTs) is of interest.

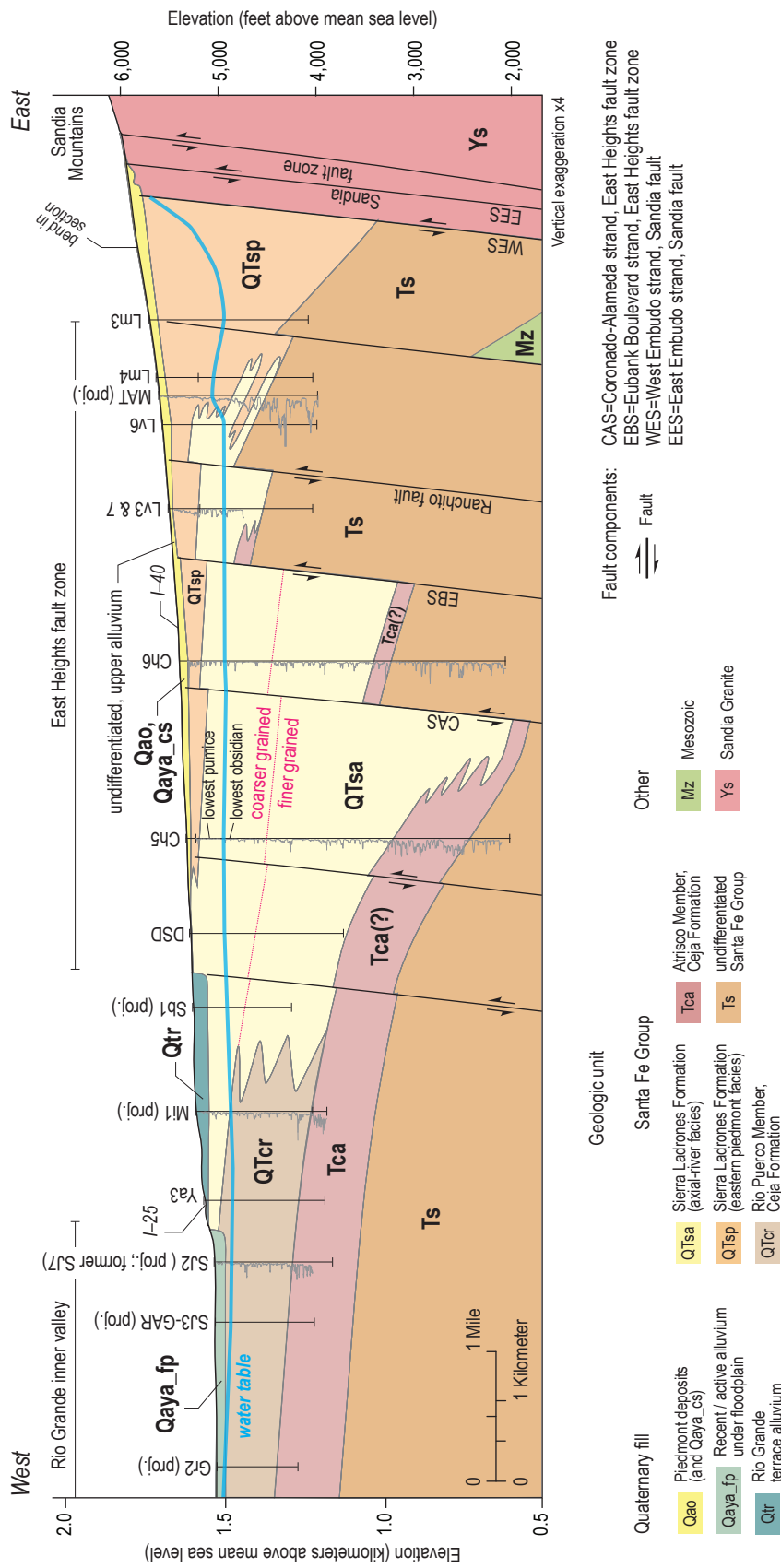


Figure 6. Central part of cross section C-C from Connell (2008b), which illustrates stratigraphic units and faults in the center of the study area. Refer to Figures 1 and 3 for location. To illustrate relative coarseness to fineness of strata, resistivity curves from downhole wireline logs are depicted next to some wells (resistivity increases to the left, and this increase likely reflects higher sand content). At wells Ch5 and Ch6, rhyolitic pebbles in the upper part of unit Ts, below the Ceja Formation (Tca), indicate older axial-river deposits (Hawley and Haase, 1992) that may have relatively high permeability. Lithological data for wells given in Appendix 1 (data reproduced from Connell, 2008b).

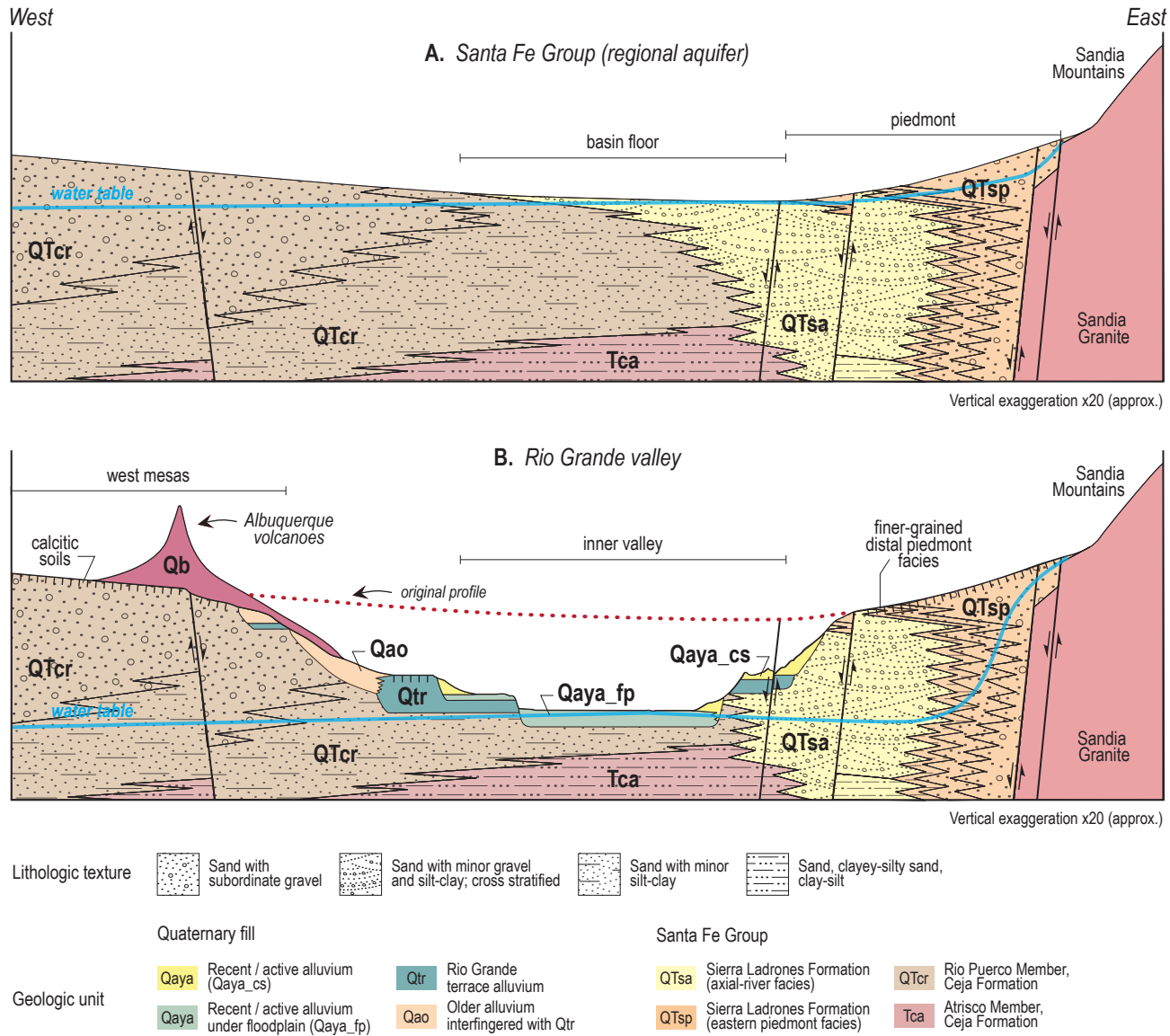


Figure 7. Schematic cross sections illustrating (A) the lithostratigraphy of the upper Santa Fe Group and (B) the lithostratigraphy of the upper Santa Fe Group and younger, middle to upper Quaternary units under and near the modern Rio Grande valley. Near the central part of the basin, the axial-river facies of the Sierra Ladrones Formation (QTsa) interfingers westward with the Ceja Formation (which includes an upper, coarser member, QTcr, overlying a finer-grained member, Tca). The axial facies, in turn, interfingers eastward with the eastern piedmont facies of the Sierra Ladrones Formation (QTsp). Within the piedmont facies, there is a westward trend from coarser sediment of sand and gravel near the mountain front to sand, clayey-silty sand, and clay-silt near the Rio Grande.

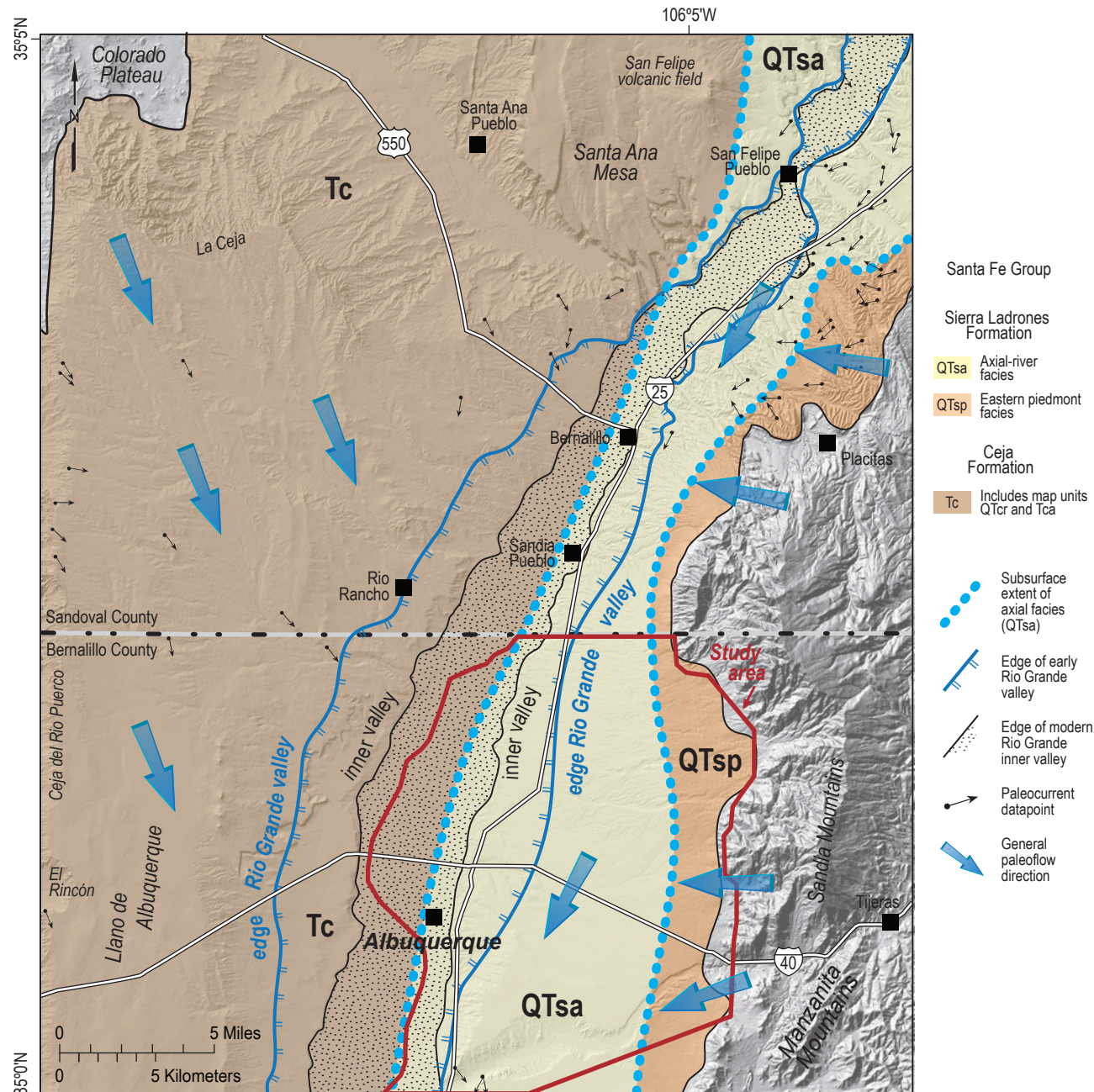


Figure 8. Distribution of strata of the upper part of the Santa Fe Group in the region around the study area: axial-river (QTsa) and eastern piedmont (QTsp) deposits of the Sierra Ladrones Formation and the large fan complex of the Ceja Formation (Tc, which includes map units QTcr and Tca). Units younger than the Santa Fe Group are not shown. Paleocurrent data (from Connell, 2008b) indicate that general paleoflow directions were to: south-southwest for the axial-river facies, west for the eastern piedmont deposits, and southeast for the Ceja Formation,

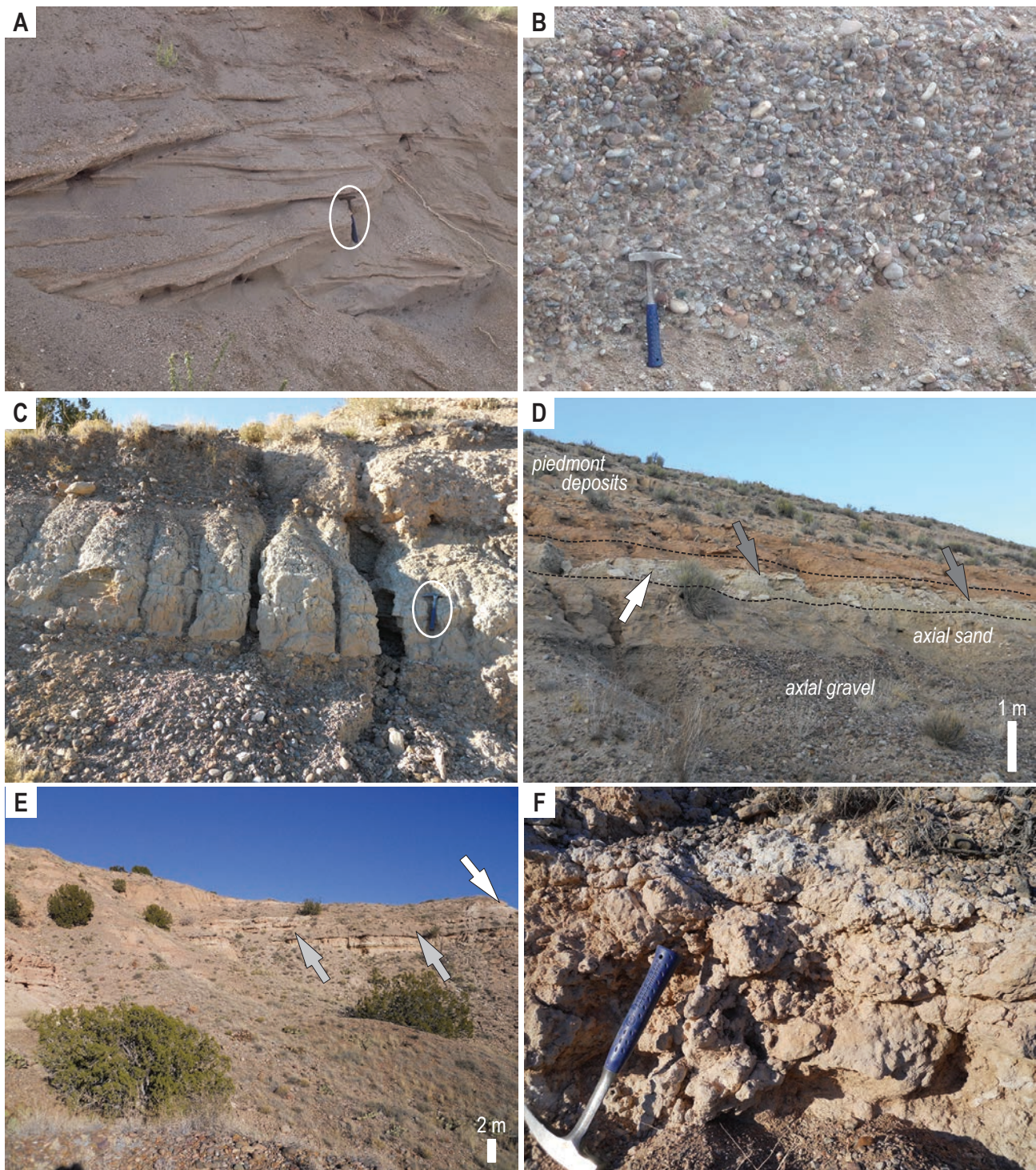


Figure 9. Axial-river facies of the Sierra Ladrones Formation (QTsa). **A.** Cross-stratified sand exposed in Tijeras Arroyo. **B.** Sandy pebbles and fine cobbles in Tijeras Arroyo; view to south-southeast. Note the clast-supported fabric and imbrication of clasts (indicating paleoflow to the right). **C.** Floodplain deposit (~4 ft, ~1.2 m) between clast-supported gravel beds near Placitas. This fine sediment comprises light greenish-yellow, very-fine sand fining upward to silt. **D.** About 20 ft (6 m) of orangish piedmont deposits (sand and clayey-silty sand) overlying axial facies (gravel overlain by grayish sand). Above the axial sand is ~1–2 ft (30–60 cm) of greenish clay-silt (white arrow), itself overlain by 10–20 cm of calcium carbonate (dark-gray arrow). A thin, reddish-brown clay immediately overlies the calcium carbonate. This fine-grained package between the axial and piedmont facies (bracketed by dashed lines) is relatively common and would be a low-permeability barrier for percolating water. **E.** Laterally extensive, tabular beds of sand and silt associated with the axial-river facies. White and gray arrows denote groundwater-precipitated calcium carbonate beds that can extend laterally for hundreds of feet (100–250 m). **F.** Close-up of a groundwater-precipitated calcium carbonate developed in a silty matrix. Bulbous texture is due to bioturbation. This type of authigenic carbonate is most abundant in zones where the axial and distal-piedmont facies are interfingered.

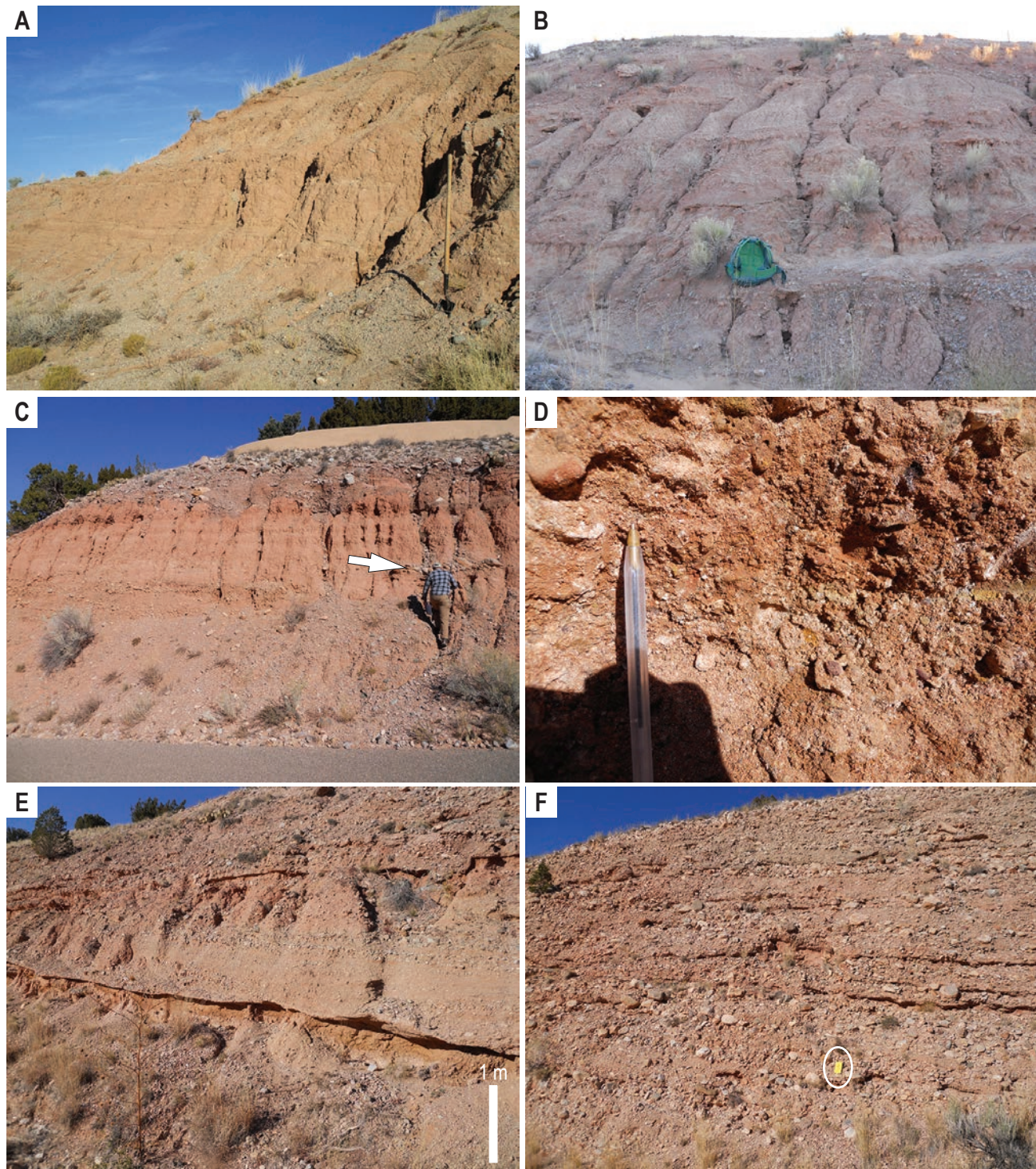


Figure 10. Eastern piedmont facies of the Sierra Ladrones Formation (QTsp and QTst). **A–B.** Distal-piedmont sediment characterized by very fine- to fine-grained sand, silty-clayey fine sand, minor pebbly sand, and minor medium- to very coarse-grained sand. Also present are beds comprising very-fine to fine sand and clayey-silty fine sand with minor, scattered coarser sand grains; this poorly sorted sediment was probably deposited by muddy water less viscous than typical debris flows (see Seager and Mack, 2003). **C.** Medial- to distal-piedmont facies, mostly consisting of fine-grained, reddish sand and silty-clayey sand with ~20–35% beds of coarse sand and gravel. **D.** Close-up of gravel bed shown in C (white arrow). Note that clay has filled much of the original porosity in the reddish-brown layer in the upper half of the photo. **E.** Medial- to proximal-piedmont facies. There is 70–80% gravelly, coarse sediment compared to 20–30% intervals of silty-clayey, very fine- to fine-grained sand that extend laterally up to ~300 ft (~100 m). **F.** Proximal-piedmont facies dominated by sandy gravel. In E–F, calcium carbonate cement is relatively pervasive, likely resulting from a nearby fault influencing groundwater flow. Most of the piedmont facies in the study area, however, is not this heavily cemented.

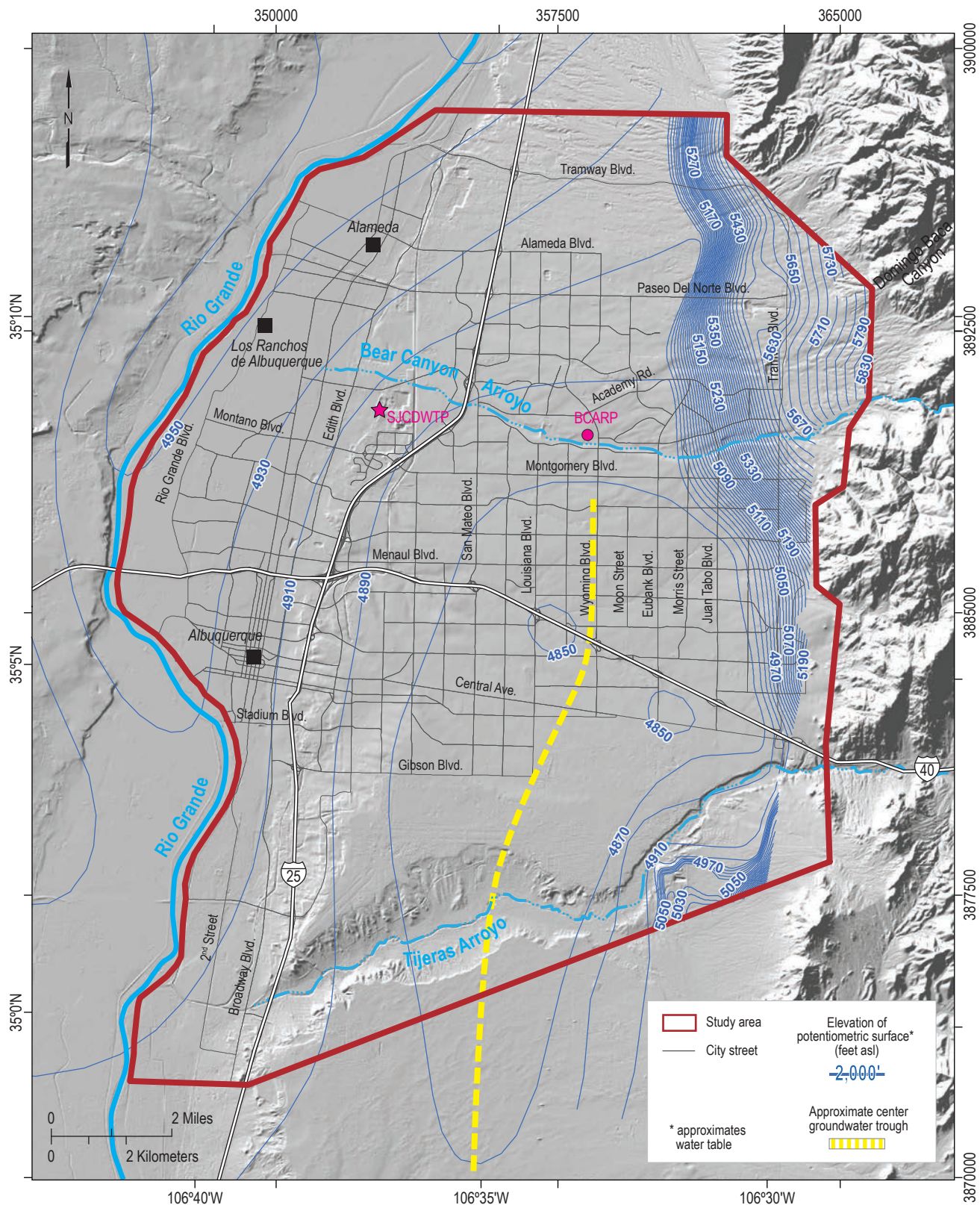


Figure 11. The potentiometric surface in the study area slopes away from the Rio Grande toward a “groundwater trough” centered near Louisiana and Wyoming Boulevards (south of Montgomery Boulevard, stepping west near Tijeras Arroyo). Another prominent feature is the steep gradient between about Juan Tabo and Tramway Boulevards, where it climbs eastward by 700 ft (210 m) over 2 mi (3.2 km). West of Juan Tabo Boulevard, contours are from the 2012 potentiometric surface by Powell and McKean (2014); east of Juan Tabo Boulevard are from this work (see text).

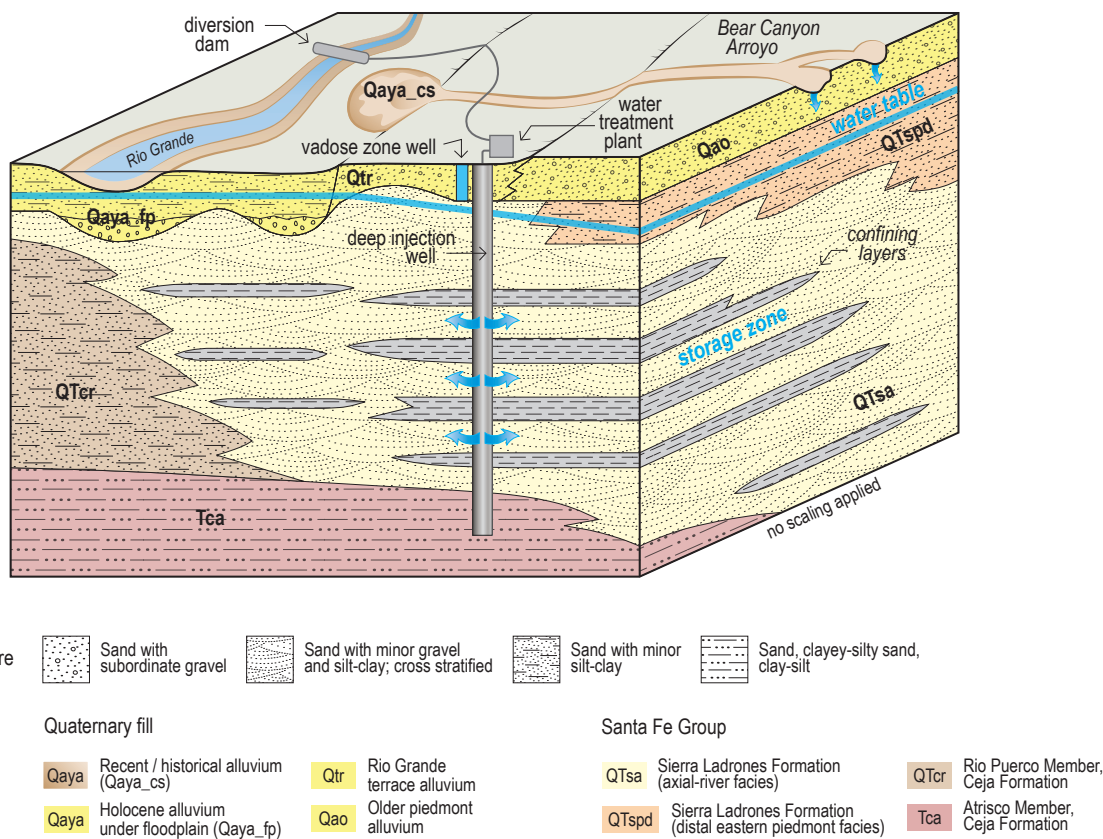


Figure 12. Schematic block diagram illustrating the subsurface geology relative to the two current MAR projects in the study area (refer to Fig. 2): the San Juan-Chama Drinking Water Treatment Plant (SJCDWTP) and Bear Canyon Arroyo Recharge Project (BCARP). Blue arrows indicate managed aquifer recharge.

V. APPROACH

Comparative approaches are needed to evaluate the suitability of areas for MAR. Considering the relatively large area under study and the available data, we elected to use an ArcGIS-based summation of weighted-ranked criteria, which is more popularly termed as a weighted overlay approach. Following a planning stage and initial data compilation, the overall workflow of the MAR suitability project involved the following phases: construction of a subsurface geologic model to incorporate subsurface hydrogeologic conditions; analysis of wireline logs for 17 wells (to ascertain the proportions of clay, clayey sand, and sand in geologic units, as well as thicknesses of permeable zones); definition of criteria and a scheme for their scoring (or ranking); Python scripting to supplement ArcGIS tools for conducting the weighted overlay analyses; and selection of the method for conversion of final weighted values to qualitative MAR suitability ratings. Two maps were created. The first map shows the suitability for MAR using deep-injection wells (where only the saturated zone was considered) and the other for suitability of MAR using shallow-based methods (where both unsaturated and saturated zones were considered).

Shallow recharge or infiltration can cause soil hydrocompaction, with the resulting subsidence potentially damaging buildings, roads, and pipelines. Thus, a separate map identifying susceptibility to soil hydrocompaction was created to compliment the shallow-recharge suitability map. The hydrocompaction-susceptibility map was made using weighted overlay analyses of factors that have been correlated to this phenomenon (Rinehart et al., 2017; Lutteneger and Saber, 1988; and Momeni et al., 2012). Using geologic units mapped by Connell (2008b), these factors include: soil type (as reflected in the soil taxonomy from order to great group); soil texture; and depth-to-groundwater derived from water-elevation contours presented in this report.

Data Compilation and Initial Work

Initial work established which geologic units are relevant for MAR studies in the Albuquerque area;

this work included description of outcrop analogs of the aquifers. Data needed to assess hydraulic properties of aquifers were compiled, as were those necessary to evaluate the hydrogeologic characteristics of the overlying unsaturated sediment (including surficial sediment deemed at risk for soil hydrocompaction). We also extended the coverage of the potentiometric surface from previous contouring efforts (e.g., Powell and McKean, 2014). Below we discuss the methods and results of the data compilation effort.

Hydrostratigraphic units

For this study, we posited 10 potential hydrostratigraphic units that reflect geologic (lithologic) units of unique paleodepositional environments and provenances (Table 1). These are based on the geologic mapping and subsurface work of Connell (2008b) and Connell et al. (1998). Surficial lithologic units of Connell (2008a, 2008b) were combined, whereas those of the Santa Fe Group were not. Note that one of our hydrostratigraphic units, QTst, is not directly associated with a map unit, but Connell (2008b) did recognize it on well logs.

A summary of well data given in Connell (2008b), as well as related lithologic picks, is presented in Appendix 1. In the course of study, we found that some of the hydrostratigraphic units possessed similar properties, such as comparable ranges of hydraulic conductivity. Nonetheless, none of the 10 units were combined, primarily to permit construction of a 3D geologic model that could be repurposed for later projects.

Units for hydrocompaction assessment

Geologic units mapped by Connell (2008b) are a high-quality dataset for estimating susceptibilities to hydrocompaction in Albuquerque. This is because they reflect paleodepositional environment, age, and permit interpretation of the more detailed information of deposits (such as grain size). These features are the primary correlative factors of hydrocompaction susceptibility (Johnpeer et al.,

Table 1. Hydrostratigraphic units.

Hydrostratigraphic unit	Name	Lithologic units of Connell (2008b) *
Qaya_cs	Coarse-grained, younger alluvium	Qa, Qpy, Qay
Qaya_fp	"Younger" alluvium underlying Rio Grande floodplain	Qrpc, Qrpf, Qrpy, Qrpyc, Qrpm, Qrpmc, Qrpo, Qrpoc
Qao	"Older" piedmont alluvium	Qam, Qam1-2, Qamt1-3, Qao, Qao1-4, Qaot1-2
Qtr	Rio Grande terrace alluvium	Qrm, Qre
QTsp	Medial-proximal piedmont facies, Sierra Ladrones Formation	QTsp
QTst	Transitional between QTsa and QTsp and the distal-piedmont facies, Sierra Ladrones Formation	QTst **
QTsa	Axial-river facies, Sierra Ladrones Formation	QTsa
QTcr	Rio Puerco Member, Ceja Formation	QTcr
Tca	Atrisco Member, Ceja Formation	Tca
Tsm	"Middle" unit of Santa Fe Group	Ts

* See text for unit descriptions; see Connell (2008b) for details.

** Not a map unit of Connell (2008b) but recognized in the Well_point feature class datatable (reproduced in Appendix 1).

Table 2. Statistics of compiled hydraulic conductivity per hydrostratigraphic unit in the saturated zone.

	Qtr	QTsp	QTst	QTsa	QTcr	Tca	Tca-Tsm * 	Tsm
Count	1	3	4	32	18	5	7	4
Mean	13.0	25.8	24.3	63.8	20.4	18.0	22.3	35.4
Std deviation	N/A	32.9	21.1	39.1	28.2	24.5	16.5	39.1
Minimum	13.0	1.0	8.0	1.5	0.0	0.2	7.0	3.5
Q1	13.0	7.1	8.8	32.5	8.3	3.6	12.1	14.4
Median	13.0	13.2	18.0	63.0	13.0	7.1	15.0	23.0
Q3	13.0	38.1	33.5	100.0	19.0	19.0	27.5	44.0
Maximum	13.0	63.1	53.0	133.0	127.0	60.0	55.0	92.0
Bottom	13.0	7.1	8.8	32.5	8.3	3.6	12.1	14.4
2Q Box	0.0	6.1	9.3	30.5	4.7	3.5	2.9	8.6
3Q Box	0.0	24.9	15.5	37.0	6.0	11.9	12.5	21.0
Whisker-	0.0	6.1	0.8	31.0	8.3	3.5	5.1	10.9
Whisker+	0.0	24.9	19.5	33.0	108.0	41.0	27.5	48.0

* Unit Tca-Tsm denotes intervals where the well screen spans across parts of both the Atrisco Member of the Ceja Formation (Tca) and the "middle" Santa Fe Group (Tsm).

1985; National Resource Council, 1999; Momeni et al., 2012). As factors for mapping hydrocompaction susceptibility, we also included soil type and texture (as reflected in soil taxonomy) using the Gridded Soil Survey Geographic Database (gSSURGO; 1:30,000 scale, Soil Survey Staff, 2014).

Hydraulic properties of saturated-zone deposits

To ascertain hydraulic properties of the hydrostratigraphic units, pump test and infiltration data from within and near the study area were compiled from literature primarily consisting of consultant reports. The following was noted for each well with pump test data: well information (e.g., location, total depth, screened depths); depths of hydrostratigraphic units (from the Well_point feature class in the GIS files of Connell, 2008b, presented in Appendix 1); and saturated hydraulic conductivity (K_{horiz}) and specific capacity. The results of this effort are in Appendix 2. Only one pump test (on the Duranes 4 well) acquired data related to storage coefficient, specific yield, and vertical

hydraulic conductivity (K_{vert}) (Appendix 2). For each well, the proportion of hydrostratigraphic units in the screened interval was calculated. Where a given hydrostratigraphic unit composed >75% the screened interval, the pump test data were attributed to that unit. The most common parameter from a pump test was horizontal saturated hydraulic conductivity. Box and whisker plots of horizontal hydraulic conductivity are shown in Figure 13, and statistical factors of this parameter (such as mean, median, and standard deviation) are presented in Table 2. In our subsequent analyses, we chose the median values of horizontal conductivity as representative of the hydrostratigraphic units.

Hydraulic properties of unsaturated sediment

Herein, infiltration rates of surficial sediment refer to the rate at which surface water is absorbed into the soil. The results of two previous studies are provided in Table 3. In these previous studies, two of our hydrostratigraphic units were tested using the falling head method: the older, post-Santa Fe Group alluvium

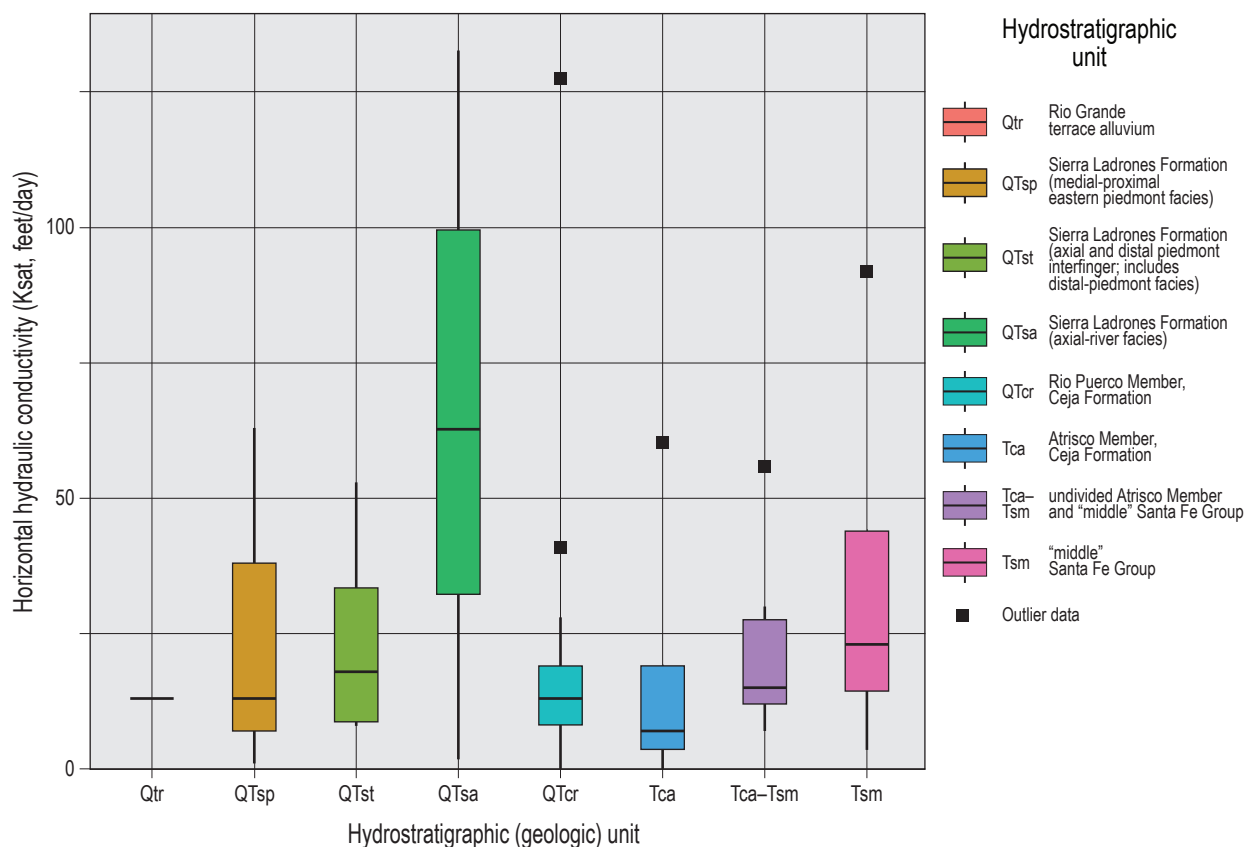


Figure 13. Box and whisker plot of hydraulic conductivities compiled for the hydrostratigraphic units, calculated from pump tests (Appendix 2). Unit abbreviations follow those in Table 1. Unit Tca–Tsm is correlated with hydraulic conductivities obtained from a set of wells with screens that extend across both the Atrisco Member (Ceja Formation) and the “middle” Santa Fe Group.

Table 3. Infiltration data from sites within 5 kilometers of the study area.

Site ID	Hydrostratigraphic unit *	Sample depth (feet)	Vertical hydraulic conductivity (cm/s)	Infiltration rate (feet/day) **	Test type	Source ***
BC3	Qaya_cs	1		25.2	Falling head	D14
BC4	Qaya_cs	1		11.3	Falling head	D14
A-1	Qao	5	3.38E-05	0.096	Falling head	A14
A-3	Qao	5	3.40E-05	0.096	Falling head	A14
B-1	Qao	5	1.08E-04	0.306	Falling head	A14
B-3	Qao	5	3.37E-05	0.096	Falling head	A14
C-1	Qao	5	1.93E-04	0.547	Falling head	A14
D-1	Qao	5	9.79E-05	0.278	Falling head	A14

Factor of safety applied to infiltration rate = 2. For sites BC3 and BC4, land-surface elevation was estimated from a DEM (USGS).

* Lithologic unit: Qaya_cs = uppermost Pleistocene to Holocene valley-floor alluvium east of the Rio Grande floodplain; Qao = middle to upper Pleistocene piedmont alluvium.

** AMEC (2014) study treats infiltration rate as equivalent to coefficient of hydraulic conductivity. This column shows original units of centimeters/second (cm/s) converted to feet/day (ft/d).

*** Data sources: A14, AMEC (2014); D14, Daniel B. Stephens and Associates (2014).

Table 4. Compilation of vertical hydraulic conductivity (Kvert).

HYDROSTRATIGRAPHIC UNIT		SOURCE			INTERPRETATION		
Unit	Representative soil texture	Wamsley (2014) * (feet/day)	Soil tables (feet/day)	Bear Canyon modeling ** (feet/day)	Representative value (feet/day)	Confidence	Notes
Qaya	sand	4-12; 12-40; 1.2-4	N/A	2.6	High	Used average of Ksat range (1.2–4 feet/day) of component GA, which is the lowest range (most conservative)	
Qaya_fp	loamy sand			1	Moderate	Assumed similar to Qtr	
Qaya and Qao	loamy sand		0.48	0.5	High	Used layer 1 in Bear Canyon model	
Qao	loamy sand	5	0.48	0.5	High	Used layer 1 in Bear Canyon model	
Qtr	loamy sand			1	Moderate	***	
QTsp	loamy sand	5		0.5	Moderate	Assumed similar to Qao	
QTst	sandy loam		0.16	0.2	Moderate	Layer 2 of Bear Canyon model equates to distal facies—alternatively, 10% of median value would be 1 feet/day ***	
QTsa	sand		1.6	1.6	Moderate	Used Bear Canyon value because accounts for interbedded clay	
QTcr	sand			1	Low	Used a value about midway between QTst and QTsa	

* Infers percolation velocity from a tracer study at North Albuquerque Acres by Thomson et al. (2000, unpublished report).

** From a data synthesis report of the Bear Canyon Recharge Demonstration Project (Daniel B. Stephens, 2010).

*** From seepage test at the San Juan-Chama Drinking Water Treatment Plant; horizontal conductivity (Khor) was 13 feet/day (ft/d) (Daniel B. Stephens and Associates, 2018).

Assume Kvert/Khor of 0.1 (from Bear Canyon modeling for layer 1, weighted by 50% because of more clay in Qaya_fp). Gb and Ge are common floodplain soil component units along the modern Rio Grande (Soil Survey Staff, 2014), with ranges from 1.2–4 ft/d to 0.4–1.2 ft/d. Older floodplain deposits in QTst could have similar Kvert. Collectively, 1 ft/d seems reasonable.

(Qao, Figs. 6–7) and the younger, coarser-grained alluvium outside the Rio Grande floodplain (Qaya_{cs}, Figs. 6–7). The infiltration rates ranged from 0.096–0.547 ft/d for unit Qao and 11.3–25.2 ft/d for Qaya_{cs}. These data were used in our compilation of representative vertical hydraulic conductivities per hydrostratigraphic unit (Table 4).

We utilized vertical hydraulic conductivity as a proxy for the percolation properties of unsaturated zones. We compiled values from a variety of sources, including: gSSURGO tables from the U.S. Department of Agriculture (USDA) (Soil Survey Staff, 2014); a 2D modeling study of the Bear Canyon Recharge Demonstration Project (Daniel B. Stephens and Associates, 2010); and studies listed in Table 3. We chose representative values based on the data and reasoning (“notes”) given in Table 4.

Potentiometric surface and depth-to-groundwater

The potentiometric surface used for this project was synthesized from several sources. Most of the study area is covered by the 2012 potentiometric surface published by the U.S. Geological Survey (USGS) (Powell and McKean, 2014). These data, however, only cover the area west of Juan Tabo Boulevard. The potentiometric surface east of Juan Tabo Boulevard was contoured from groundwater-level data obtained from the USGS (A. Galanter, personal commun., 2018) and the New Mexico Office of the State Engineer-Water Rights Reporting System (WRRS). Perched groundwater and water levels of shallow aquifers were excluded.

Following Powell and McKean (2014), only groundwater-level measurements from November through February (i.e., the time interval of greatest seasonal aquifer recovery) were used to contour the potentiometric surface east of Juan Tabo Boulevard. In most cases, groundwater levels were taken from non-pumping wells measured during the years 2011–2013 in order to temporally match the 2012 USGS dataset. It was necessary, however, to also use some WRRS data spanning years 2010–2016 to expand coverage.

Once groundwater-level data were compiled, we interpolated the potentiometric surface east of Juan Tabo Boulevard using a regularized spline function in ArcGIS. The spline tool was selected instead of other methods because it forces the interpolated surface through the data points (i.e., it more directly honors the data within the input gridding environment). A weight of 0.1 was applied to create a smoother surface. The splined surface was then contoured

at 20-ft intervals to match the 2012 USGS dataset (Powell and McKean, 2014). Manual adjustments to contours were made in order to better account for specific geologic information and accommodate coverage constraints:

1. No measurements were available on Sandia Pueblo in the northeastern part of the study area, so it was assumed that steep contours continue northward to that area along the range-front fault system.
2. Contours shallower than 5,610 ft above mean sea level (amsl) were modified to follow the trend of a paleovalley near Domingo Baca Canyon, improving correlation with cross section B–B' in Connell (2008a).
3. In the absence of better data in the central-eastern part of the study area, two contours (i.e., 4,870 ft and 4,890 ft) were adjusted to better conform to the 2012 USGS data (Powell and McKean, 2014) and to follow the range-front fault system.
4. Contours were generalized near Tijeras Arroyo in the southeastern part of the study area, where a poorly understood fault system west of the Sandia fault appears to have induced complex patterns of groundwater level.

Once these modifications were complete, we merged our interpolated potentiometric surface with the 2012 USGS contours. The resulting map of the potentiometric surface is shown in Figure 11. The map of depth-to-groundwater, made by subtracting the elevation of the potentiometric surface from the land-surface elevation at grid cells, is provided in Figure 14. Note that the potentiometric surface approximates the water table because they are relatively close (<100 ft, typically 10s of feet per Powell and McKean, 2014) in the context of our investigated depth interval of 1,500 ft.

Subsurface Geologic Model

The 3D geologic model was constructed using the lithologic units derived from the Well_point feature class in the GIS files of Connell (2008b) (Appendix 1). Using these data, the bases of the hydrostratigraphic units listed in Table 1 were manually contoured in ArcMap; structural contours were also created for relatively large fault planes by assuming constant

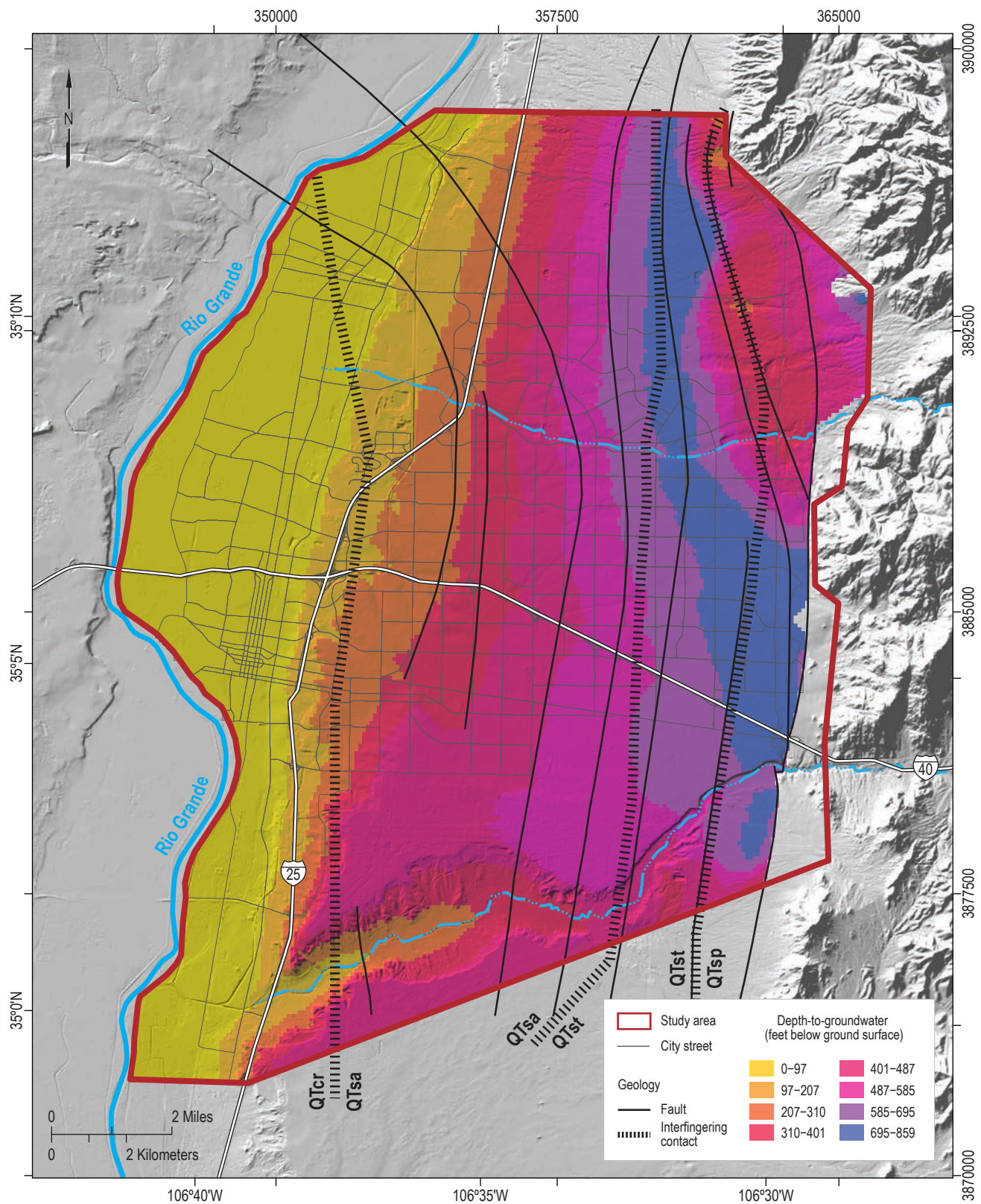


Figure 14. Depth-to-groundwater. Map constructed by subtracting the elevation of the potentiometric surface from the elevation of the land surface. Hatched lines are generalized, laterally gradational contacts between hydrostratigraphic units, from west to east: Rio Puerco Member of the Ceja Formation (QTcr) and the axial-river (QTsa), transitional and distal-piedmont (QTst), and eastern medial-proximal piedmont (QTsp) facies of the Sierra Ladrones Formation.

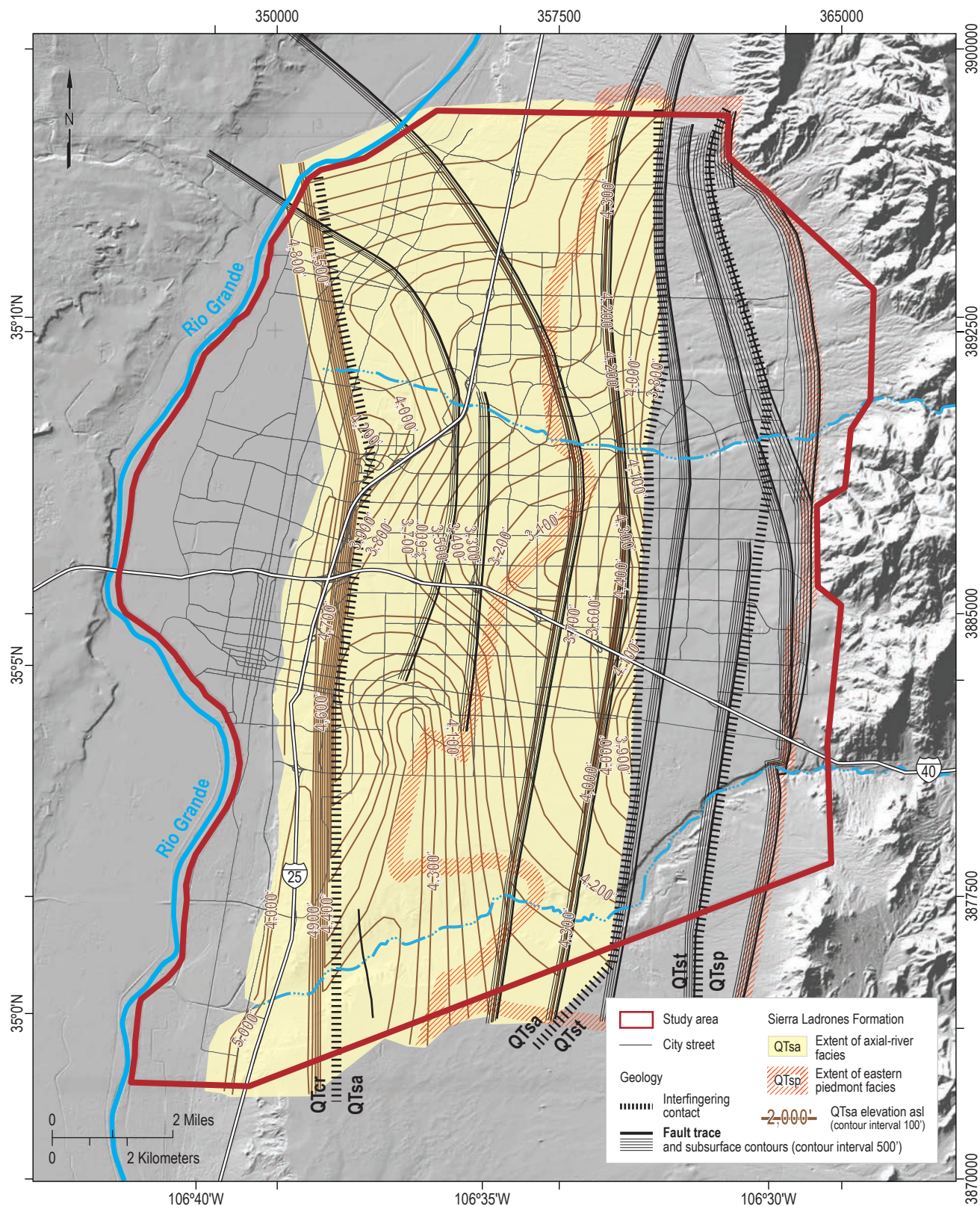


Figure 15. Structural contour maps of two facies of the Sierra Ladrones Formation. Contours are in feet-elevation.

See Appendix 3 for structural contour maps of all hydrostratigraphic units.

Figure 15A (above) presents the axial-river facies (QTsa). The extents of units QTsa and QTsp in the subsurface are shown by shading and colored hatched lines (yellow for QTsa, orange for QTsp). Hatched lines represent generalized, laterally interfingering contacts, from west to east, between hydrostratigraphic units QTcr, QTsa, QTst, and QTsp. Note that structural contours of unit QTst are not shown.

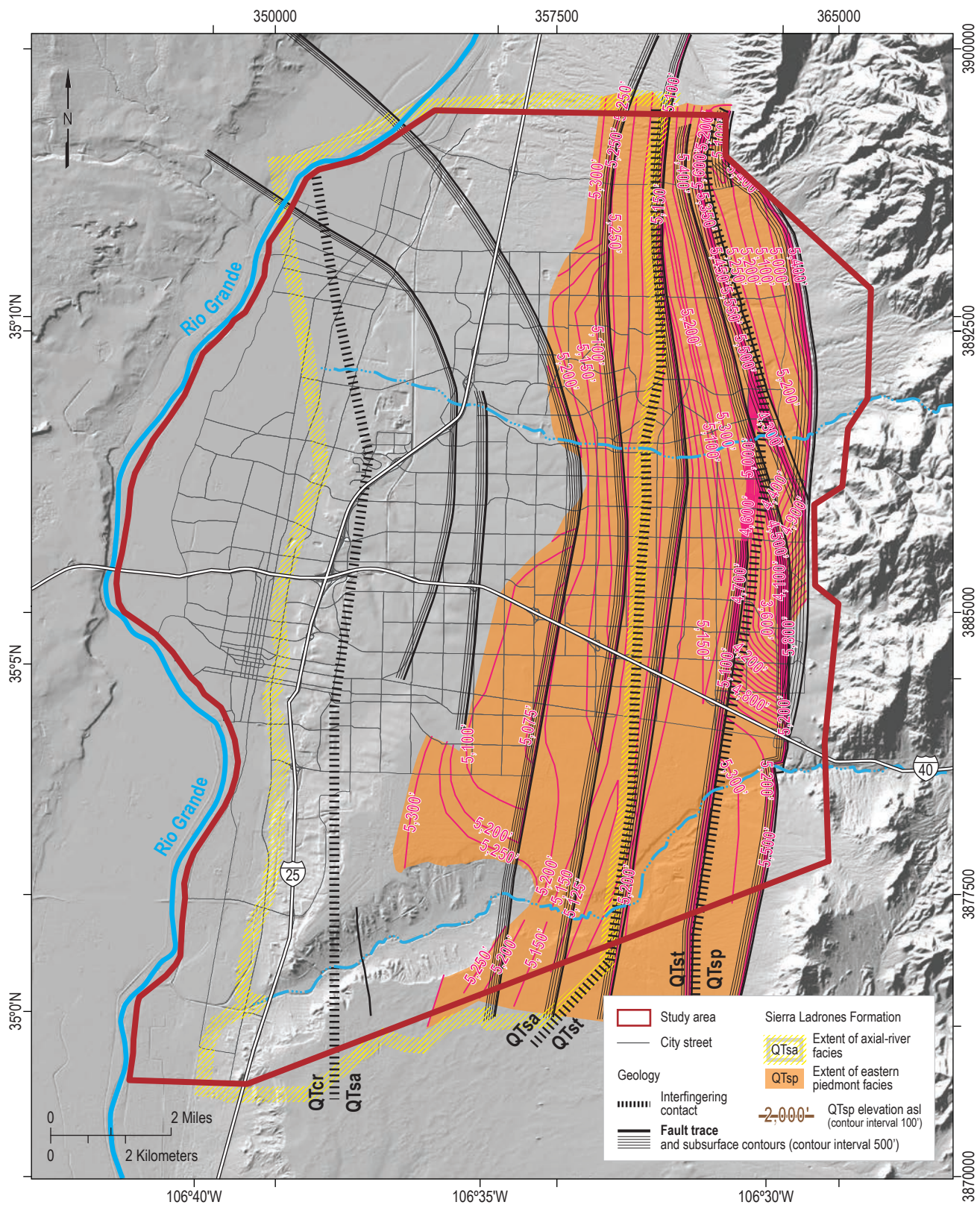


Figure 15—continued. Structural contour maps of two facies of the Sierra Ladrones Formation. Contours are in feet-elevation.

See Appendix 3 for structural contour maps of all hydrostratigraphic units.

Figure 15B (above) presents the eastern medial-proximal facies (QTsp). The extents of units QTsa and QTsp in the subsurface are shown by shading and colored hatched lines (yellow for QTsa, orange for QTsp). Late in Santa Fe Group deposition, the piedmont facies prograded westward, illustrated by the shading of QTsp extended west of its generalized western contact. Note that structural contours of unit QTst are not shown.

dips of 67° . The structural contour maps for each lithologic unit, as well as the fault planes, are presented in Appendix 3. Example structural contour maps of two geologic units (the axial and piedmont facies of the Sierra Ladrones Formation, QTsa and QTsp, respectively) are shown in Figure 15.

Several ArcGIS tools were used to generate the geologic model from the subsurface contours (Fig. 16; Appendix 3). The generation of the 3D surfaces, as well as later rating of parameters and the weighted overlay analyses, utilized a 100x100 m snap raster to ensure collocated pixel cells. ArcGIS terrain datasets were used as an intermediate between the structure contours and the final basal surfaces of units.

To contour each unit, as well as the potentiometric surface, the interpolation extent (i.e., the gridding environment) in ArcMap was drawn beyond the study area (where data allowed) in order to avoid edge effects within the study area during the interpolation process. Lines representing structural troughs and ridges were drawn across contours to

force the interpolation to honor linear trends in unit surfaces. Elevation controls were either manually entered along the troughs, ridges, and the edges of the extent polygon based on structural elevations or, where the base of a unit is exposed at the surface, were assigned based on topographic elevations. Structural contours, structural ridges and troughs, and the extent polygon were then added to the terrain dataset. The Terrain to Raster conversion tool was used to generate an initial base-of-unit surface for each unit and the potentiometric surface.

The 3D geologic model was produced sequentially by defining the base of each unit at every pixel, beginning with the land surface and progressing down the stratigraphic section. Where a unit is absent in the subsurface, the elevation of the base of the unit was set to the elevation of the base of the first overlying unit at that location, or the land surface if no other units are present. In this way, the missing unit is defined everywhere in the model extent and will have zero thickness wherever the unit is not present in the subsurface. This prevents processing errors associated

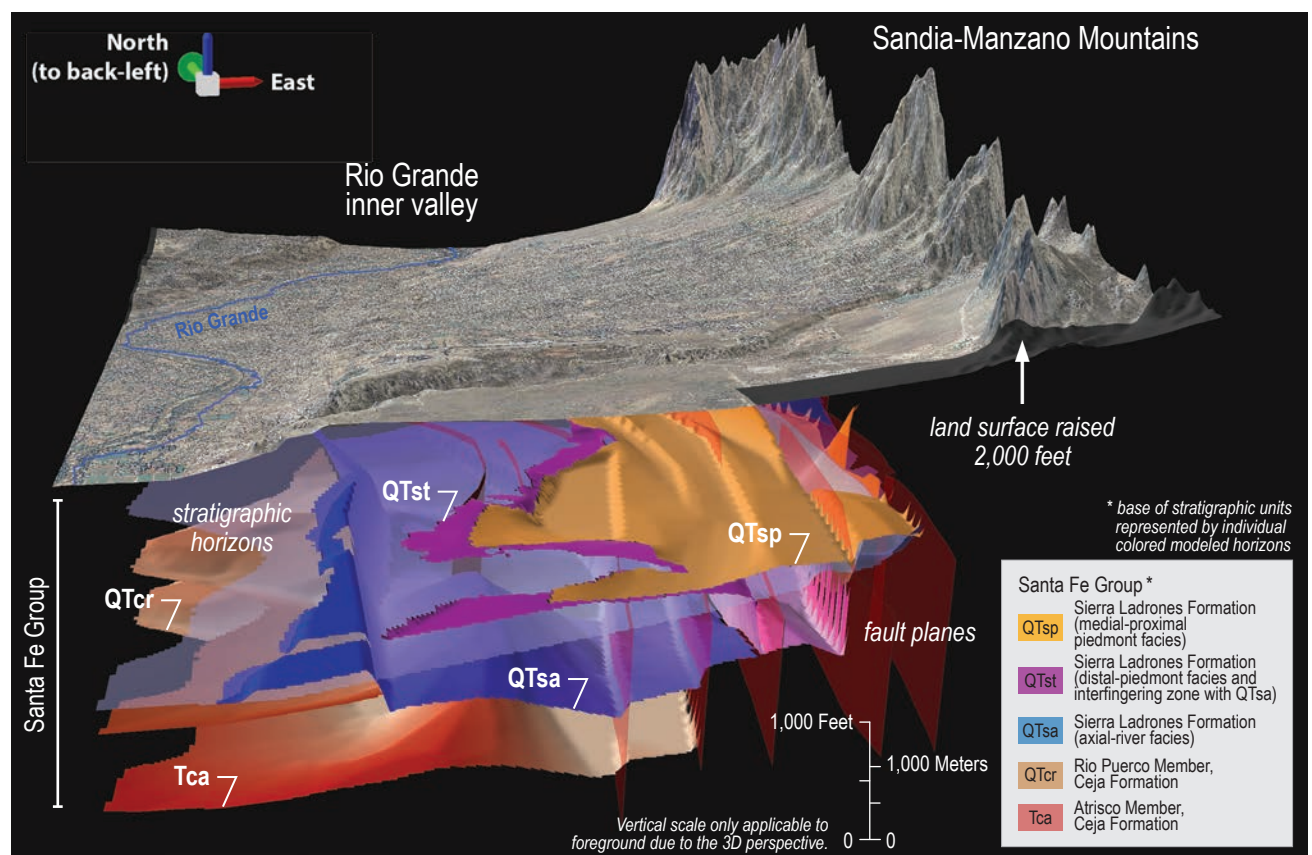


Figure 16. 3D subsurface geologic model of the Santa Fe Group underlying topography of the Earth's surface. The land surface is raised by 2,000 ft, and the post-Santa Fe Group section between it and the Santa Fe Group is artificially removed for easier viewing of the stratigraphic interval of interest.

with “null” values and results in a closed geologic model. During suitability processing, each unit was weighted by its thickness such that it does not affect the suitability determined at that location if below a certain thickness threshold (of 20 ft, 6 m).

A limitation of this method is that contacts of interfingered units had to be simplified as steeply dipping surfaces in order to make one unit overlie the other, but this is not believed to be a significant constraint of our model. Three-dimensional depictions of the model units (via Esri ArcScene) are shown in Appendix 4. Figure 16 depicts the Santa Fe Group in the 3D model under a raised topographic surface; post-Santa Fe Group units are not shown.

Wireline Log Analyses

Several deep water wells are located in the Albuquerque area, of which ~90 have wireline logs. We examined 17 logs to determine the thicknesses of storage zones and ascertain the proportions of sand, clayey sand, and clay in the following units of the Santa Fe Group: younger alluvium under the Rio Grande floodplain (Qaya_fp); Rio Grande terrace deposits (Qtr); axial-river facies of the Sierra Ladrones Formation (QTsa); medial-proximal piedmont facies of the Sierra Ladrones Formation (QTsp); distal piedmont and its transition with the axial facies (Sierra Ladrones Formation, QTst); Rio Puerco Member of the Ceja Formation (QTcr);

and Atrisco Member of the Ceja Formation (Tca). Table 5 provides detailed subsurface information germane to these wireline analyses, including the depth ranges inspected in each well. Note that the proportions of sand, muddy sand, and clay were only differentiated in the unsaturated zone and the upper ~500 ft of the underlying saturated zone.

Storage-zone thickness is defined as the thickness of permeable sediment between impermeable layers (Figs. 12, 17). For our study, we defined impermeable layers as clay beds, which were inferred from resistivity curves (Table 5, Fig. 17). Permeable sediment includes sand, gravelly sand, and clayey or silty sand. In some wells, strata deeper than intervals used to determine textural proportions were still analyzed for storage-zone thicknesses; corresponding depths are shown in Table 5.

Although supplemented by gamma ray and neutron curves, our lithologic interpretations were primarily made using resistivity curves. The types of resistivity curves are listed in Table 5. We usually used induction curves, but other types of resistivity curves were more useful for some cases: resistivity 16" normal curves were used for two wells, a microlog for one, and the microinverse of 2" resistivity for another (Table 5). For the chosen type of resistivity curve, we defined a “shale baseline” from which to select a relatively narrow range of low resistivity values (ohms-m) we deemed to represent clay (Fig. 17). Clayey sand was determined from intermediately low values. Higher ranges of resistivity values indicated

Figure 17 (next page). Santa Fe Fairgrounds monitoring well in the City of Santa Fe, New Mexico, illustrating how resistivity curves were used to assess lithologic textures—the proportions of clay, clayey sand, and sand—in the Santa Fe Group. This well is used here for demonstration purposes because of ready availability of digital data, although we did not use this well in our study. The 16-inch Normal Resistivity (R16) is utilized in this example because it corresponds well with picks using Gamma Ray (GR). Right deflections in the resistivity curve (i.e., increasing resistivity) are referred to as “peaks” and left deflections (i.e., decreasing resistivity) as “troughs.” The red dotted lines demarcate the respective ranges in resistivity values that correspond to the three lithologic textures. Low resistivity values near the shale baseline, corresponding to leftmost troughs, are interpreted as clay. Intermediary leftward curve deflections (troughs) are inferred to represent clayey sand, and right-deflections (peaks) were assigned as sand. The specific (range of) resistivity values corresponding to inferred clay, clayey sand, and sand are unique to each of the 17 wells studied for Albuquerque. Other data were used to place boundaries of textures as necessary. Annotations on the right denote storage-zone thickness.

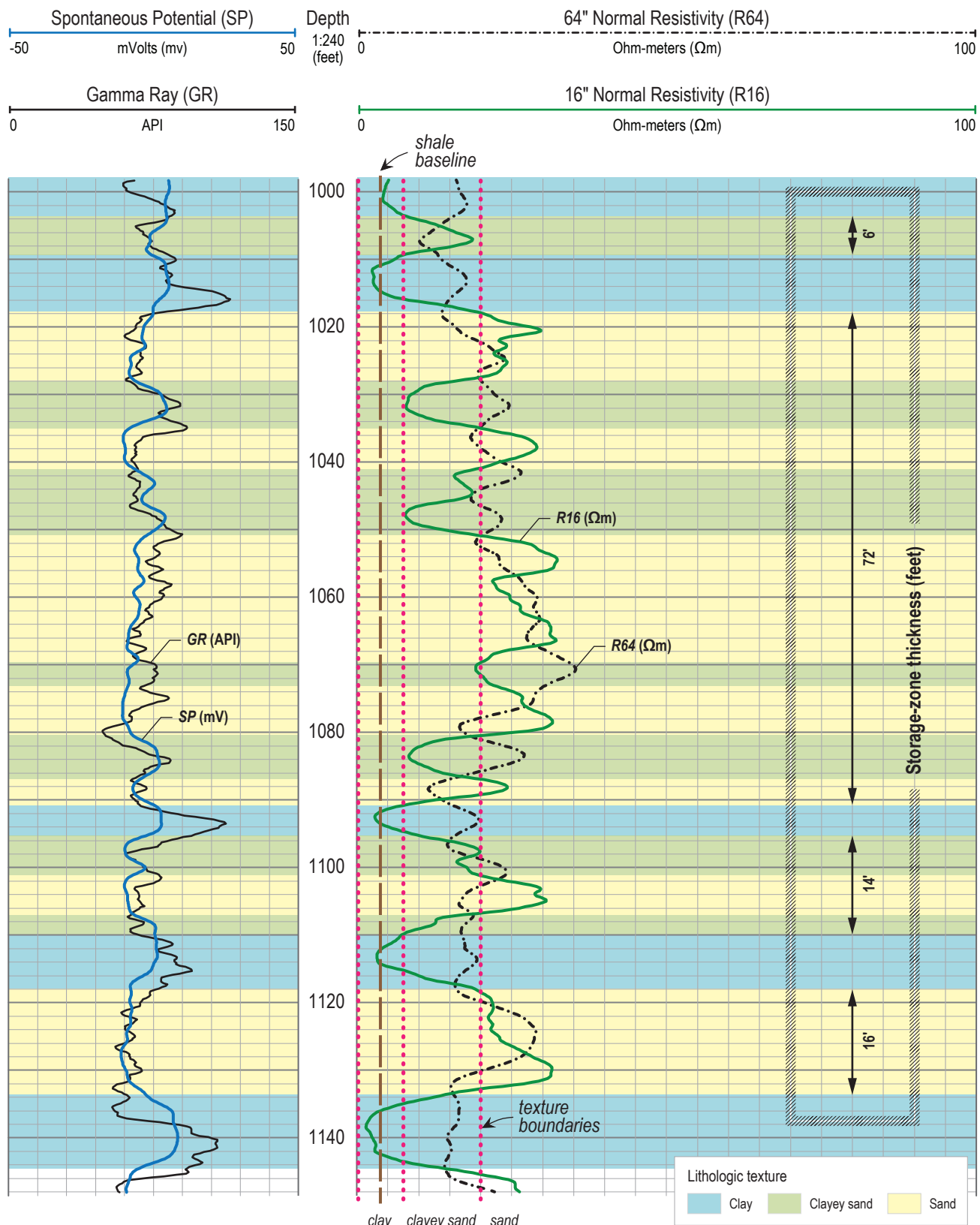


Table 5. Wireline log analyses for sand, clayey sand, and clay intervals.

Well	Depth interval (feet)	Geologic unit	%sand/ %clayey sand/ %clay	Storage- zone thickness only	RESISTIVITY			
					Curve type	Depth (feet)	Clay (ohm-m)	Clayey sand-silt (ohm-m)
ASR-1	0–148	Qtr	7/30/63	16" Normal	0–138	8–18	18–30	>30
	148–650	QTsa	10/14/75		138–650	8–20	20–30	>30
Bursum-1	124–599	QTsa	6/28/66	Microlog		4–8	8–16	>16
Bursum-5	50–192	QTsp	6/13/80	Induction	50–251	<22	22–26	>26
	192–251	QTst	22/75/3	Induction	251–747		22–27	>27
	251–747	QTsa	10/32/58					
Charles-5	100–668	QTsa	8/22/71	Medium Induction (ILM)	100–350	<40	40–70	>70
	2,020–2,855	Tca			350–668	<30	30–40	>40
	2,855–3,215	Tsm		Yes				
Miles-1	53–404	QTcr	20/22/58	Induction	53–175	<25	25–50	>50
	404–1,198	QTcr		Yes	175–404	0–15	15–30	>30
	1,198–1,342	Tca	88/X/12	Yes				
Ponderosa-1a	70–100	Qao	0/7/93	Induction	70–610	<20	20–50	>50
	100–497	QTsp	0/23/77					
Ponderosa-4	105–562	QTsp	1/42/57	16" Normal		0–15	15–40	>40
	562–649	QTst	85/5/10					
San Jose-2	30–115	Qaya_fp	27/6/67	Induction	30–115	0–25	25–40	>40
	115–528	QTcr	26/38/36	Induction	115–1,008	0–15	15–30	>30
	528–814	QTcr		Yes				
	821–1,008	Tca		Yes				
Santa Barbara-1	116–119	Qtr	16/40/44	40" Induction	116–183	0–25	25–45	>45
	119–724	QTsa	11/44/45	40" Induction	183–1,001	0–15	15–30	>30
	660–1,001	QTsa		Yes				
Thomas-1	84–224	Qao	0/13/87	Microinverse 2" Resistivity	84–1,023	≤4	4–8	>8
	224–311	QTsp	3/28/69					
	311–339	QTst	0/11/89					
Volandria-3	339–1,023	QTsa	1/23/76					
	14–58	Qao	0/77/23	Induction		0–25	25–40	>40
	58–671	QTsa	9/32/59					
Walker-1	680–1,006	QTsa		Yes				
	110–608	QTsp	5/52/43	Deep Induction	110–431	0–25	25–56	>56
				Deep Induction	431–608	0–15	15–30	>30
Walker-2	90–144	Qao	0/70/30	Deep Induction (RILD)	90–1,095	≤30	30–60	>60
	144–455	QTsp	10/52/38					
	455–485	QTst	54/46/0					
Webster-1	806–1,095	QTsa	13/1/45					
	110–276	QTsp	24/38/38	40" Induction	110–478	0–30	30–60	>60
	276–350	QTst	37/53/11	40" Induction	478–700	0–30	30–55	>55
Webster-2	350–958	QTsa	16/31/54	40" Induction	700–958	0–25	25–50	>50
	126–219	QTsp	2/11/87	Deep Induction (RILD)	126–450	≤10	10–60	>60
	219–279	QTst	41/38/21	Deep Induction (RILD)	450–850	≤10	10–30	>30
Yale-3	279–850	QTsa	10/14/76					
	56–131	Qtr	11/41/48	40" Induction		<10	10–20	>20
	131–733	QTsa	14/54/32					
	712–964	QTsa		Yes				

VI. MAPPING MANAGED AQUIFER RECHARGE SUITABILITY

Weighted Overlay Analyses

The procedure for weighted overlay analyses is illustrated in Figure 18. The study area was subdivided into a grid corresponding to that of the geologic model (see above), in which each cell is 100x100 m. Each category of criteria was binned and scored (rated) on an integer scale of 0 to 2, with 0 being the least favorable for MAR and 2 being the most favorable. For criteria that vary for a geologic unit (e.g., transmissivity, storage-zone thickness), the score for each unit was weighted for thickness, summed, then normalized to between 0 and 2 at each cell, producing a single (sometimes non-integer) score for each criterion (as illustrated in Figure 19).

These criterion scores were weighted (using values of 0, 1, 2, and 3, as determined by consultation with the ABCWUA), and the weighted scores were summed and normalized to a scale of 0 to 2 (with 0 being the least suitable to MAR and 2 being most suitable) (Figs. 18–19). We compared the overall ratings to previous maps of known or hypothesized locations suitable for MAR and used histogram analyses to translate the scores into three qualitative MAR suitability ratings of low, moderate, and high suitability.

Exclusionary (Unsuitable) Buffers

We designated three types of exclusionary buffers, where we *a priori* deemed the area to be “unsuitable” for MAR projects (Fig. 20). This is an additional qualitative suitability rating. The first type of exclusionary buffer incorporates known groundwater-contamination sites. The ABCWUA provided the corresponding GIS polygons. The second type of exclusionary buffer encompasses the modern floodplain of the Rio Grande. This buffer was recommended by the ABCWUA to address concerns regarding the potential flow of inputted MAR water back to the Rio Grande and of groundwater mounding in areas with shallow water

tables (<140 ft, <43 m). Another type of exclusionary buffer extends 500 ft (152 m) from both sides of a dipping fault zone. The resulting three-dimensional feature in the subsurface was projected to the land surface, resulting in a two-dimensional polygon. On maps, this buffer only extends for 500 ft (152 m) onto the footwall but much further in the hanging wall (on account of the fault dip). The exclusionary buffers around faults were only applied to the deep-injection suitability map (Fig. 20A). In contrast, faults in dry sand in unsaturated zones may actually enhance recharge (Sigda and Wilson, 2003). For example, the fault in the Bear Canyon Arroyo does not hamper shallow-based recharge efforts of that project (Daniel B. Stephens and Associates, 2010), so the fault-related exclusionary zones are not shown in shallow-based recharge suitability maps (e.g., Fig. 20B).

Estimating Susceptibility to Soil Hydrocompaction

Soil hydrocompaction results from the combined wetting and loading of a surficial deposit. Naturally, this is a gradual process (hundreds to thousands of years), and it is rare in the arid southwestern U.S. Soil hydrocompaction can happen suddenly (days to months) if human activity causes rapid infiltration of unnaturally high volumes of water, such as from the diversion of rainwater in populated areas.

The challenge of mapping the susceptibility of surficial sediment to hydrocompaction is that quantitative estimates require exhaustive and expensive geotechnical sampling. We instead evaluate the general hazard in the study area based on overlay analysis of correlative factors (see Lutteneger and Saber, 1988; Momeni et al., 2012). Recent, dry and well-drained, clay-rich sediment that was rapidly deposited is of primary concern (Momeni et al., 2012). The collapse potential study by Momeni et al. (2012) was done in a semi-arid climate similar to Albuquerque. Momeni et al. (2012) found that the age and type of deposit, including the grain-size

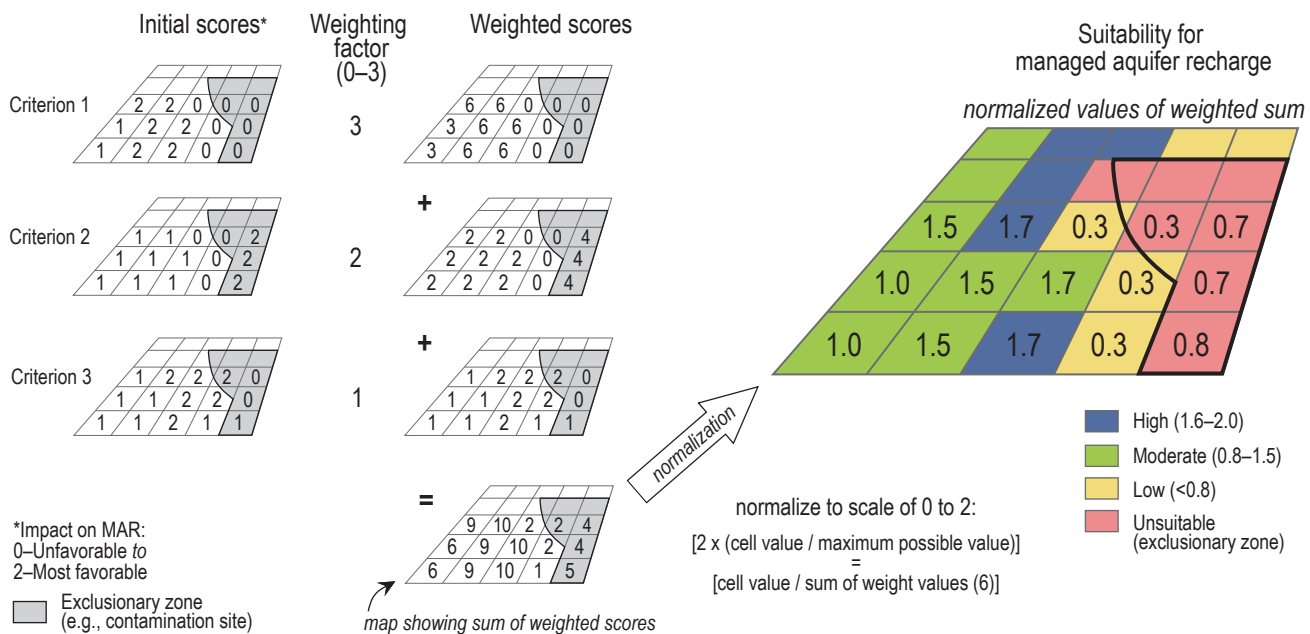


Figure 18. Illustration of the weighted overlay method used in this study, showing generic criteria (labeled Criterion 1–3) and their corresponding GIS raster maps. Each criterion is initially scored for its impact on MAR on a scale of 0 to 2, with 0 the least favorable and 2 having the most positive effect. Each criterion is then multiplied by a weighting factor (0 to 3 based on group consensus of staff at the New Mexico Bureau of Geology and Mineral Resources and the Albuquerque Bernalillo County Water Utility Authority). Weighted scores are summed and normalized to a scale of 0 to 2. The process also calculates values for buffered (exclusionary) zones, but such areas are *a priori* identified as unsuitable. (Scoring and qualitative ratings in this figure are schematic).

distribution, and the degree of saturation were the main controls on the formation of collapsible soil.

Characterization of soils is important in assessing hydrocompaction susceptibility. As an example using soil texture, sandy soils are less susceptible and loamy soils more susceptible (Momeni et al., 2012). Data for important factors like age, texture, paleodepositional environment, climate, and parent material can be derived from soil taxonomy (Soil Survey Staff, 1992) and soil texture reported as part of soil map units (Soil Survey Staff, 2014).

Another important criterion is depth-to-groundwater. The deeper the water table, the less likely a soil is to have been entirely saturated in the past, increasing the likelihood of future hydrocompaction. We follow Rinehart et al. (2017) for setting susceptibility thresholds based on recent water levels. Rinehart et al. (2017) used engineering knowledge of how likely previous water tables were near the surface. The assessment was based on a statewide review of tens of thousands of hydrographs (reflecting recent water levels), as well as geologically inferred estimates of groundwater-level variations in the historical past and the Holocene (using spring

deposits, phreatic cementation, liquefaction features, and erosional history).

We mapped soil-hydrocompaction susceptibility for Albuquerque using a weighted overlay method with the following criteria: age and depositional environment associated with surficial units mapped by Connell (2008b); soil type, using soil taxonomic order, suborder, and great group, and soil texture, all of which are mapped (Soil Survey Staff, 2014); and depth-to-groundwater as a proxy for the degree of saturation (refer to Powell and McKean, 2014). For each criterion, we assigned each map grid cell a quality (or weighting) factor (of 0–10) and a susceptibility value (ranging from 1 to 4, with higher values indicating higher susceptibility), based on Rogers (1995), Momeni et al. (2012), and Rinehart et al. (2017). For full discussion of susceptibility assignment, see Rinehart et al. (2017).

The Quaternary map units of Connell (2008b) reflect landform, deposit age, sorting, and depositional environment, all of which can be used to estimate susceptibility based on the fuzzy weightings of Momeni et al. (2012). We assigned hydrocompaction susceptibilities to the Quaternary

map units (polygons) of Connell (2008a) by comparing their lithologic properties with the landform map of New Mexico (Hawley et al., 2005) (refer to Rinehart et al., 2017, for more detail). Consistent with the framework of Hawley et al. (2005) and Momeni et al (2012), uppermost Pleistocene to historical-age units of poorly sorted sediment were assigned the highest susceptibility; older, better sorted, non-alluvial units were assigned lower susceptibilities. Because the map units directly reflect age and depositional environment, two of the strongest correlative factors (Momeni et al., 2012), we assigned the highest quality (weighting) to this layer (10).

Susceptibilities using both geologic data (polygons from Connell, 2008b) and soil type and texture (10x10 m grid, Soil Survey Staff, 2014) were initially estimated in the original format and scale. Because layers used in the overlay analysis of hydrocompaction susceptibility were originally mapped in different formats, we resampled them to the same, coarse grid (i.e., 100x100 m) used elsewhere in this study using the majority value in the grid cell. Depth-to-groundwater was estimated from the land-surface elevation DEM and water-elevation contours constructed in earlier parts of this study.

After all susceptibility layers were resampled, we calculated the weighted-average susceptibility at each grid cell following Rinehart et al. (2017). Because

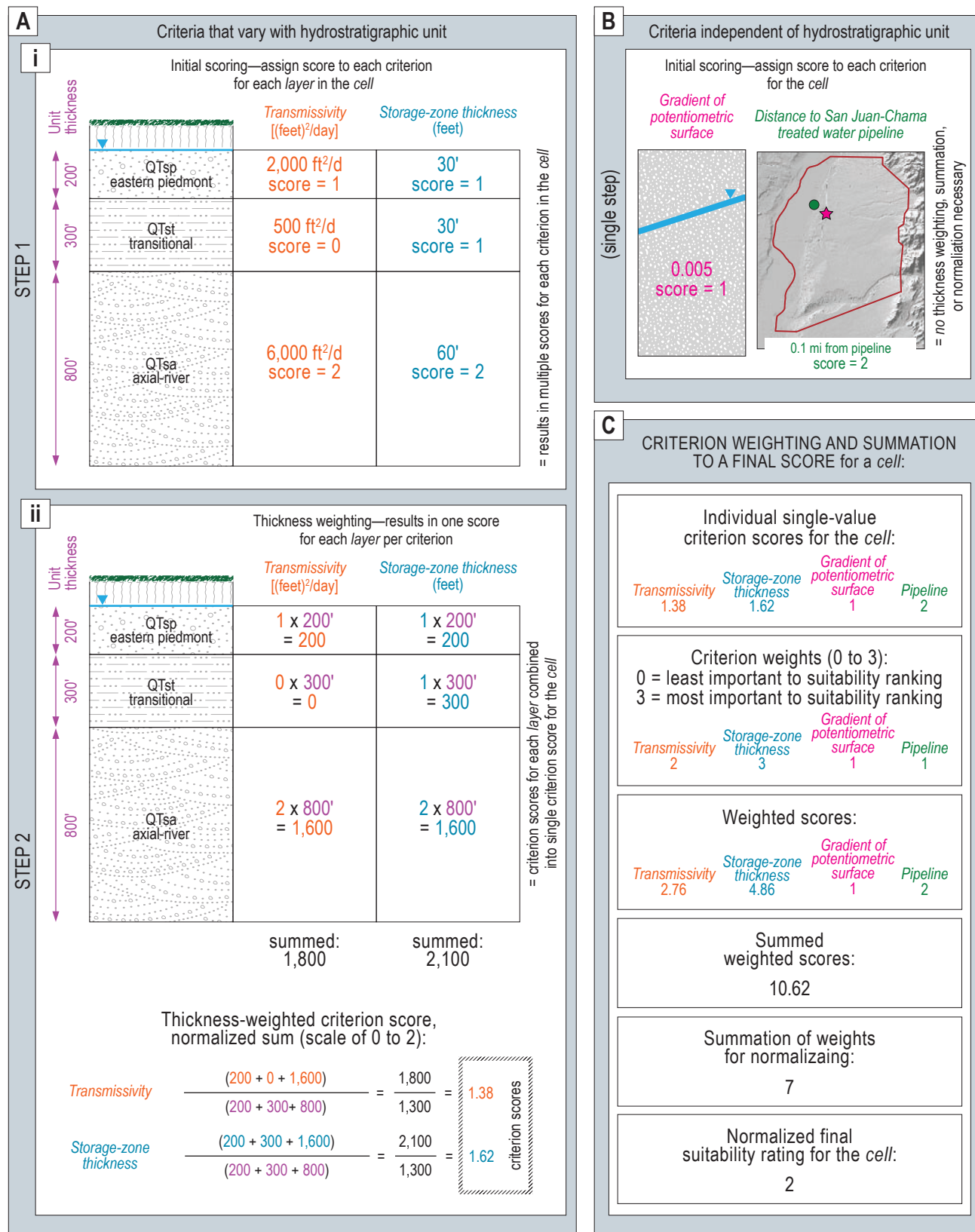
not all layers are present throughout the study area, the number of layers used to determine susceptibility is provided on a separate map (Plate 4). In Rinehart et al. (2017), the average weighting (quality) factor was also reported. In this study, however, the range of variation across map units was within one quality factor, too uniform to be informative (but it is available in Appendix 8).

It is vital to recognize the limitations of this method prior to planning projects. First, we used the method of Rinehart et al. (2017), which was developed for a scale of 1:500,000—as a general planning tool, not as an engineering estimate. It was verified by comparison with the distribution of known collapsible soils in New Mexico, several of which are located around the current study area. These locations, however, were only reported at the scale of 1:500,000, limiting their use in verifying our current analysis.

Like Rinehart et al. (2017), we are limited by the lack of geotechnical data to confirm our susceptibilities; thus, the weighted overlay method produces qualitative estimates of susceptibility rather than quantitative predictions. This implies that the hydrocompaction susceptibility maps (Plate 3) can be used for planning strategies but not in site-specific design. In areas mapped as highly to extremely susceptible, soils should be examined by a qualified engineer before site-specific design and construction.

Figure 19 (next page). Illustration of how the workflow differs between criteria using the geologic model versus criteria independent of the geologic model. **Panel A.** illustrates the process for two criteria used in the geologic model for deep-injection recharge, transmissivity and storage-zone thickness. These criteria must be thickness weighted. **Panel B.** instead shows two criteria that are independent of hydrostratigraphic unit, potentiometric-surface gradient and distance to water infrastructures (i.e., San Juan-Chama treated water pipelines), which do not need to be thickness weighted. **Panel C.** illustrates how all four criteria are treated for weighting, summation of weighted scores, and normalization to produce a final rating of between 0 and 2 for the grid cell.

Scoring of criteria



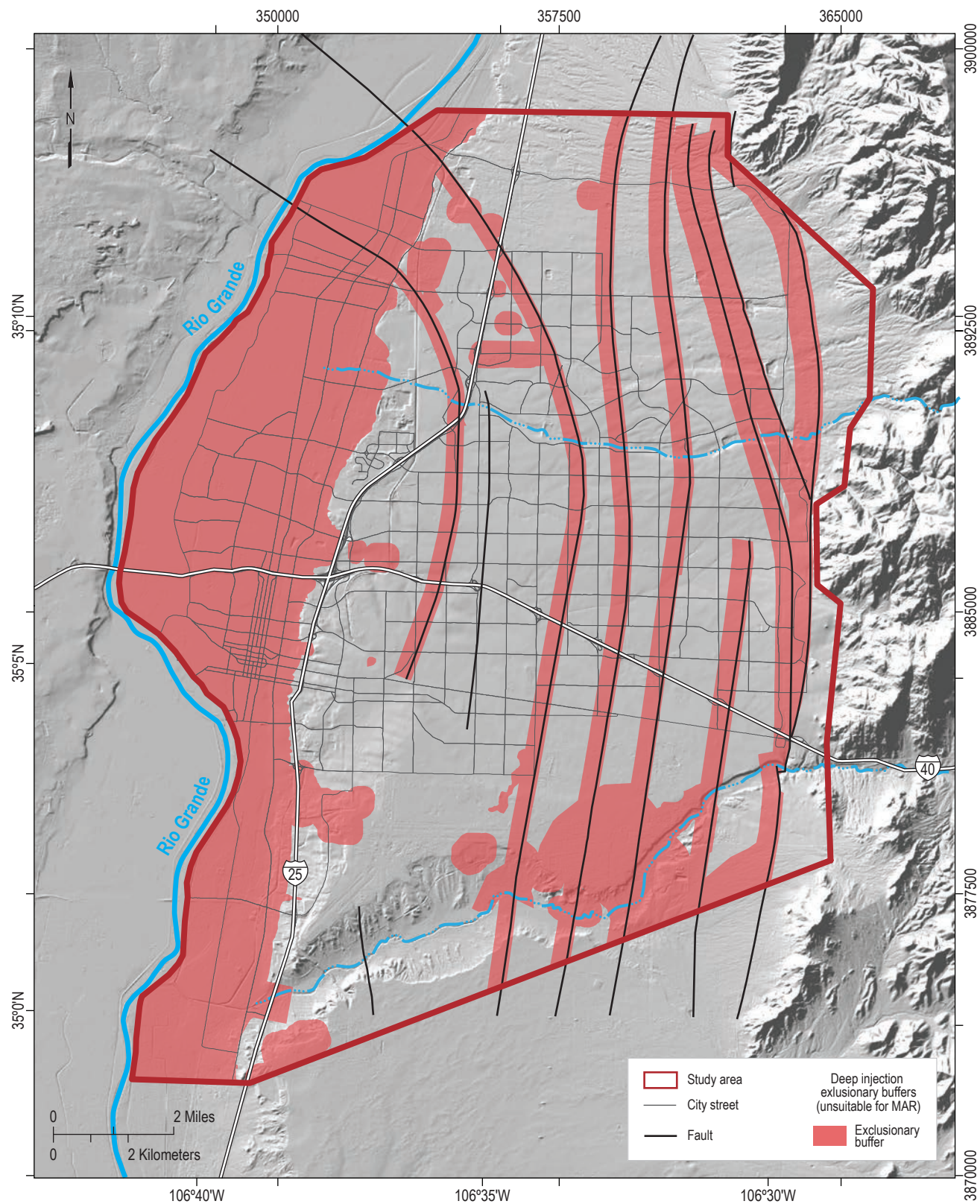


Figure 20. Exclusionary buffers (i.e., areas *a priori* identified as unsuitable for managed aquifer recharge, or MAR).

Figure 20A (above). Exclusionary buffers used in this study for deep-injection recharge. These buffers include known groundwater-contamination sites, the modern Rio Grande floodplain, and fault zones (500 ft on both sides of the dipping fault zone, projected upward to the land surface).

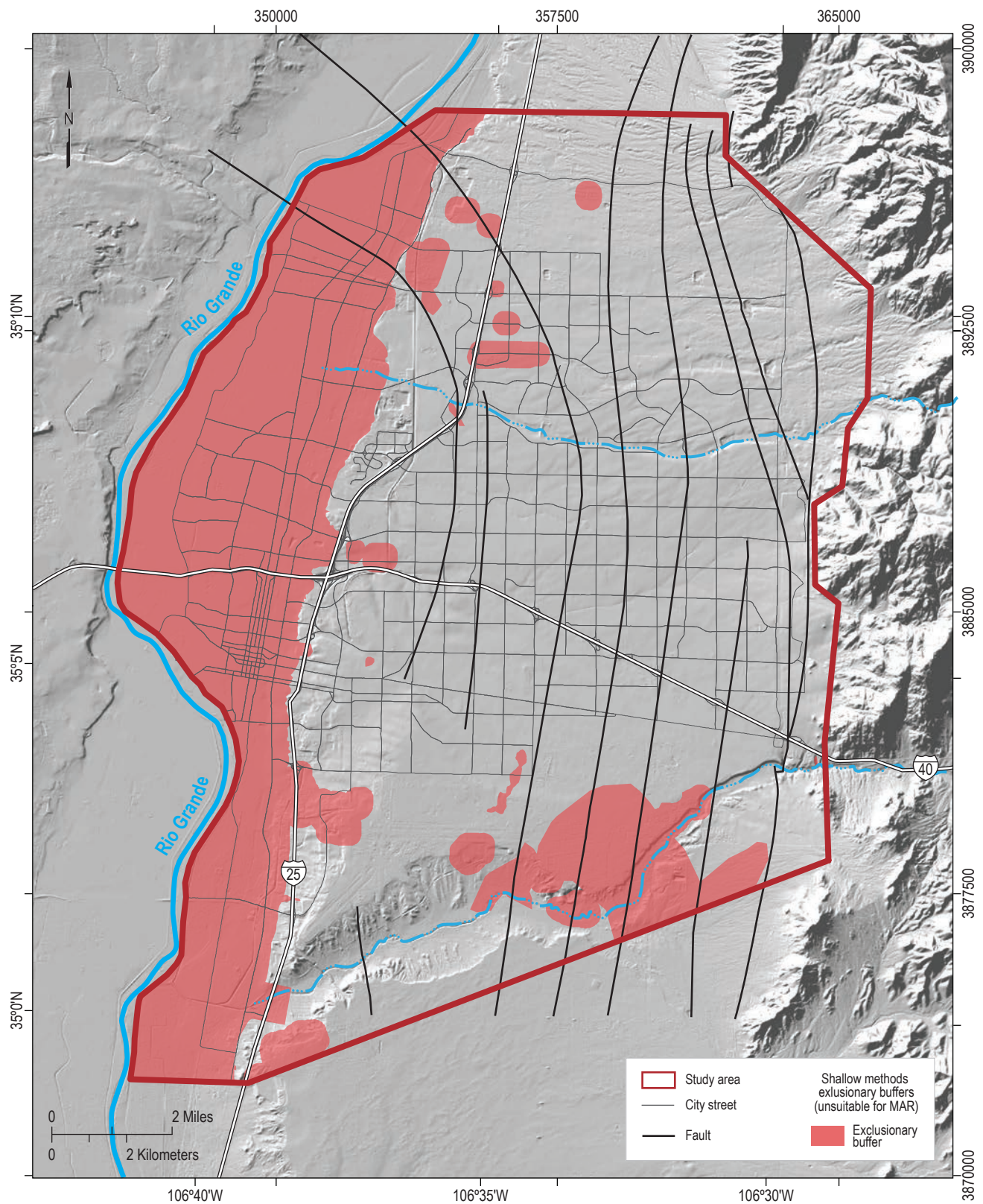


Figure 20—continued. Exclusionary buffers (i.e., areas *a priori* identified as unsuitable for managed aquifer recharge, or MAR).

Figure 20B (above). Exclusionary buffers used in this study for shallow-based recharge. These buffers include known groundwater-contamination sites and the modern Rio Grande floodplain.

VII. METHODS

This section explains the methods we used to map MAR suitability—for both deep-injection recharge and shallow-based recharge of aquifers—and for mapping the susceptibility of areas to soil hydrocompaction. We justify our choices of criteria, the classification of criteria for scoring (i.e., the binning of criteria for rank-based metrics), and how we scored each criterion.

Suitability for Deep-Injection Recharge

The workflow for mapping the suitability for deep-injection recharge is shown in Figure 21. Based on previous research on MAR, goals of the ABCWUA, and the subsurface geology of the study area, criteria for this study are organized into: geologic; adverse groundwater mounding; hydraulic properties; and water and well infrastructure.

Geologic criteria

Transmissivity and storage-zone thickness are the geologic criteria for evaluating suitability for deep-injection recharge. Most studies consider transmissivity a key parameter in assessing the potential success of recharge into an aquifer (e.g., Brown et al., 2005; Chowdhury et al., 2009; Nasiri et al., 2013; Gibson et al., 2018). In our study, it was calculated as the product of the hydraulic conductivity (compiled from pump tests, Appendix 2) and the saturated thickness of a hydrostratigraphic unit. To account for multiple hydrostratigraphic units within a given grid cell, we applied the thickness-weighting scheme shown in Figure 19. The greater the transmissivity of an aquifer unit, the more easily that injected water can move away from the source well and the less pressure needed in the well during injection (Brown, 2005). We modified the scoring of Brown et al. (2005) for this important metric: up to 1,000 ft²/d ranked as 0; 1,000 to 5,000 ft²/d ranked 1; and >5,000 ft²/d ranked 2 (Fig. 21).

To calculate storage-zone thicknesses, we used the same depth intervals for which the proportions of clay, clayey sand, and sand were assessed in the

aquifer and overlying vadose zone (see shallow-based MAR methods below). Because this metric is for the deep-injection map, however, we also investigated deeper sections for storage-zone thicknesses, as tabulated in Table 5. Results of the downhole wireline log investigation are given in Appendix 5. For a given hydrostratigraphic unit, permeable layers were sorted from thinnest to thickest to produce a cumulative distribution curve (fraction of the total on x-axis versus permeable thickness on y-axis). The permeable thickness at the 0.5 fraction was chosen as representative of that hydrostratigraphic unit (Fig. 22). The resulting storage-zone thicknesses are shown in Figure 23. We divided storage zones into three classes based on Brown (2005), in which a storage-zone thickness of: 0–25 ft is scored as 0; 25–50 ft scored 1; and >50 ft scored 2 (Fig. 21).

Summation of geologic unit scores

Transmissivity and storage-zone thickness vary depending on hydrostratigraphic units. For each pixel cell, a separate score was assigned to each criterion per hydrostratigraphic unit (layer) in the subsurface. Individual scores were aggregated into a singular rating for each cell using the following procedure (Fig. 19):

1. Each criterion score weighted by its respective thickness within the hydrostratigraphic unit;
2. Summation of resulting thickness-weighted scores of all criteria; and
3. Summed scores divided by the total saturated thickness to produce final normalized scores of 0 to 2.

Hydrostratigraphic units with <20 ft of saturated thickness were disregarded as minimally influential to the overall suitability of a location, and units or parts of units or units more than 1,500 ft bgs were excluded because these depths are greater than the interval of focus.

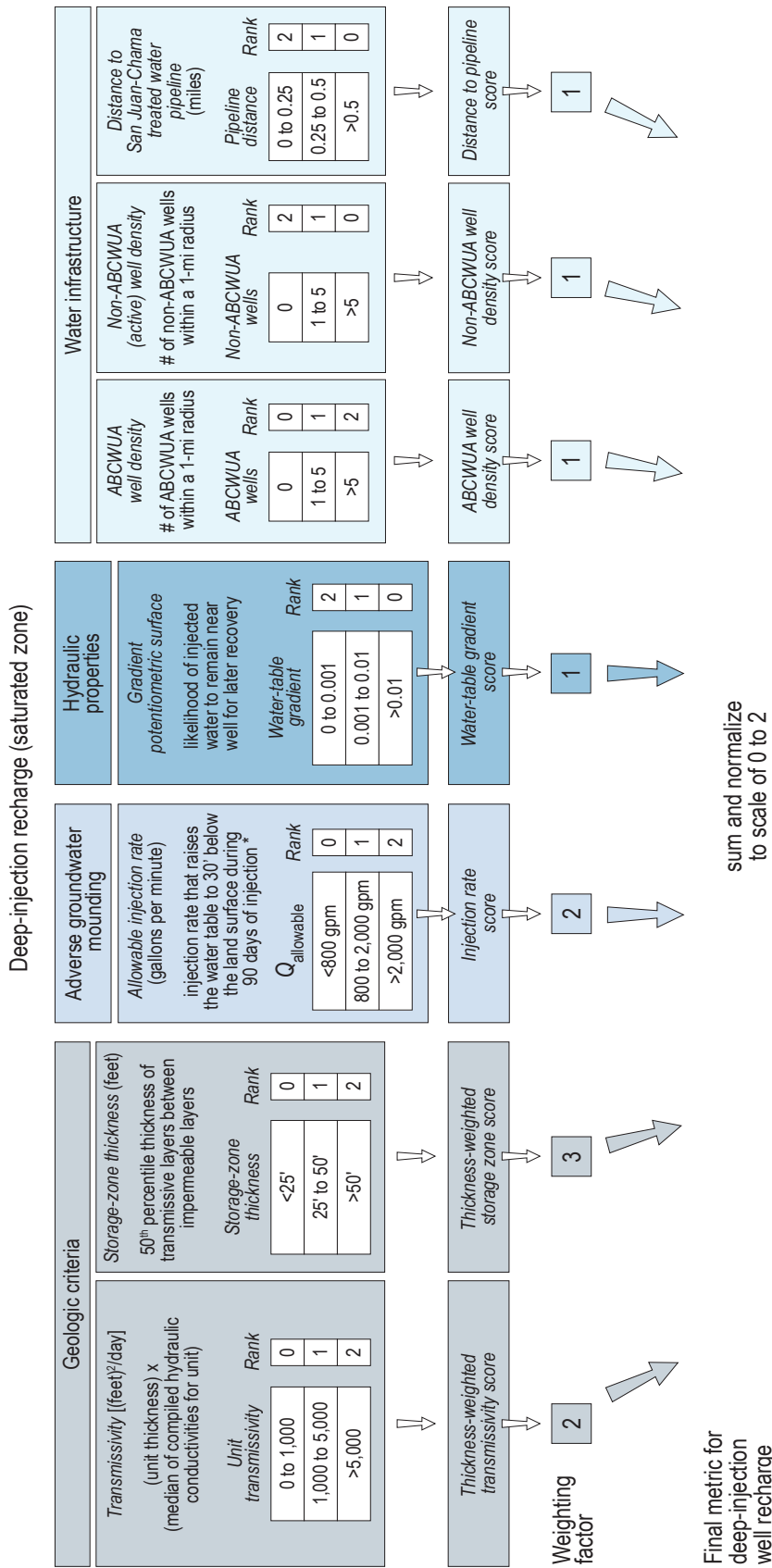


Figure 21. Flow chart for scoring and weighting criteria for deep-injection recharge. Criteria were grouped into four categories: geologic, adverse groundwater mounding, hydraulic properties, and water infrastructure. These criteria were subdivided into ranking classes and scored (0 being the least favorable, 2 being the most favorable; see text for more detail). Scores for criteria that vary with geologic unit were thickness-weighted, summed, and normalized at each grid cell location. A weighting factor was applied to each criterion (0 to 3 based on group consensus by the ABCWUA and NMBGMR). Values of weighting factors are shown in the next to last row. The weighted scores were then summed and normalized to a scale of 0 to 2.

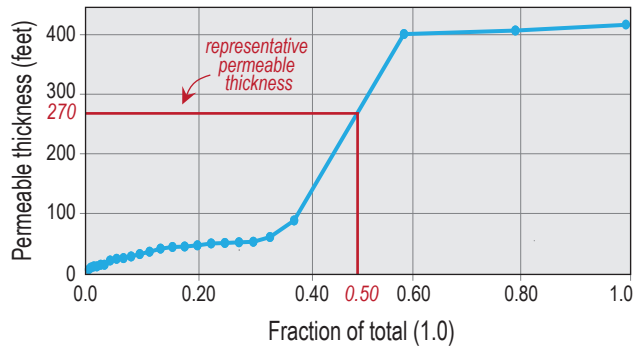


Figure 22. Depiction of how the storage-zone thickness of a hydrostratigraphic unit was determined, in this case the medial-proximal piedmont facies of the Sierra Ladrones Formation (QTsp). A storage zone is defined as the permeable interval, comprising sand and clayey sand, between layers of impermeable clay. The thicknesses of all permeable units were plotted from thinnest to thickest to create a cumulative distribution [with fraction of the total (1.0) on the x-axis and permeable thickness on y-axis]. For our analyses, we chose the 50th percentile (0.5 fraction value) of the cumulative distribution as representative of the storage-zone thickness for a given hydrostratigraphic unit.

Adverse groundwater mounding

Injection operations may be adversely affected if injection causes the local water table to rise too close to the land surface, due perhaps to already shallow groundwater or low transmissivity of the targeted hydrostratigraphic unit. The ABCWUA indicated that a facility will likely cease injection if the water table rises to within 30 ft (10 m) of the ground surface (personal commun., February, 2019). The amount that a groundwater rises is a function of many local variables, and it is beyond the scope of this project to thoroughly predict specific water-table rises for the study area. Given that mounding can inhibit the efficacy of MAR projects, however, the potential for mounding to restrict operations was roughly estimated.

Following Gibson et al. (2018), we used the Cooper-Jacob approximate solution to the Theis equation at large pumping times (Cooper and Jacob, 1946) to estimate the potential for groundwater mounding to restrict an injection operation. The Cooper-Jacob equation is commonly given as:

$$hw - h\theta = \frac{2.3Q}{4\pi T} \log \left[\frac{2.25Tt}{r^2S} \right]$$

where:
 hw = depth of water table at time t
 $h\theta$ = depth of static water level
 Q = injection rates (volume rate)
 T = transmissivity
 r = well radius
 S = storativity

We defined the allowable amount of groundwater rise to be that which brings the water table to a chosen buffer depth below the ground surface; following current operations, we set this buffer at 30 ft. To understand how groundwater mounding may inhibit operations, we set $hw - h\theta$ equal to the permissible amount of groundwater rise (i.e., up to 30 ft bgs) and rearranged the equation to estimate the corresponding allowable injection rate ($Q_{allowable}$) that would bring the water table no shallower than this buffer, given the hydraulic properties of an aquifer unit and a presumed duration of injection. That is:

$$Q_{allowable} = \frac{(DTW - 30) * 4\pi T}{2.3 * \log \left[\frac{2.25Tt}{r^2S} \right]}$$

where:
 $Q_{allowable}$ = allowable injection rate
 DTW = the local depth to groundwater

We again followed Gibson et al. (2018) in using an average well radius (r) of 7.75 in and injection period of 90 days, and we used their conservative estimate of 0.01 for storativity (S) for all units, as storativity data are unavailable for most hydrostratigraphic units in the study area (Appendix 2). The allowable injection rate was evaluated for each hydrostratigraphic unit at each cell location in the model area, using the transmissivity calculated for the unit at that location (i.e., the median hydraulic conductivity, listed in Table 2, multiplied by the unit thickness at the grid cell). To obtain a single value per grid cell, the results for each hydrostratigraphic unit were combined via a thickness-weighted averaging scheme. To translate allowable injection rates into scores, we considered that two projects in development in the study area are targeting injection rates of 2,000 to 2,500 gpm (Daniel B. Stephens and Associates, personal commun., January, 2019; ABCWUA, personal commun., February, 2019) and thus scored areas with allowable rates more than 2,000 gpm with a 2. We scored rates between 800 and

2,000 gpm with a 1, as Gibson et al. (2018) reported injection rates as low as~800 gpm in Washington state. Injection rates below 800 gpm were scored as 0.

We recognize that the Cooper-Jacob equation, as given, is only accurate for confined aquifers but not necessarily for the largely unconfined aquifers encountered in the study area. The formulation, however, concisely and explicitly relates the parameters of interest (depth-to-groundwater and allowable injection rate) to factors that are known or can be estimated without numerical methods. We further suggest that this method is conservative because confined aquifers (modeled by the Cooper-Jacob equation) typically show higher-magnitude hydraulic head responses to pumping or injection than unconfined aquifers. Experimental calculations using other equations for unconfined conditions nearly always yielded higher allowable injection rates as compared to the results from this method. Therefore, for identifying areas where shallow water tables or low transmissivity will potentially inhibit the efficacy of injection projects, we believe this method is beneficial.

Hydraulic properties

The regional gradient of the potentiometric surface (approximating the water table in the study area) conceptually reflects the propensity of injected water to stay near the injection well, which is ideal for aquifer storage and recovery (ASR) (Pyne, 1995). Steeper gradients translate to faster groundwater-flow velocities and gentler gradients to slower velocities. Thus, comparatively steep potentiometric-surface gradients can be viewed as unfavorable because the injected water is more likely to move further away from the injection well, compromising the effectiveness of its repurposed use later as an extraction well when the stored water is needed. Both Brown (2005) and Gibson et al. (2018) considered regional horizontal hydraulic gradients ≤ 0.01 to be most suitable for ASR. Following Gibson et al., 2018, we assigned regional gradients: of >0.01 a score of 0; intermediate gradients of 0.01 to 0.001 a score of 1; and gradients <0.001 as 2.

Water and well infrastructure

Two criteria relate to well density (Fig. 21). A higher density of non-ABCWUA wells near the injection well is considered detrimental. The injection or extraction of water could negatively impact third parties, or third parties could potentially withdraw

(pump) water rightfully belonging to the ABCWUA. In contrast, a high density of wells owned by the ABCWUA is favorable because the injected water has a better chance of being recovered by the ABCWUA. Thus, we established separate criteria for non-ABCWUA versus ABCWUA well density. The classification of each was based on the number of wells within a 1-mi radius of a pixel (per Brown et al., 2005, and Gibson et al., 2018). For non-ABCWUA wells: no wells within the 1-mi radius was scored as 2; 1 to 5 wells scored 1; and >5 wells scored 0. For ABCWUA-owned well density: >5 wells within the 1-mi radius was scored 2; 1 to 5 wells scored 1; and no wells scored as 0.

The ABCWUA requested that we also consider the distances of potential MAR sites to the San Juan-Chama treated water pipelines. Infrastructure costs are less if injection wells are installed nearer to existing pipelines (by minimizing the costs of new pipelines). Based on consultation with ABCWUA, we devised three classes for this criterion and scored them according to the distance (in miles) from the San Juan-Chama treated water pipeline: scored 2 for 0–0.25 mi; 1 for 0.25–0.5 mi; and scored 0 if >0.5 mi (Fig. 21).

Suitability for Shallow-Based Recharge

The workflow for mapping the suitability for shallow-based recharge is shown in Figure 24. Criteria can be organized as: surface characteristics; adverse groundwater mounding; and deep-geology considerations. We also incorporated three criteria from the deep-injection recharge assessment: transmissivity; storage-zone thickness; and gradient of the potentiometric surface. Below, we detail the criteria and how they were scored. See the preceding section for discussion of transmissivity, storage-zone thickness, and potentiometric-surface gradient.

Surface characteristics

Multiple soil and surficial characteristics were considered in the shallow-based recharge suitability analysis due to their potential to limit project efficiencies. These included: soil-profile average hydraulic conductivity; soil drainage class; Low profile conductivities and poorly drained soils may inhibit water percolation, and shallow-recharge projects could be restricted by resulting soil saturation. Topographic slope may impose limits to projects that do not modify the land surface, such

as arroyo-bottom recharge, because the added water would travel longer distances prior to complete infiltration. Steep slopes may also cause the recharge water to flow beyond the project site and impact downstream landowners. The Bear Canyon Recharge Demonstration Project, for example, adds water upstream of the Arroyo del Oso Golf Course, which must enter the vadose zone prior to reaching a golf cart crossing (A. Ewing, personal commun., January, 2019).

Soil saturated hydraulic conductivity—Soil-profile average hydraulic conductivities used in this study were derived from the Natural Resources Conservation Service (NRCS) Soil Survey Geographic Database (SSURGO) (Soil Survey Staff, 2018). Soils comprise stacked layers called horizons that have different properties (e.g., color, structure, clay or calcium carbonate content). A soil profile is a vertical representation of the stacked horizons found at a given location. A soil pedon is the smallest volume of soil that contains all horizons of a particular soil type. A soil map shows the spatial distribution of soil map units for a given area. A soil map unit, in turn, consists of one or more components that describe the properties of natural bodies of soils, or miscellaneous areas of nonsoil, in a particular landscape (Soil Science Division Staff, 2017). The SSURGO database provides estimated vertical hydraulic conductivities and thicknesses for typical soil profiles of each component of a soil map unit. We averaged the individual conductivities of soil horizons to a single soil-profile value by calculating the harmonic mean using the following equation (after Fisher et al., 2017):

$$K_{hm} = \frac{\sum d_i}{\sum \left(\frac{d_i}{K_i^G} \right)}$$

where:
 K_{hm} = the harmonic mean of the vertical hydraulic conductivity or the soil component
 d_i = the thickness of horizon
 K_i^G = the geometric mean of the conductivity provided for horizon i:

$$K_i^G = \begin{cases} \sqrt{K_{min} * K_{max}} & \text{if } K_{min}, K_{max} \text{ provided} \\ K_{typical} & \text{if } K_{min}, K_{max} \text{ unavailable} \end{cases}$$

where K_{min} , K_{max} , and $K_{typical}$ are the minimum, maximum, and typical vertical conductivity listed for each soil horizon in the soil components table. The harmonic mean was used instead of the arithmetic mean because the former emphasizes lower, limiting values (Fisher et al., 2017). Figure 25 shows the distribution of harmonic means for soil-saturated hydraulic conductivities of all soil components encountered in the study area. Along the left margin of the chart are those components with a negligible conductivities of <1 micrometers per second ($\mu\text{m/s}$), including soil map unit components comprising: shallow bedrock; ‘cut and fill’ areas, for which no conductivity values were provided; and clay and clay loams that strongly inhibit percolation. A pronounced gap is present between ~30 and 50 $\mu\text{m/s}$; values <30 $\mu\text{m/s}$ mostly are for soils with loam or loamy textures of various types, whereas >50 $\mu\text{m/s}$ are soils dominated by sand, loamy sand, and sandy loam textures. We utilized these natural breaks in the distribution of the harmonic mean conductivity to establish the following shallow-recharge suitability ratings: 0 to 1 $\mu\text{m/s}$ was rated as 0; 1 to 30 $\mu\text{m/s}$ rated as 1; and >30 $\mu\text{m/s}$ rated as 2 (Figs. 24–25).

Soil drainage class—Soil drainage class was also taken from the SSURGO soils map data (Soil Survey Staff, 2018), which provides drainage classes for most soil map unit components, with the exception of such features as bedrock, badlands, and ‘cut and fill’ land. Drainage classes are qualitative assessments of the capacity of a soil and its landscape position to allow water to percolate into the soil and, hence, permit assessment of the potential for an area to become swampy due to inadequate drainage during shallow-recharge operations.

Figure 26 shows the frequency of each drainage class among the soil map unit components present in the study area. The histogram illustrates that most soil components are well drained to excessively well drained, with subordinate components being somewhat poorly drained to poorly drained. Poorly to somewhat poorly drained soil components are mainly loamy soils along river valleys and floodplains, whereas better-drained classes are typically loams to sands occupying interfluves and upland areas. We rated “poorly drained” and “somewhat poorly drained” classes with a score of 1 and higher drainage classes (well drained through excessively drained) with a 2 (Fig. 24). Because map unit components with no specified drainage class are generally bedrock areas or areas with impervious surfaces (in the case of ‘cut and fill’ land), we rated those areas with a score of 0.

Summation of soil map unit component scores—Soil maps consist of soil map units. Some units are collective, in that they contain multiple soil map unit components. In these collective map units, the spatial distribution of components is not mapped, only the overall distribution (proportion) of the soil map units. For soil-profile hydraulic conductivity and soil drainage class, each map unit component received a score as described above, but the individual component scores needed to be aggregated into a single score for a collective map unit for use in the weighted overlay analysis. The SSURGO datatables provide the estimated percent abundance of the individual soil map unit components for the dominant soils within each collective soil map unit. This typically characterizes between 75 and 95% of the soil map unit, with the remaining 5 to 25% being minor components rarely included in the datatables. To aggregate component scores, we weighted each component by its percent abundance, summed the weighted score, then normalized this to between 0 and 2 by dividing the summed weighted score by the total percentage of the soil map unit that was characterized in the datatables. In this way, for a given soil map unit, we calculated a single abundance-weighted score for each soil drainage class and soil-profile hydraulic conductivity criteria.

Surface slope

Authors have incorporated surface slope into assessments of shallow-recharge suitability in several ways. Chowdhury et al. (2009) and Mahmoud et al. (2014) used slope as an independent variable, separately scored from other variables and incorporated into their suitability maps as they did for other weighted factors. Russo et al. (2015), however, only indirectly included slope as a variable in their equation for ‘effective infiltration capacity,’ alongside estimates of Manning’s roughness factor and an estimate of soil-infiltration capacity derived from soil type. Fisher et al. (2017), meanwhile, used slope as a filter, removing from final consideration all areas with slopes >10%, but they did not directly use slope in their initial calculations for suitability.

We incorporated slope as its own variable, similar to Chowdhury et al. (2009) and Mahmoud et al. (2014), as this minimizes the number of variables to estimate (versus adding Manning’s roughness factor and infiltration capacity). Also, the variability in topographic relief across this study area is less than of areas examined by Fisher et al (2017). We considered

the ratings used by Chowdhury et al. (2009) and Mahmoud et al. (2014), and additionally considered the limiting slope used by Fisher et al. (2017), to derive the following scoring: areas with slopes <5% were scored as a 2; areas with slopes between 5 and 10% were scored as 1; and areas with slopes >10% were scored a 0 (Fig. 24). Surface slope was calculated from the land surface digital elevation model (DEM) used in the 3D subsurface geologic model.

Adverse groundwater mounding

As with deep injection, focused shallow recharge has the potential to raise the local water table close enough to the land surface to impact drainage and cause oversaturation of soils, leading to swamping. Because this issue is not uncommon, particularly in areas where recharge impoundments are used to manage storm floodwaters, the USGS (Carleton, 2010) released a macro-enabled Microsoft Excel spreadsheet predicting the amount of water-table rise anticipated for a specified basin geometry, duration of recharge efforts, and hydraulic properties of the underlying aquifer. These estimates were based on a numerical solution to the Hantush equation (Hantush, 1967).

We used this spreadsheet to estimate the amount of water-table rise that may result under certain conditions plausible along the margins of the Rio Grande floodplain, where the water table is relatively shallow and mounding may be induced. The inputs for this were:

1. Recharge rate (rate at which injected water is added to the groundwater; excludes storage within and percolation rates through the vadose zone);
2. Horizontal saturated hydraulic conductivity of the aquifer zone (all flow is assumed horizontal and away from the mound);
3. Initial saturated thickness of the aquifer zone (changes in transmissivity with mound height are ignored);
4. Specific yield (S_y) of the aquifer;
5. Recharge duration (note that the spreadsheet only provides the maximum expected water-table rise following this length of time); and
6. Dimensions of the recharge basin (assumed rectangular).

We anticipate that groundwater mounding will only be an issue along the margins of the Rio Grande floodplain, and, hence, designed our mounding scenario using hydraulic properties that could characterize that area. The eastern part of the floodplain is generally underlain by some thickness of young alluvium (Qaya_{cs} or Qaya_{fp}) overlying the axial-river facies of the Sierra Ladrones Formation (QTsa) (Connell, 2008b). As an estimate for the saturated thickness through which a mound must dissipate, we chose 17 ft based on the expected storage-zone thickness for the floodplain unit (Qaya_{fp}, Fig. 23), and we used a posited horizontal conductivity of 63 ft/d for Qaya_{fp} (assuming it is similar to QTsa, Table 2). For recharge rate, we selected the larger constant-rate infiltration of 25 ft/d, which was determined by Daniel B. Stephens and Associates (2014) from an *in situ* falling head infiltration test at the Bear Canyon Recharge Demonstration Project site (Table 3). Due to the paucity of specific yield (Sy) data (Appendix 2), we chose a conservative value of 0.01. Finally, the duration of recharge was presumed 90 days and the dimensions of the recharge basin arbitrarily set to 100x100 ft (30x30 m). A physical setting where this scenario could be established would be an

arroyo-bottom recharge site that adds water to a modern channel filled with coarse gravel and inset into floodplain deposits, the latter being fine grained except for relatively thin, conductive sand bodies. Under these conditions, the predicted water-table rise is ~110 ft (~34 m).

Given that the ABCWUA currently plans to cease injection at their vadose-zone recharge sites if the water table rises to within 30 ft of the land surface (ABCWUA, personal commun., February, 2019), we incorporated an additional 30 ft of buffer for a total scoring-limit boundary of 140 ft (43 m) and recognized that areas with depth-to-groundwater already at or shallower than 30 ft bgs are even more concerning. Therefore, we used depth-to-groundwater to rate areas as follows: shallower than 30 ft bgs scored as 0; between 30 and 140 ft bgs as 1; and deeper than 140 ft bgs scored as 2 (Fig. 24)

Deep-geology considerations

A constraint of shallow (above the water table) MAR projects is that infiltrated or injected water must percolate vertically through the vadose zone before contributing to an aquifer. Flow through a vadose zone is complex. Fine-grained units interbedded with

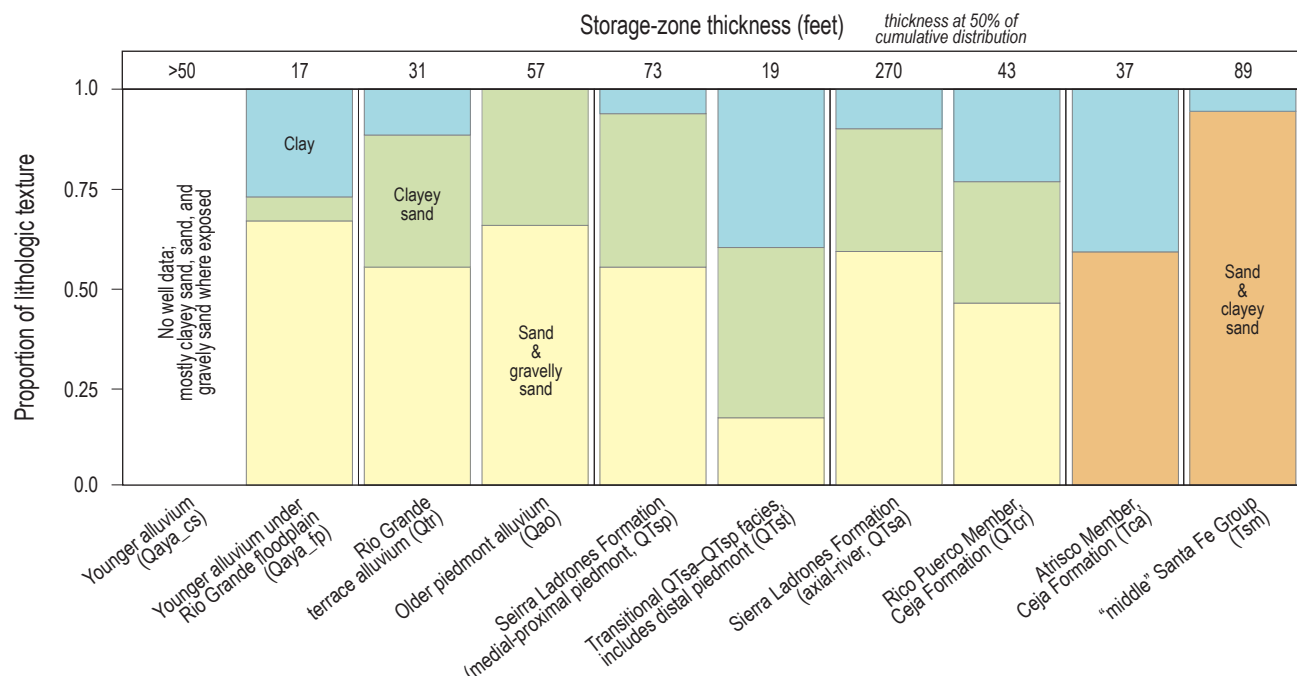


Figure 23. Lithologic textures for hydrostratigraphic units in the “middle” and upper parts of the Santa Fe Group and younger deposits. The proportion of sand (and gravelly sand), clayey sand, and clay were determined using well data (see example in Fig. 17). Note that sand and clayey sand textures are combined for the Atrisco Member of the Ceja Formation (Tca) and the “middle” Santa Fe Group (Tsm).

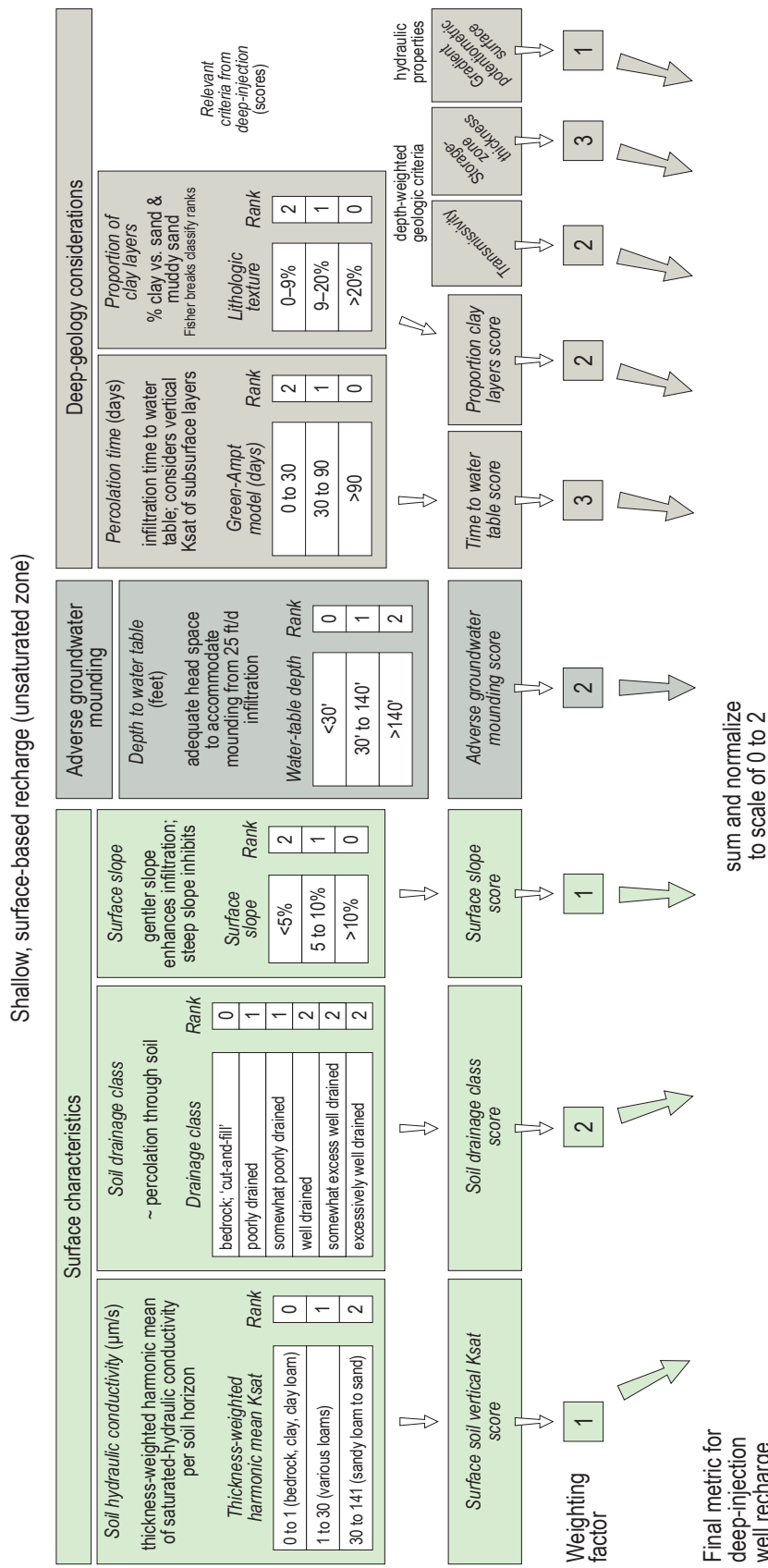
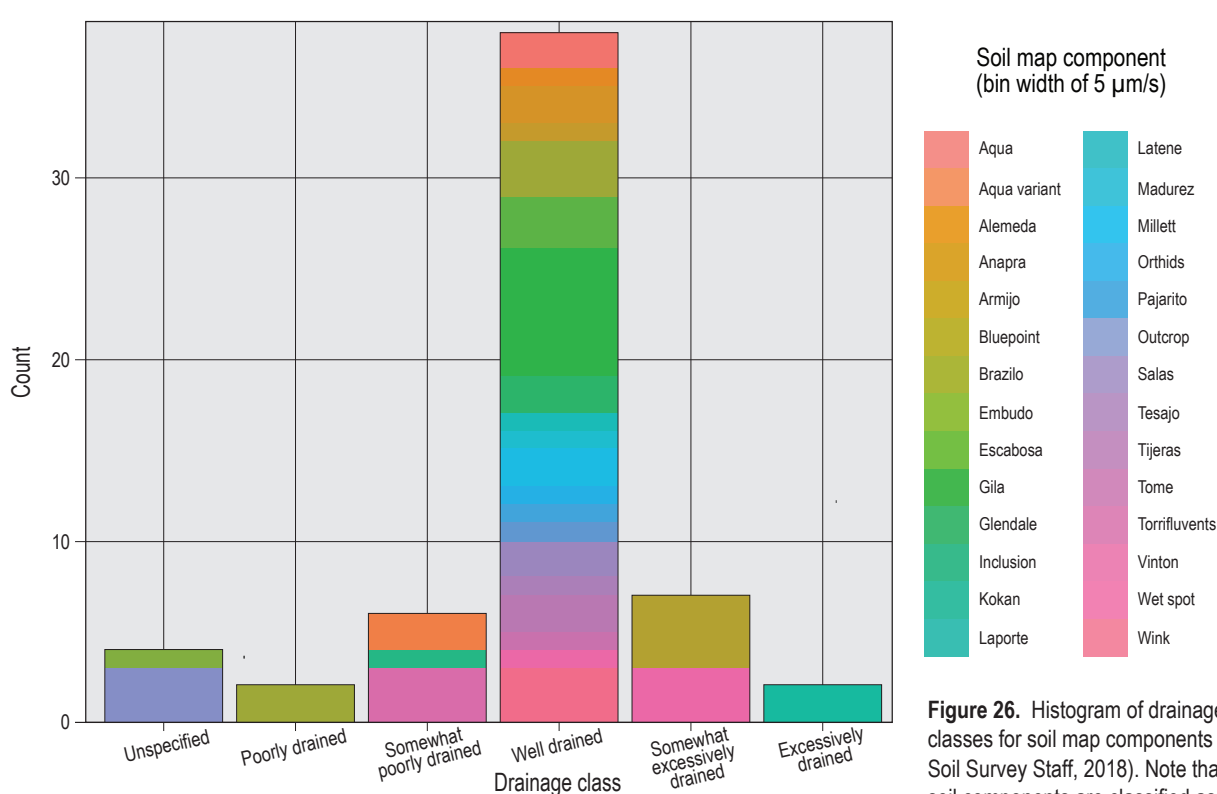
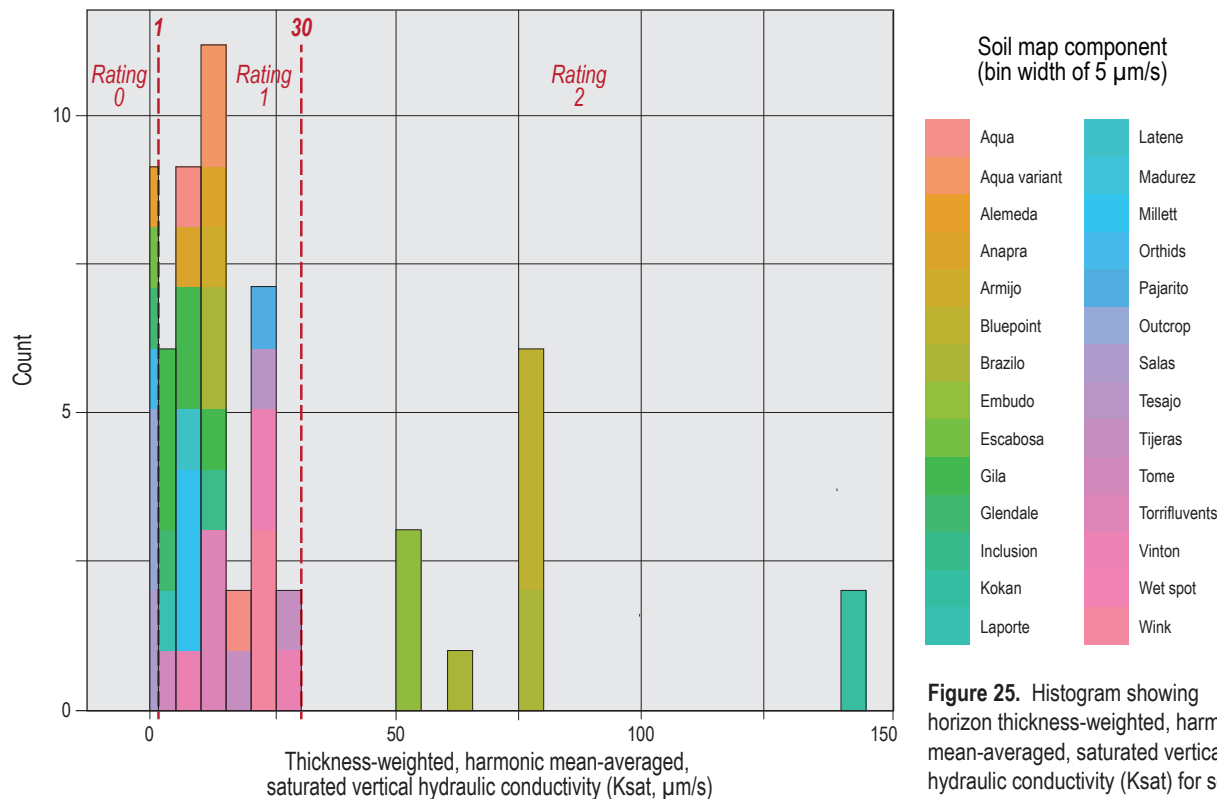


Figure 24. Flow chart for scoring and weighting criteria for shallow-based recharge. Criteria were grouped into three categories: surface characteristics; adverse groundwater mounding, and deep-geology considerations. These criteria were subdivided into ranking classes and scored (0 being the most favorable; 2 being the least favorable; see text for more detail). We also considered the scores of three criteria from deep-injection recharge that were calculated for grid cells: thickness-weighted transmissivity, thickness-weighted storage zone thickness, and porosity gradient. A weighting factor was then applied to each criterion (0 to 3 based on group consensus by the ABCWUA and NMBGMR). Values of weighting factors are shown in the next to last row. The weighted scores were summed and normalized to a scale of 0 to 2.



coarse-grained layers can cause significant barriers to percolation, whereas the development of dynamic preferential flow paths can result in rapid percolation. We approximated the capacity of a location to permit effective recharge to a groundwater aquifer through the vadose zone by: (1) estimating the amount of time it takes for percolating water to reach the water table from the surface through the geologic layers at and above the water table; (2) evaluating the abundance of fine-grained sediment in the vadose zone that could impede downward percolation.

Percolation time—Estimated percolation time incorporates the amount of time for a wetting front to pass through each geologic unit in the unsaturated zone at each raster cell location and the summation of individual breakthrough times. Breakthrough times were estimated by dividing the unsaturated thickness of each unit by an average velocity of the wetting front calculated from a derivative property of the Philip (1957) infiltration model at long infiltration times (Jury and Horton, 2004):

$$Vf = \frac{K(\theta_0) - K(\theta_i)}{(\theta_0) - (\theta_i)}$$

where: Vf = the velocity of the wetting front
 $K(\theta_0)$ = the (vertical) hydraulic conductivity at the surface water content
 $K(\theta_i)$ = the (vertical) hydraulic conductivity at the initial water content
 θ_0 = the surface soil water content
 θ_i = the initial water content

We assumed that at long infiltration times, the surface soil water content equals the saturated soil water content (i.e., the actual quantity of water in the surface soil is the maximum amount of water that the soil can store), and, hence, $K(\theta_0)$ is the vertical saturated hydraulic conductivity. We further assumed that the initial water content equals the field capacity water content as approximated by the water content at one-third a bar of pressure head. Because information regarding the water content of the geologic units was not available, we estimated these properties by assigning representative soil texture classes to each (Table 4). We applied the typical hydraulic properties for the texture classes from the datatables in Williams et al. (1998; specifically, their table 11, originally in Rawls et al., 1992). To assign a

vertical saturated hydraulic conductivity value to each of our hydrostratigraphic units, we compared vertical conductivities determined from projects having infiltration or percolation data from within the study area (Table 4). We used lithologic similarities among the hydrostratigraphic units to assign values to those for which there are no direct estimates of vertical hydraulic conductivity (Table 4). Finally, we assumed that $K(0i)$ was 0 for the purpose of assigning ratings. Based on guidance from the ABCWUA (personal commun., February, 2019), we assigned all cells with percolation times shorter than 30 days a score of 2; times between 30 and 90 days as 1; and times >90 days with 0 (Fig. 24).

Proportion of clay layers—We inductively postulated that impermeable subsurface layers, such as clay or well-cemented units, could inhibit infiltration from the surface to an aquifer. It was difficult to identify well-cemented layers only using wireline logs. We thus focused our efforts on the proportion of clay using interpretations of 17 wireline logs in the Albuquerque area. How these logs were interpreted was discussed earlier and is illustrated in Figure 17. Data are compiled in Appendix 5. Clustering of the data was evaluated by Fisher natural breaks classification (i.e., using the classIntervals function from the classInt package for the R statistical computing language), which indicated that three groupings of the data best corresponded to 0–9%, 9–20%, and >20% proportion of clay. We scored 0–9% as a 2; 9–20% as 1; and >20% as 0 (Fig. 24).

Soil-Hydrocompaction Susceptibility Map

This method mostly followed Rinehart et al. (2017). As described above, we used a weighted overlay method in ArcGIS, which is a spatial weighted average of correlative susceptibility factors. These factors included: for each soil map unit, the majority pedon soil taxonomic classification (which reflects the environment and age of the soil; we used order to great group); soil texture from Soil Survey (2014) sources; depth-to-groundwater (derived from the water-elevation contours presented in this report); and the geologic map units of Connell (2008b). For each layer, a quality factor of 0 to 10 was assigned, with 10 being the highest quality. These quality factors indicate the degree of confidence and relative importance of each correlative factor to the hydrocompaction of soil. Similar to susceptibilities of individual units, these quality factors were decided

by: (1) iterative comparison of total estimated susceptibility (i.e., the quality-weighted average of susceptibility) to total susceptibilities within a 500-m radius around a subset of known hydrocompactive soil locales in the state (Rinehart et al., 2017); (2) by the fuzzy-logic weightings developed by Momeni et al. (2012) from the correlation of indirect proxies to direct engineering measurements in a similar arid-basin environment. Some layers, however, were more challenging to assign than others and required engineering judgment.

The susceptibilities and weighting of quality factors, described below, were based on soil taxonomy and soil texture of map unit pedons as described in Rinehart et al. (2017) using the gSSURGO dataset, which was mapped at a scale of 1:30,000 (Soil Survey Staff, 2014). Taxonomic classifications reflecting youth, aridity, and relatively high clay content (in a mixture of sand and clay) were assigned higher susceptibilities. Taxonomic classifications of older units indicating humid conditions and lower clay content (in a mixture of sand and clay) were assigned lower susceptibilities. Quality (or weighting) factors of 8, 7, and 6 were given to the order, suborder, and great-group classification levels, respectively. Soil texture was determined for the bottom one-third of each pedon of a map unit component. This was to focus on non-pedogenically altered material within the profile. Each pedon was assigned a susceptibility from texture thresholds in Rinehart et al. (2017). A frequency of susceptibility was determined by accounting for the areal frequency of each component within a map unit, and the 0.9 percentile of soil texture susceptibility was applied to the entire map unit. This prevents a rare but extremely susceptible component from overwhelming the rating of an entire unit (Rinehart et al., 2017). Soil texture was assigned a quality of 7. The shallower a water table, the more likely the overlying sediment has been saturated in the past, leading to the collapse of the pore space of hydrocompactive soils. Natural fluctuations of deeper water tables are more likely to leave upper, dry parts of the sediment column unwetted—the fluctuation are not commonly large enough to reach 10s to 100s of feet. By examining hydrographs around the Albuquerque Basin (Powell and McKean, 2014; Rinehart et al., 2016) and reviewing the history of incision and backfill of the Rio Grande valley (Connell and Love, 2007; Connell, 2008a), susceptibilities based on depth-to-groundwater were assigned using:

$$s_{dtw} = \begin{cases} 1, & \text{if } d_w \leq 15 \\ 2, & \text{if } 15 \leq d_w \leq 40 \\ 3, & \text{if } d_w \geq 40 \end{cases}$$

where s_{dtw} is the susceptibility based on depth-to-groundwater (d_w , obtained from subtracting the potentiometric-surface elevation from land elevations at grid cells). Potentiometric-surface elevation was obtained from the maps generated in this report (see above), which used a grid of 100x100 m. The land elevation was obtained from digital elevation models (DEM) that were resampled to the same grid used for the potentiometric-surface elevation map. We also used predevelopment water-table elevation maps, but found little difference in susceptibilities. The quality factor for this layer was 6, reflecting the uncertainty of depth-to-groundwater with varying drainage and the lack of correlation of depth-to-groundwater with any texture or age information.

The highest-quality layer we used, which is considerably different than in Rinehart et al. (2017), was susceptibility assigned to geologic units mapped by Connell (2008b) that we explicitly incorporated in our analyses. These values were made by comparing the age, depositional environment, and texture of a given geologic unit to landform map units of Hawley et al. (2005) that were previously assigned susceptibilities by Rinehart et al. (2017) using procedures and criteria listed in Beckwith and Hansen (1989) and Momeni et al. (2012). Appendix 7 summarizes the susceptibilities we assigned to map units, with higher susceptibilities assigned to younger units that are more clay rich (e.g., distal-piedmont environments). The layer quality weighting was 10 because the geologic units were mapped by a specialist in Albuquerque Basin geology and directly correlate to the factors of Rogers (1995) and Momeni et al. (2012) without need for reinterpretation. Geospatially, these units were also located with more confidence than other units—they are not interpolations of subsurface point data, like depth-to-groundwater maps, nor are they based on the studies of numerous workers, like the gSSURGO maps. The map units were not biased by specific application, such as agriculture for the gSSURGO units focus on agriculture. Rather, Connell (2008b) documented the age, provenance, thickness, precise location, and grain-size distribution of surficial deposits. Connell (2008b), did not, however, map the entire area of interest in our study. In particular, the southwestern corner of the study area extends beyond the southern boundary of his map. As a result, we did not consider this layer outside of his map area.

VIII. RESULTS

Subsurface Lithologic Interpretations

Figure 23 summarizes storage-zone thicknesses and lithologic textures of the Santa Fe Group and younger units. The complete dataset is given in Appendix 5 (note that we did not acquire well data for unit Qaya_{cs}). Clay is relatively abundant (25–40%) in the: Holocene (“younger”) alluvium under the Rio Grande floodplain (Qaya_{fp}); transitional unit between the axial and piedmont facies of the Sierra Ladrones Formation (i.e., QTst), which includes the distal-piedmont facies; and Atrisco Member of the Ceja Formation (Tca). Less clay (10–25%) is present in the: Rio Grande terrace alluvium (Qtr); axial-river and medial-proximal piedmont facies of the Sierra Ladrones Formation (QTsa and QTsp, respectively); and Rio Puerco Member of the Ceja Formation (QTcr). The “middle” unit of the Santa Fe Group (Tsm, axial and piedmont facies older than unit QTsp) and post-Santa Fe Group piedmont deposits (Qao) have the least amount of clay (0–5%).

Storage zones are thickest in the medial-proximal piedmont facies (QTsp) and “middle” Santa Fe Group (Tsm), for which thicknesses at 50% of the cumulative distribution (assigned as the representative storage-zone thickness of a unit) are 270 ft and 89 ft, respectively. Storage zones in the axial facies (QTsa) and older alluvium (Qao) are also relatively thick at 73 ft and 57 ft, respectively. Notably thin storage zones are present in: younger alluvium under the Rio Grande floodplain (Qaya_{fp}, 17 ft); Rio Grande terrace alluvium (Qtr, 31 ft); the transitional unit between the axial and piedmont facies of the Sierra Ladrones Formation (QTst, 19 ft); and the Atrisco Member of the Ceja Formation (Tca, 37 ft).

MAR Using Deep Injection

In this section, we present maps showing the normalized results (ratings) for the metrics related to each criterion (0 to 2, with 0 being least suitable and 2 being most suitable). Ratings are presented as three

color-coded bins in some maps (i.e., 0, 1, 2), but in other maps the ratings are depicted as four or more color-coded bins to show more detail. Note that the “best-expert” weighting factor (next to last row on Figs. 21) is not reflected in these interim maps (Figs. 27–33) but is used to calculate the final summed metric for the deep-injection recharge suitability maps (Plates 1–2).

On each of the following maps, the generalized location of three laterally gradational contacts are depicted as hatched lines (refer to Fig. 15). Most of the axial-river facies of the Sierra Ladrones Formation (QTsa) lies between the western and central contacts. The Rio Puerco Member of the Ceja Formation (QTcr) is west of the western contact (map left). To the east of the central contact (toward map right) is the distal-piedmont facies and its transition with the axial facies (QTst). The eastern contact near the foot of the Sandia Mountains (map right) separates QTst from the medial-proximal piedmont facies of the Sierra Ladrones Formation (QTsp). Saturation of deposits younger than the Santa Fe Group is limited (except for Qaya_{fp}), so the distribution of some of the scoring appears to directly correlate with the spatial distribution of hydrostratigraphic units in the Santa Fe Group, as noted below.

Geologic criteria

Normalized criterion ratings for thickness-weighted transmissivity range from 0 to 2, but most are 1.6 to 2.0 (Fig. 27). From the prevalence of the highest-suitability bin, one can conclude that transmissivity is not a limiting factor within the study area (using our elected scoring system). Summed and normalized ratings for storage-zone thickness are more evenly distributed compared to transmissivity (Fig. 28). Storage-zone thicknesses directly correspond with the main geologic unit within 1,500 ft of the ground surface. The axial-river facies (QTsa) and medial-proximal piedmont facies (QTsp) returned high ratings (mostly 1.6–2.0). Lower ratings (0.6–1.5) are associated with younger alluvium under the modern floodplain (Qaya_{fp}) and the two members

of the Ceja Formation (QTcr, Tca). The lowest ratings (0–1.5) correlate to the distal-piedmont facies and where it is interfingered with axial sediment (QTst).

Allowable injection rates

Summed and normalized criterion ratings for allowable injection rates ($Q_{allowable}$) are relatively high across most of the study area (Fig. 29). Most values are 1.76 to 2.0. Low values are associated with the Rio Grande floodplain where unit Qaya_fp is underlain by unit QTcr, indicating that adverse groundwater mounding may be a problem in the area. Intermediate values are present under much of the Rio Grande floodplain north of Paseo del Norte Boulevard, where units Qaya_fp and Qaya_cs are underlain by unit QTsa.

Hydraulic properties

Gradients of the potentiometric surface are shown on Figure 30. Steep gradients of >0.01 (rated as 0) are present near the base of the Sandia Mountains. Most of the study area is characterized by intermediate gradients of 0.01 to 0.001 (rated as 1). Shallow gradients most suitable for MAR are present along the Rio Grande floodplain at the southern end of the study area and locally in the “groundwater trough” (illustrated in Fig. 11). Artifacts parallel the potentiometric surface in the southern part of this trough (near Tijeras Arroyo) and near downtown Albuquerque.

Infrastructure properties

The scoring of well density is shown in Figure 31 (for non-ABCWUA wells) and Figure 32 (for ABCWUA wells). Non-ABCWUA wells are relatively dense near the Rio Grande and in the northern part of the study area (rated as 0 on Fig. 31). ABCWUA wells are concentrated in the northern and central parts of the “trough” in the potentiometric surface (cf. Fig. 11 and Fig. 32) as well as south of the University of New Mexico (southwest of the intersection of Central Avenue and San Mateo Boulevard) and on the Rio Grande floodplain north of I-40. Figure 33 maps the scoring of the distance to water supply distribution pipelines carrying treated San-Juan Chama water.

Mapped Suitability for Deep-Injection Recharge

After a consensus was reached between the authors and the ABCWUA regarding values of the final, “best expert” weighting factors (values shown on next to last row on Fig. 21), the score of each criterion was multiplied by the relevant weighting factor. The post-weighted values were then summed for all criteria and normalized to a scale of 0 to 2 (Fig. 21).

The final step for mapping the suitability of deep-injection recharge was translation of the numeric weighted sums of ratings into qualitative categories of suitability. At this stage, most previous workers simply binned the range of values (in this case, 0 to 2) into equal parts. Instead, we advocate assigning qualitative suitability terms to bins that reflect natural clustering, and we also considered what has been previously interpreted as favorable for recharge. For this binning analysis, known or previously hypothesized areas suitable for deep recharge were:

1. The deep-injection well at the San Juan-Chama Drinking Water Treatment Plant (SJCDWTP, Fig. 2), whose aquifer has been demonstrated to have properties favorable for deep-injection recharge (Daniel B. Stephens and Associates, 2018). We added a ~500-ft (150-m) buffer around the well to provide a polygonal area from which to determine suitability representative of the subsurface conditions at that location.
2. A hypothesized “suitable deep injection zone” approximated using descriptions and cross sections in Hawley (1996), implying that a promising site is located in the East Heights sub-basin north of Gibson Boulevard (where substantial thicknesses of his lithofacies I and II for USF-2 are present in the subsurface). The northern boundary of this suggested area was not described. As mapped, however, the sub-basin ends south of Bernalillo County. Therefore, we arbitrarily extended the corresponding map polygon northward to the east-west part of Tramway Boulevard (Fig. 42).

Figure 34 is a histogram of the final sum of the weighted-ratings values for all criteria, normalized to 0–2, used to make the suitability map

of deep-injection recharge. In the histogram, grid cell counts corresponding to previously hypothesized recharge areas (items 1 and 2 above, from Hawley, 1996) are differentiated with orange shades. Note that these previously hypothesized areas mostly correspond to the higher suitability ratings of our work (i.e., they lie on the right side of the histogram). Agreement of these independent analyses corroborates our method. We determined that two natural clusters compose the distribution: a lower range of values mostly <0.9 and a higher range that overlaps with the distribution of ratings for the previously hypothesized recharge areas. We thus fit the overall distribution of ratings with a two-bin Gaussian mixture model (GMM), which conformed well to the histogram. The resulting Gaussian curves are shown in Figure 34; the purple curve fits the lower range of the ratings, and the green curve fits the higher range of ratings. For comparison, a Gaussian curve (brown) was also fitted to the ratings of grid cells that correspond to previously interpreted favorable areas (items 1 and 2 above). Note that the Gaussian curve for the previously hypothesized recharge areas is comparable to the higher-range of the two-bin GMM curve (green).

To translate the histogram analysis (Fig. 34) into suitability ratings, we considered that the higher-range curve (green) for the overall distribution is comparable to the curve fit to the previously hypothesized recharge areas (brown curve), such that the former curve likely represents those values suitable for deep-injection MAR projects. In contrast, the lower-range curve (purple) appears to represent areas not considered suitable for injection projects. We thus chose the intersection of the curves (at 0.85) to separate the “low suitability” and “moderate suitability” ratings. We further inferred that ratings in the upper one-half of the higher-range curve, above the peak at 1.33, indicate sites with the most favorable characteristics, classifying these as having “high suitability.” We assigned all cells within an exclusionary buffer to the “unsuitable” class.

Figure 35 and Plate 1 show the results of our efforts to qualitatively categorize suitability for deep-injection recharge for the Albuquerque area under the jurisdiction of the ABCWUA. Outside the Rio Grande floodplain, most of the map area is classified as either moderately or highly suitable. Highly suitable areas are commonly associated with substantial thicknesses of the axial-river deposits (QTsa); there is also some correspondence with the medial-proximal piedmont

facies (QTsp). Areas of low suitability east of the floodplain are associated with the distal-piedmont facies and its interfingering zone with QTsa, both of which are incorporated into hydrostratigraphic unit QTst. All cells within an exclusionary buffer are deemed “unsuitable.”

MAR Using Shallow-Based Recharge

In this section we present the normalized results for scoring (rating) of each criterion for shallow-based MAR (0 to 2, with 0 least suitable and 2 as most suitable).

Surface characteristics

Surface criteria included: the soil horizon (layer) thickness-weighted harmonic mean of vertical hydraulic conductivity (for saturated conditions); drainage characteristics based on soil drainage class; and surface slope. The distribution of ratings for soil vertical hydraulic conductivity, weighted with respect to the relative abundance of a soil in a map unit, is shown in Figure 36. There is a wide range in the normalized ratings for hydraulic conductivity, and the resulting boundaries of the binned ratings mimic many boundaries in the USDA soil map for Bernalillo County (Soil Conservation Service, 2019). Low hydraulic conductivities of 0–0.5 correspond to ‘cut-and-fill’ map units.

To a lesser extent, the mapped distribution of ratings for soil drainage class also follows the boundaries of the USDA soil map (Soil Conservation Service, 2019) (Fig. 37). Low ratings for ‘cut-and-fill’ land away from the Rio Grande are particularly evident. Most of study area, however, exhibits relatively suitable drainage classes (Fig. 37). The coincidence of boundaries of soil-related criteria with the Soil Survey map reflects our use of it and related datatables to score them.

Surface-slope ratings are shown in Figure 38. Most of the study area has favorable slopes of <5% (scored as 2). Undesirable slopes (scored as 0) are locally found along Tijeras Arroyo and at the base of the Sandia Mountains. Intermediary slopes (5–10%, scored as 1) are along much of the remainder of Tijeras Arroyo and on proximal parts of modern alluvial fans at the foot of the Sandia Mountains (Fig. 38).

Adverse groundwater mounding

A minimum depth below the water table is desired as “headroom” to avoid the adverse effects of groundwater mounding. We used a macro-enabled Microsoft Excel spreadsheet from Carleton (2010) that employs the Hantush equation (Hantush, 1967) to predict the amount of water-table rise using a specified recharge basin geometry, the duration of recharge, and the hydraulic properties of the unsaturated zone. The resulting depth-to-groundwater ratings are shown in Figure 39. Ratings of 0 (<30 ft, <10 m depth) are restricted to along the central and southern parts of the Rio Grande in the study area. The remainder of the floodplain, and recent, “young” alluvial fans that merge with the floodplain along its eastern edge, are rated as 1 for depths of 30–140 ft (10–43 m). To the east, groundwater is sufficiently deep that adverse groundwater mounding is not expected.

Deep-geology considerations

Ratings based on estimated percolation times were obtained by dividing the unsaturated thickness of each unit by the average velocity of the wetting front. This velocity was calculated using a derivative property of the Philip (1957) infiltration model at long infiltration times (Jury and Horton, 2004). Figure 40 shows the resulting ratings in the study area. Estimated percolation times are shorter (0–30 days) under the floodplain and adjoining young alluvial fans where groundwater is relatively shallow. Intermediate lengths of time of 30–90 days (rating of 1) are along I-25. Percolation is estimated to be longer than 90 days (rating of 0) under the central and eastern extents of the modern piedmont surface. These long percolation times are probably a function of deeper water tables in the areas 400–860 ft, 122–262 m).

Clay abundance is presented in Figure 41; the ratings have been thickness-weighted according to the geologic units present between the land surface and water table. Low ratings are present under the modern floodplain, due to the relatively high (27%) clay content of unit Qaya_fp (Fig. 19, Appendix 5). High ratings are observed in the proximal-medial piedmont deposits of the Sierra Ladrones Formation (QTsp). High ratings also correspond to alluvial-fan deposits (Qaya_cs) adjoining eastern floodplain sediment because these deposits lack clay and occupy most of the subsurface interval above the water table.

Moderate ratings lie in a north-south trend across the central part of the map area, which is mostly underlain by the axial-river facies (QTsa).

Other deep-geology criteria were considered relevant for assessment of saturated-zone suitability (i.e., via deep injection), including depth-weighted transmissivity, storage-zone thickness, and potentiometric-surface gradient. Scores of these criteria were imported from the deep-injection recharge map (Fig. 35, and are illustrated in Figs. 27–38, and 30).

Mapped suitability for shallow-based recharge

After a consensus was reached between the authors and the ABCWUA regarding the final weighting factors, we multiplied the score of each criterion by the relevant weighting value (next to last row in Fig. 24). The post-weighted values were then summed for all criteria and normalized to a scale of 0 to 2.

The final step for mapping the suitability of areas for shallow-based recharge was translation of numeric weighted sums of ratings into qualitative, descriptive categories of suitability. The procedure was similar to that for the deep-injection recharge suitability map (see above). We considered a different set of areas, however. These areas included those previously thought by Hawley (1996) to be suitable for shallow-based recharge as well as sites that have proven successful using shallow methods (Fig. 42):

3. The reach of Bear Canyon Arroyo used for the Bear Canyon Recharge Demonstration Project, where >95% of applied surface water percolates into the aquifer (Daniel B. Stephens and Associates, 2010);
4. A modification of the mountain-front recharge areas of Hawley (1996)—but because they are mostly located outside the study area, each was continued as a ‘recharge reach’ downstream into the study area, to the edge of the raster extent of the water table and continuing another five pixels further downstream (~1,650 ft, ~500 m);
5. Floodplain recharge windows recognized by Hawley (1996), modified as lines paralleling the Rio Grande inner valley;
6. Two non-floodplain recharge windows described by Hawley (1996):
 - a. Along Tijeras Arroyo from Pennsylvania Avenue westward to the bridge past the

- convergence with Coyote Arroyo, extending to the western edge of the eastern recharge circle (see Hawley, 1996, his plate 20A);
- b. Along Tijeras Arroyo between the Kirtland Air Force Base and I-25; and
7. The vadose-zone well at the San Juan-Chama Drinking Water Treatment Plant (SJCDWTP, Figs. 2 and 12), located 200 ft (60 m) north of the deep-injection well, where injection tests and theoretical calculations indicate allowable injection rates of 350–587 gpm.

A buffer of ~500 ft (150 m) was applied around these hypothesized recharge areas in which to determine suitability using our methods.

Figure 43 is a histogram of suitability ratings corresponding to known or hypothesized recharge areas in floodplains, ratings for similarly known or hypothesized non-floodplain areas, and suitability ratings for the remainder of the study area. The x-axis of the histogram corresponds to the final normalized summed ratings. In contrast to the histogram for deep injection (Fig. 34), there is less correspondence between our ratings and the recharge areas inferred by Hawley (1996). The ratings for hypothesized non-floodplain recharge areas, however, mostly reside in the middle to lower-upper parts of the overall distribution, a correspondence that offers some corroboration of our method.

The overall distribution of ratings is characterized by two natural, overlapping clusters (as with the deep-injection suitability assessment). In contrast to the deep-injection suitability histogram, the two clusters are closer and less clearly defined, but a two-bin Gaussian mixture model (GMM) again adequately fits the distribution, with peaks at 1.16 and 1.38 and a cross-over intersection at 1.24 (Fig. 43). We also fit a Gaussian curve (brown) to the ratings for non-floodplain areas previously hypothesized favorable (items 1–2 and 4–5 above), which is somewhat comparable, albeit slightly shifted, to the higher-range GMM curve (green).

As with the deep-injection suitability histogram analysis above, we utilized the GMM results to translate suitability ratings to qualitative suitability classes by using the cross-over intersection and the peak of the higher-range curve as boundaries. We again suggest that the higher-range curve (green) is comparable to the curve fit to known or previously hypothesized suitable non-floodplain recharge areas (brown curve), such that this range of values likely reflects sites suitable for shallow-based MAR. The lower-range GMM curve (purple) appears to reflect

ratings of less suitable sites. We used the intersection at 1.24 as the divider between “low suitability” and “moderate suitability” and the peak of the higher-range curve at 1.38 as the boundary between “moderate suitability” and “high suitability.” We assigned all cells within an exclusionary buffer to the “unsuitable” class. Note that exclusionary zones for the shallow-based recharge map do not include those for faults because faults in dry sand in an unsaturated zone may act as preferential pathways for groundwater flow, rather than impede flow as in a deeper saturated zone (Sigda and Wilson, 2003).

Figure 44 and Plate 2 show the results of this qualitative categorization of suitability for shallow-based recharge. There is a relatively positive correlation with the subsurface geology. Areas where there are abundant axial-river deposits (QTsa) are ranked as moderately or highly suitable. Non-lithologic factors appear to play a role in the differentiation between moderate suitability and high suitability. High to moderate suitability corresponds to the medial-proximal piedmont facies (QTsp), probably due to the general lack of clay and moderately shallow water tables. Low suitability commonly correlates to areas overlying the two members of the Ceja Formation (units QTcr, Tca), together with many areas overlying the distal-piedmont facies and its transition into axial facies (QTst).

Mapped Susceptibility to Soil Hydrocompaction

Figure 45 shows the susceptibility of each layer used to assess soil-hydrocompaction suitability. The taxonomic order layer shows a generally high susceptibility (Fig. 45A). The taxonomic suborder shows moderate to high susceptibilities where there is coverage, but suborder does not yield additional information over much of the region (Fig. 45B). The susceptibility map from taxonomic great group shows moderate to high susceptibilities for much of the region, with younger deposits (having relatively high susceptibilities) interspersed amongst older soils (with moderate susceptibilities) (Fig. 45C). Soil texture susceptibilities are high to extreme in fine-grained piedmont and floodplain deposits (Fig. 45D). Sandy channels and other sandy deposits have moderate susceptibility. Groundwater in much of the region is deep enough to default to an extreme susceptibility, with susceptibility decreasing toward the Rio Grande as the water table becomes

shallower (Fig. 45E). Susceptibility directly based on geologic units are extreme in the youngest alluvial deposits, with map patterns reflecting modern stream networks and most recent stream terraces (Fig. 45F). Susceptibility decreases with increasing unit age and grain size for reasons elaborated in the methods section.

Classifications of low, moderate, high, and extreme were made by breaking the distribution of total susceptibility into quartiles (25% quantiles). Results are shown in Plate 3, with the number of layers used in the analyses depicted in Plate 4. Plate 3 features four regions with unique soil-hydrocompaction susceptibility characteristics:

1. Pleistocene-age Tijeras canyon fan complex (region south of I-40): Older surfaces of low susceptibility are inset by younger, highly to extremely susceptible, fine-grained deposits.
2. Northern piedmont complex (region north of I-40) with generally high susceptibilities: On older surfaces, susceptibilities are controlled by a balance of age and grain size; increasing age

lowers susceptibility, whereas finer grain size elevates susceptibility. Younger surfaces include young, distal-fan deposits (Qaya_{cs}) having extreme susceptibility. Some relatively recent inset streams, however, are coarse grained, locally lowering susceptibility east of I-25.

3. Alluvial fans along the margins of the Rio Grande inner valley (“Bosque” region): Alluvial fans prograded over terraces around Edith and Broadway Boulevards, and the relatively fine grain size of these young fans resulted in a north-south band of extreme susceptibility west of I-25.
4. Active floodplain, with shallow water tables and wetter soils resulting in low susceptibility: These soils, although young, were repeatedly wetted naturally by floods before construction of dikes in the early 1900s and flood control dams at Cochiti and Jemez in the late 1900s. In addition, the soils were subject to much higher water tables before the basin-wide drain system was cut in the early 1900s.

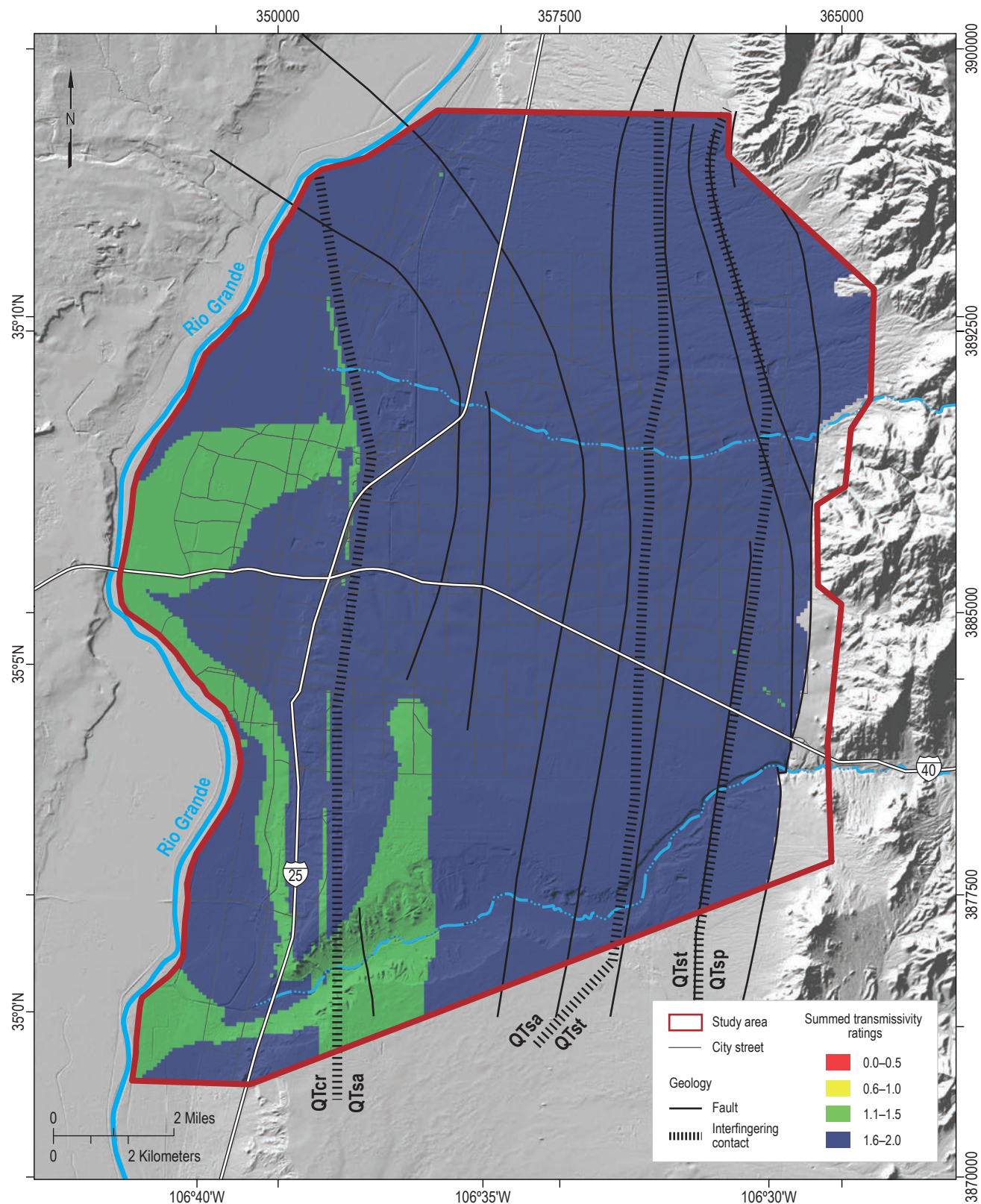


Figure 27. Ratings for transmissivity after initial thickness-weighting (Fig. 19), which produced non-integer values. These ratings are divided into four bins (lower values being less favorable and higher values more favorable). Hatched lines are the generalized, laterally gradational contacts between hydrostratigraphic units QTcr, QTsa, QTst, and QTsp.

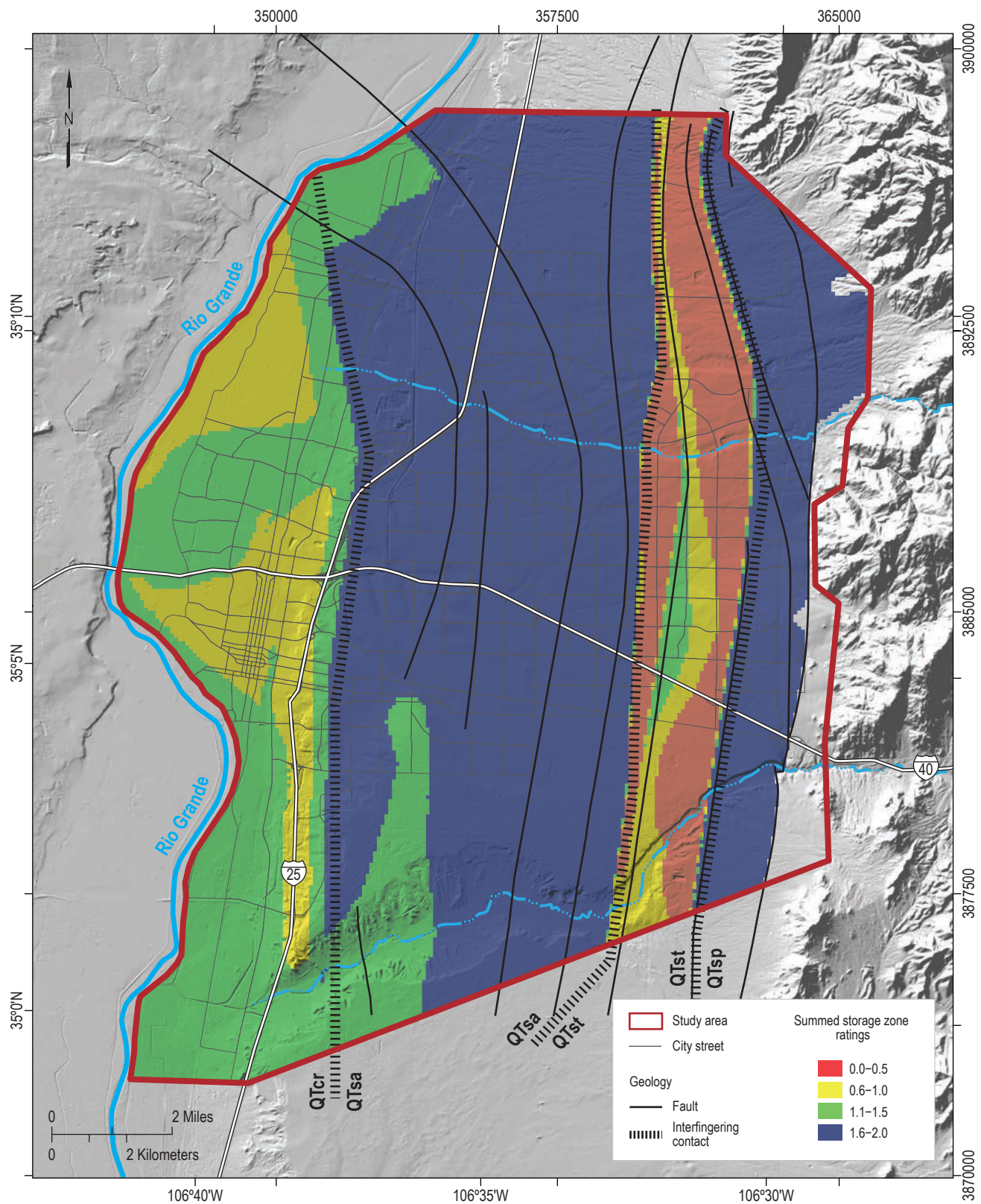


Figure 28. Ratings for storage-zone thickness after the initial thickness-weighting, which produced non-integer values. These ratings are divided into four bins (lower values being less favorable and higher values more favorable).

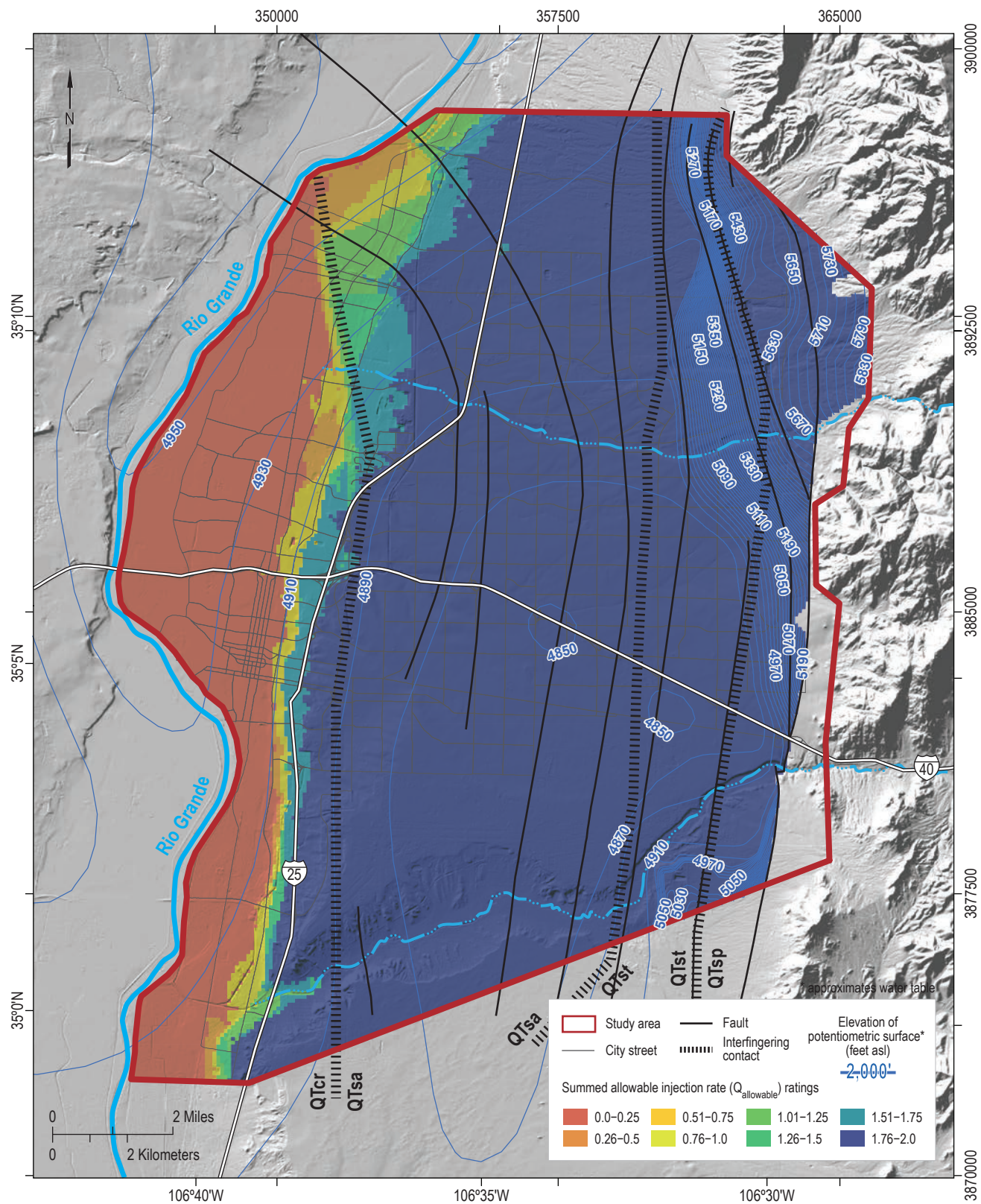


Figure 29. Summed and normalized ratings for allowable injection rate ($Q_{allowable}$), which produced non-integer values. These ratings are divided into eight bins (lower values being less favorable and higher values more favorable).

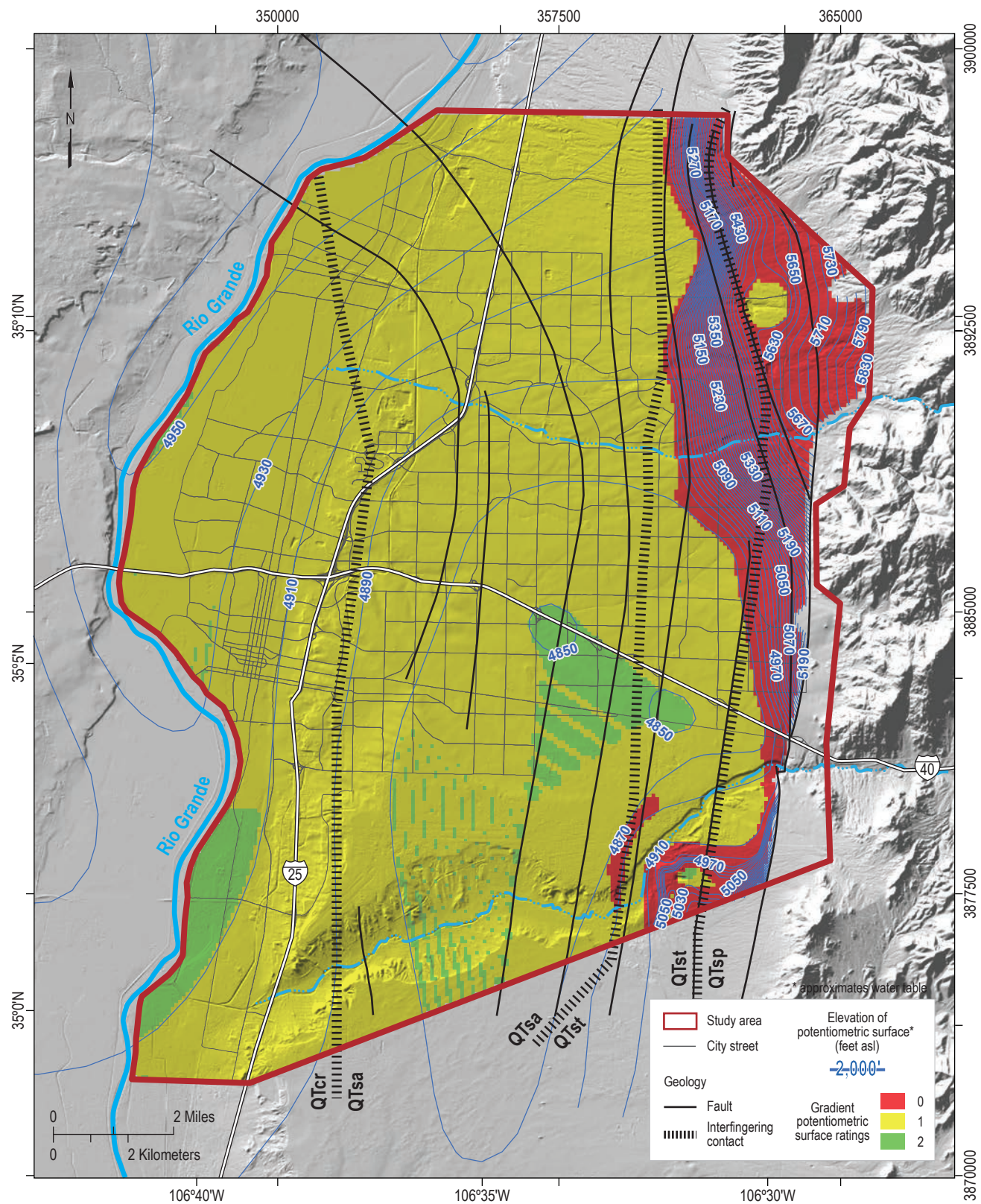


Figure 30. Ratings for the potentiometric-surface gradient. A gradient of 0 to 0.001 is rated as a 2; 0.001 to 0.01 rated as a 1; and >0.01 rated as a 0 (Fig. 21). The parallel bands are processing-related artifacts.

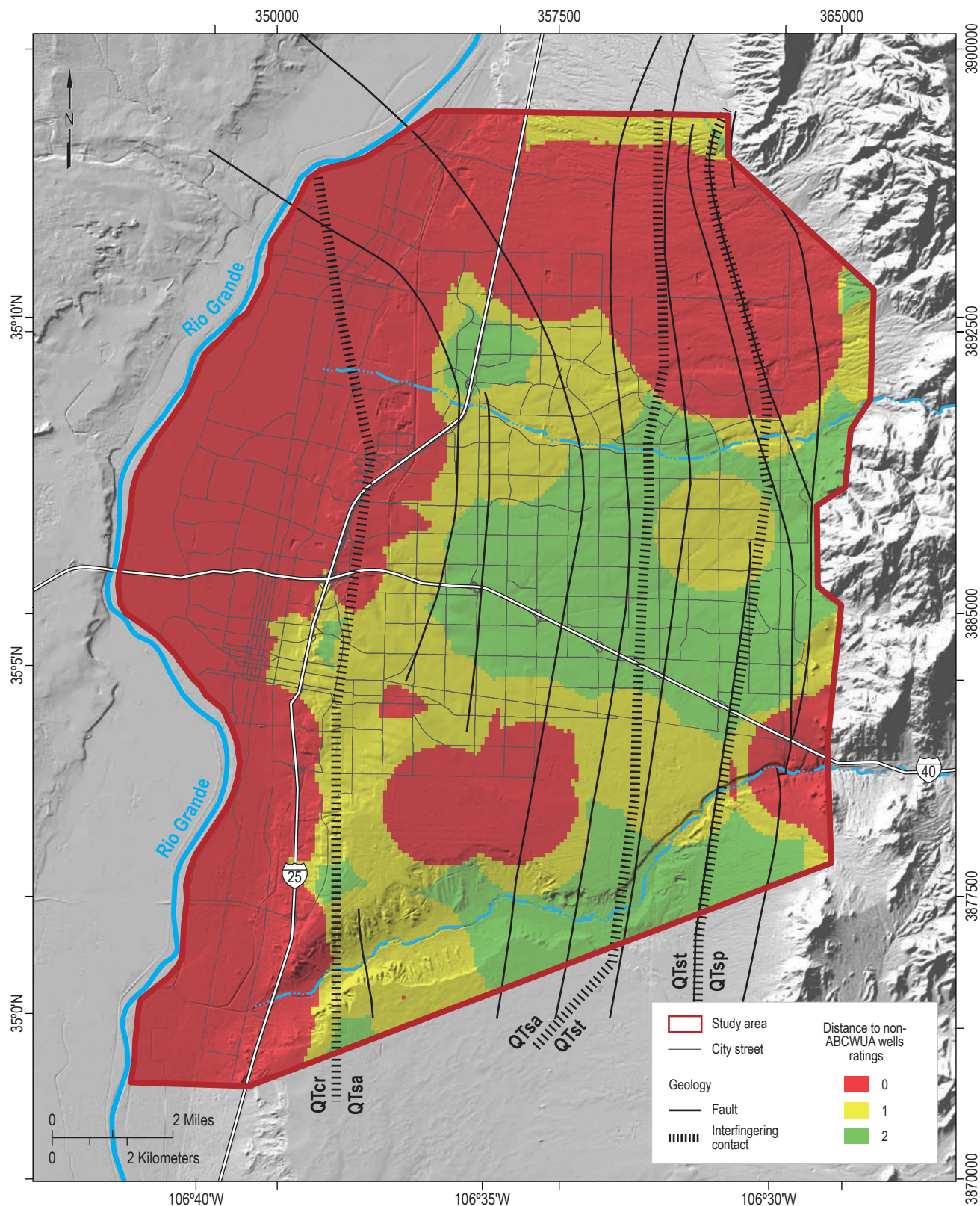


Figure 31. Ratings for non-ABCWUA well density. Zero wells within a 1-mi radius of a grid cell is rated as a 2; 1 to 5 wells rated as a 1; and >5 wells is rated as a 0 (Fig. 21).

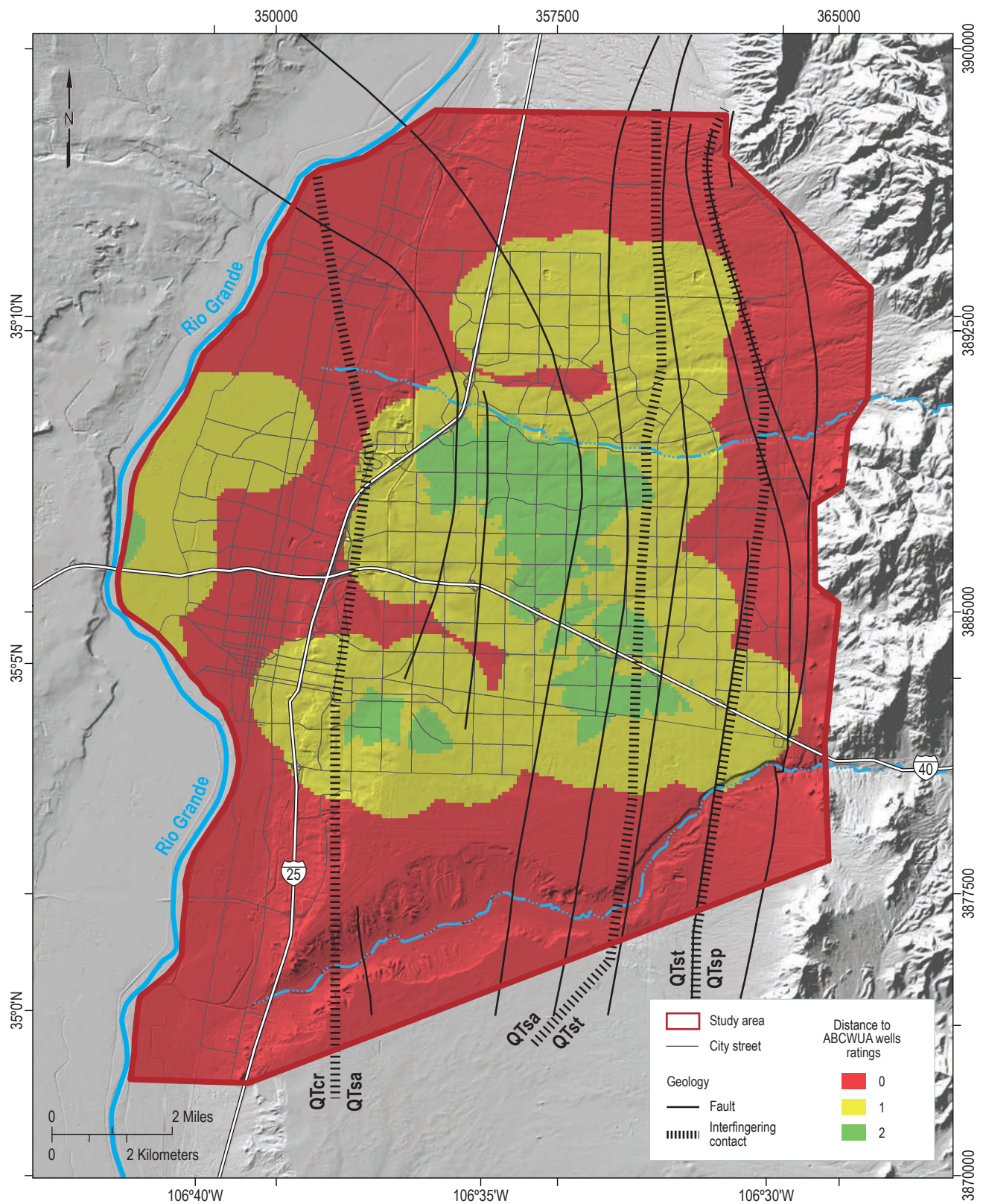


Figure 32. Ratings for ABCWUA well density. More than 5 wells within a 1-mi radius of a grid cell is rated as a 2; 1 to 5 wells rated as a 1; and 0 wells is rated as a 0 (Fig. 21).

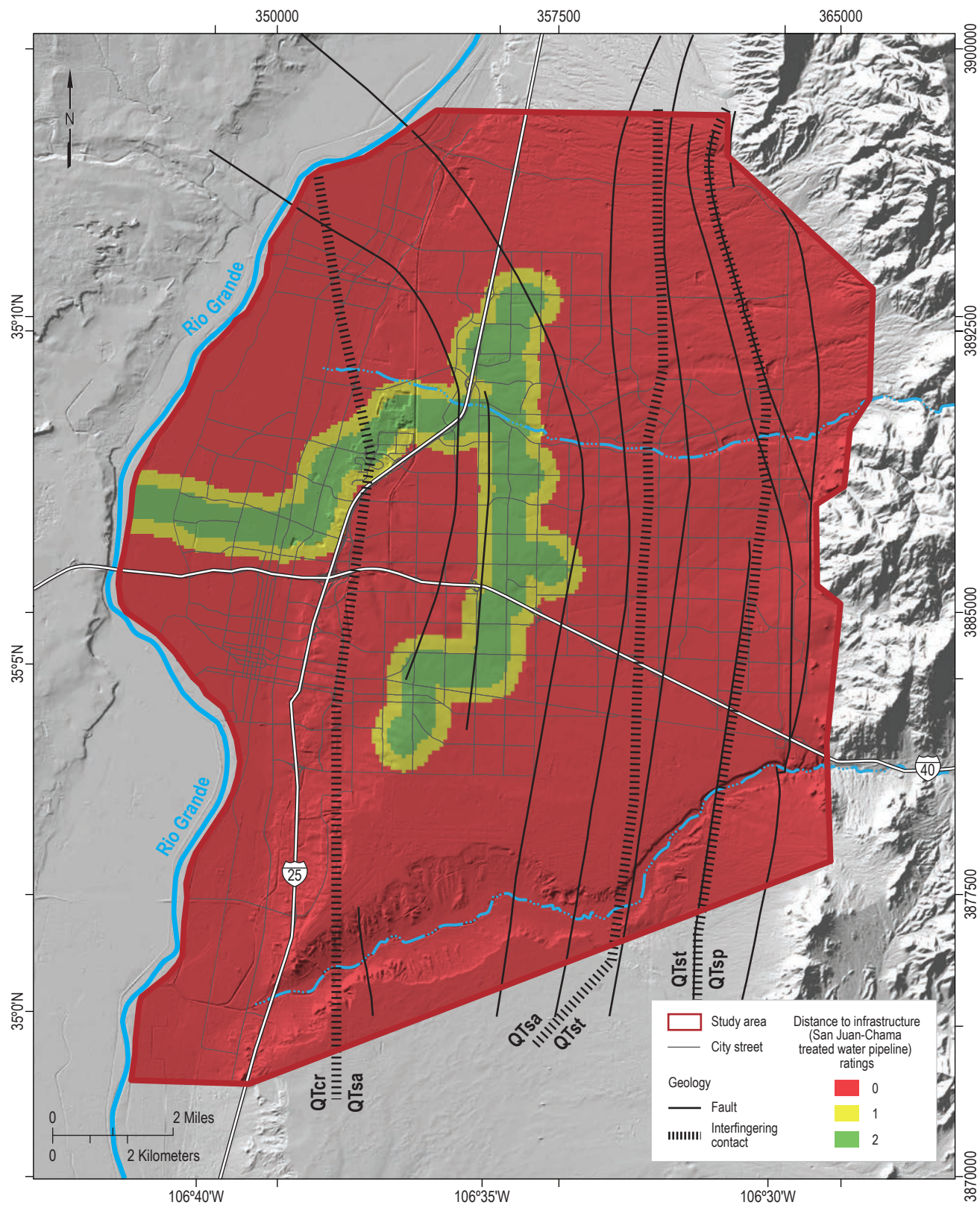


Figure 33. Ratings of the distance to San Juan-Chama treated water distribution pipelines. A distance of 0 to 0.25 mi is rated as a 2; 0.25 to 0.5 mi as a 1; and >0.5 mi as a 2 (Fig. 21).

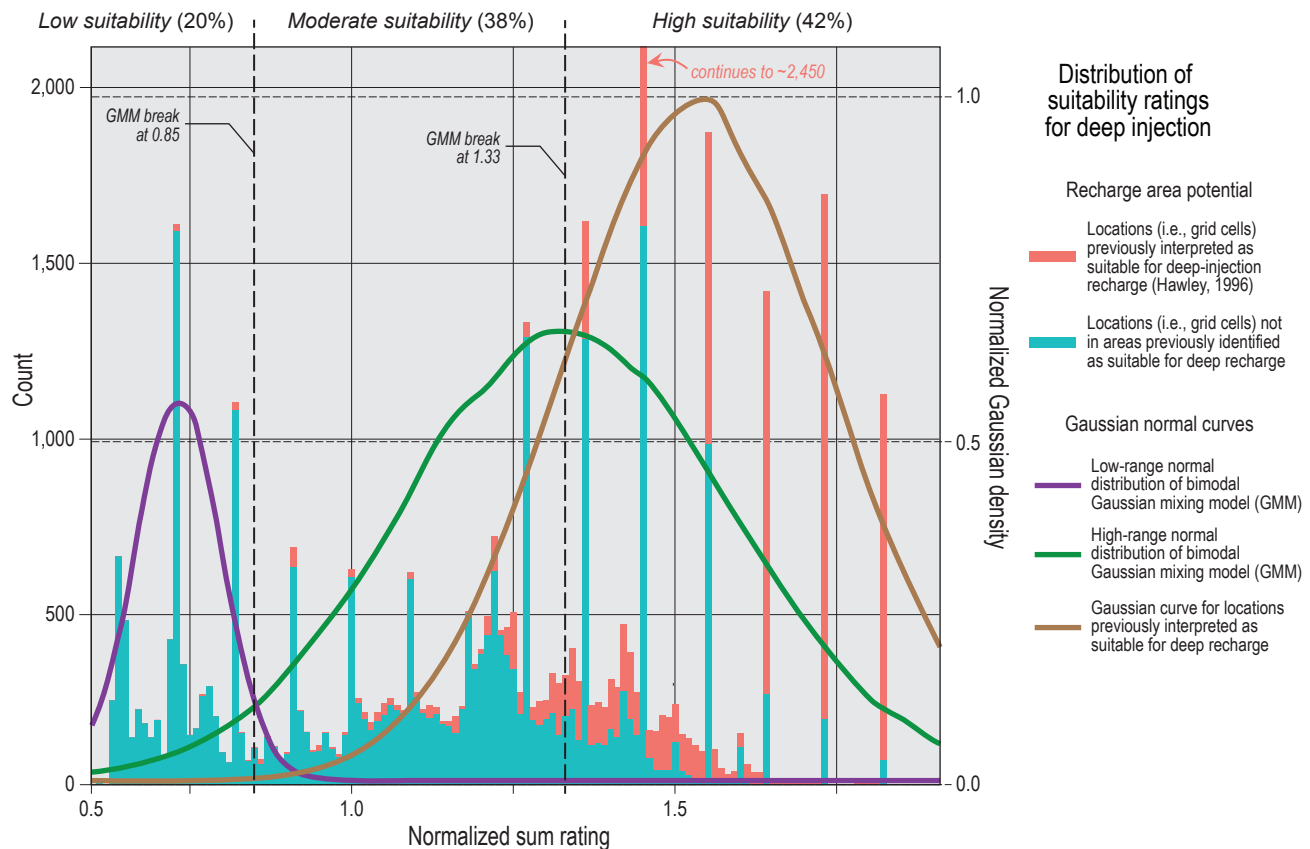


Figure 34. Histogram showing the sum of weighted-ratings values, normalized to 0–2, of all map grid cells for deep-injection MAR. The low-range (purple) and high-range (green) Gaussian normal curves are from bimodal Gaussian mixing models (GMM). Another Gaussian curve (brown) was fitted for grid cells corresponding to hypothesized recharge areas. Dashed lines represent breaks used to separate data into three qualitative bins of low, moderate, and high suitability. The boundaries of bins correspond with the peak of the higher-range GMM (1.33) and the trough between the lower-range and higher-range GMM peaks (0.85).

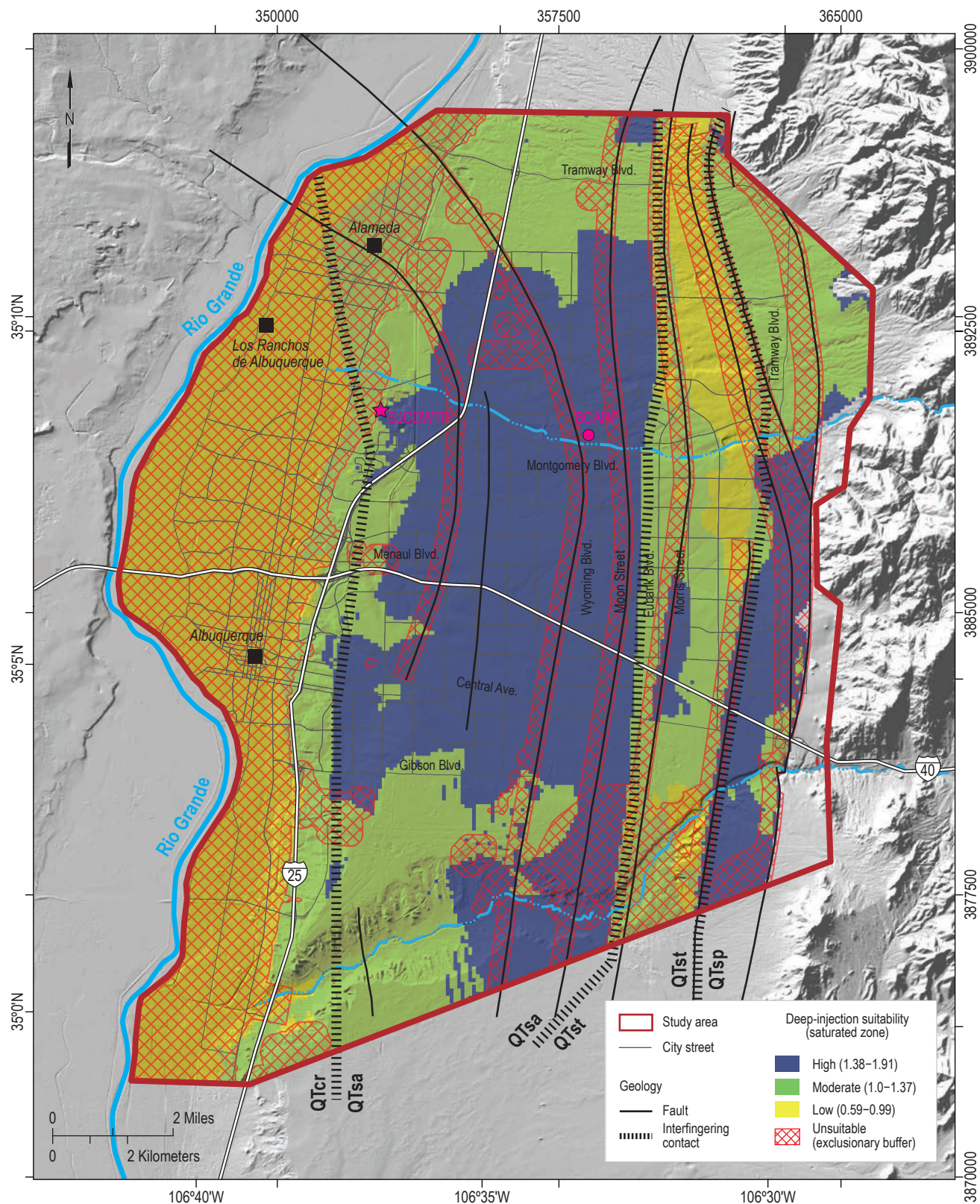


Figure 35. Map showing the final color-coded suitability bins—of unsuitable and low, moderate, and high suitability—that permits qualitative assessment of the efficacy of deep-injection recharge.

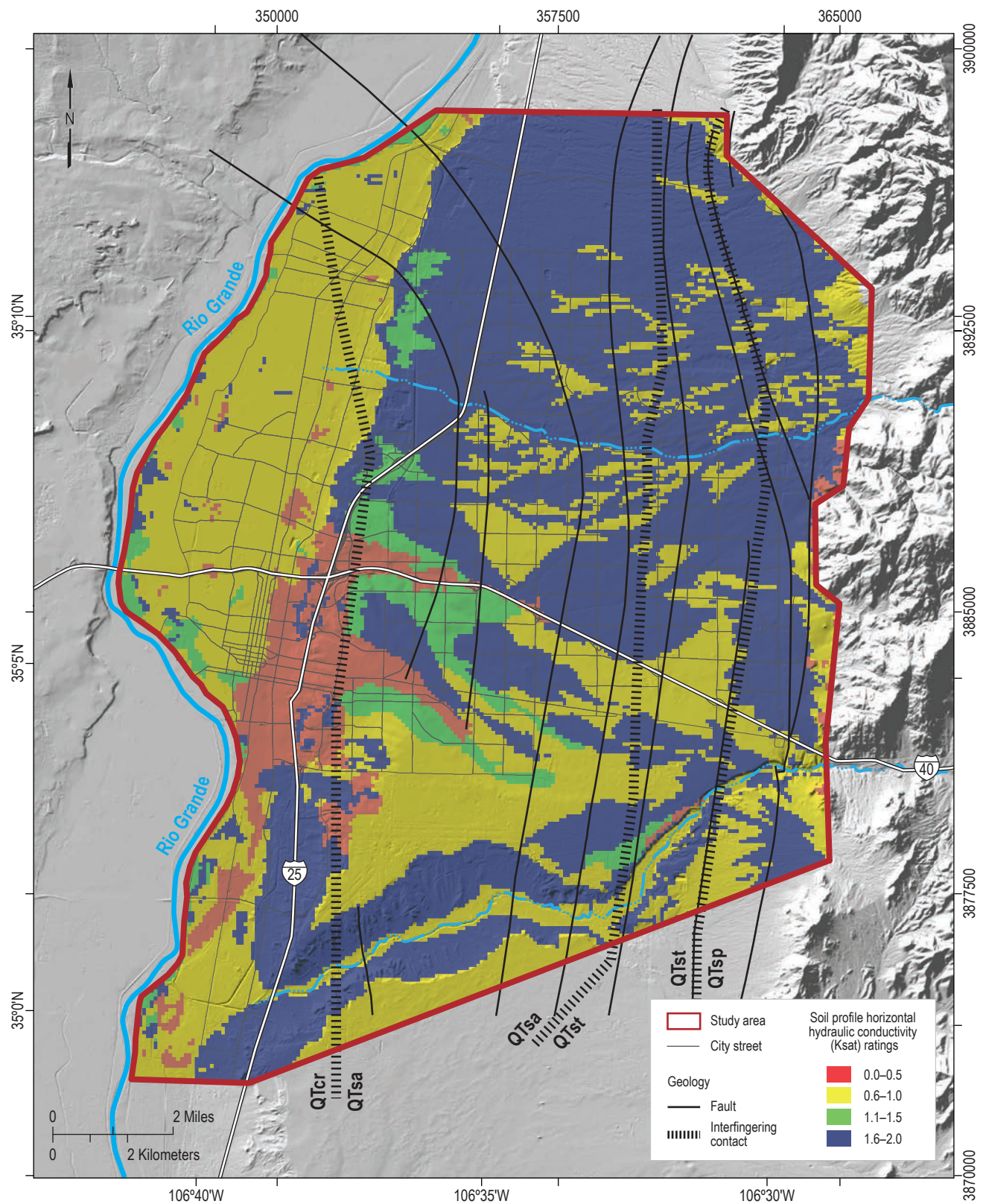


Figure 36. Distribution of ratings for soil vertical hydraulic conductivity (Ksat), weighted according to the relative abundance of a soil in a grid cell. Ratings are grouped into four bins, with higher values being more favorable for recharge. These ratings are relevant to the top 6 ft (~2 m) of sediment below the land surface and, in many cases, may be modified by urbanization.

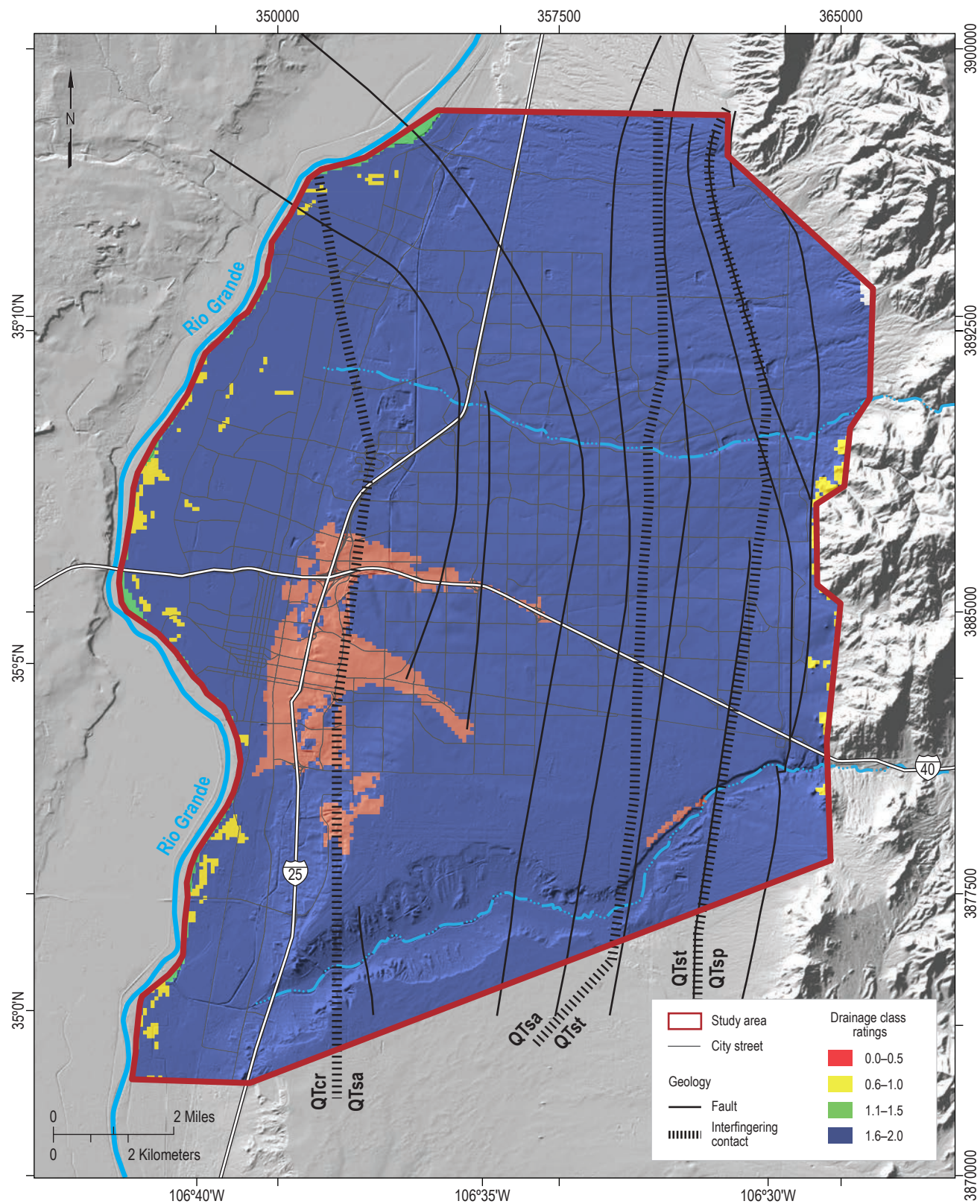


Figure 37. Distribution of drainage class ratings, weighted according to the proportion of a soil component in a soil map unit. Ratings are grouped into four bins, with higher values being more favorable for recharge. These ratings are applicable to the top 6 ft (~2m) below the land surface and, in many areas, may be modified by urbanization.

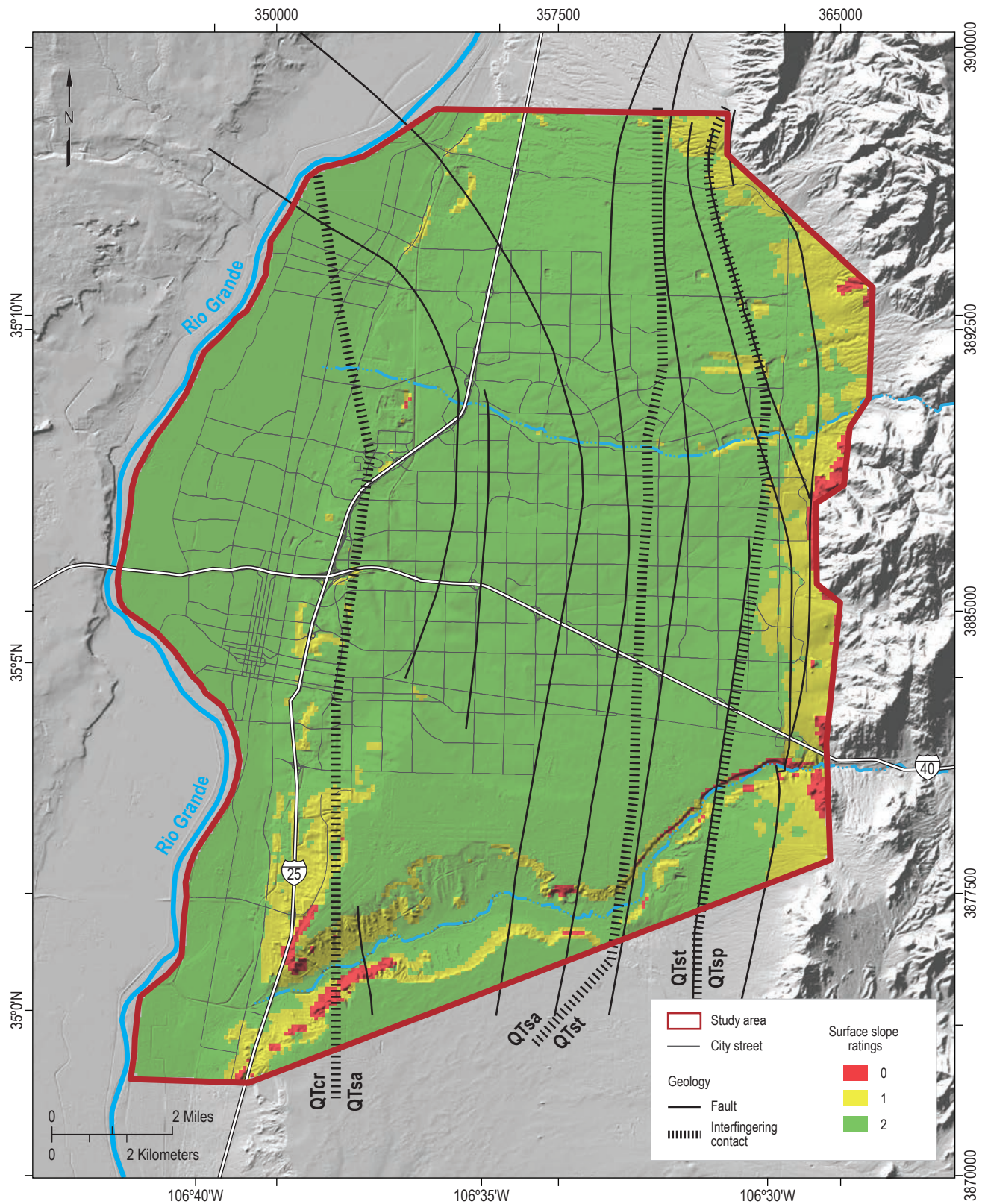


Figure 38. Distribution of surface slope ratings. Slopes <5% are rated as 2; 5 to 10% as 1; and >10% as 0 (Fig. 24). Most of the study area has favorable slopes of <5% (scored as 2).

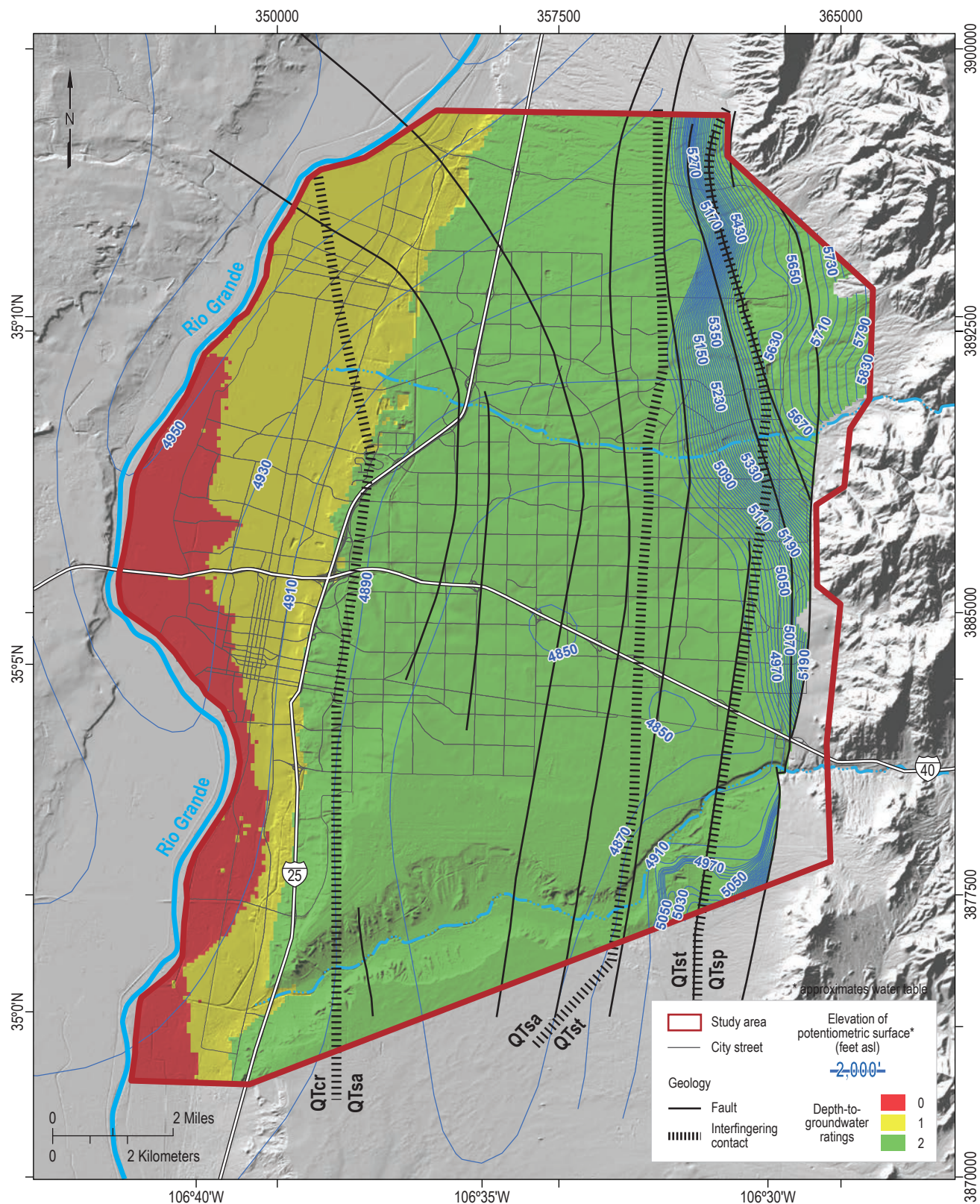
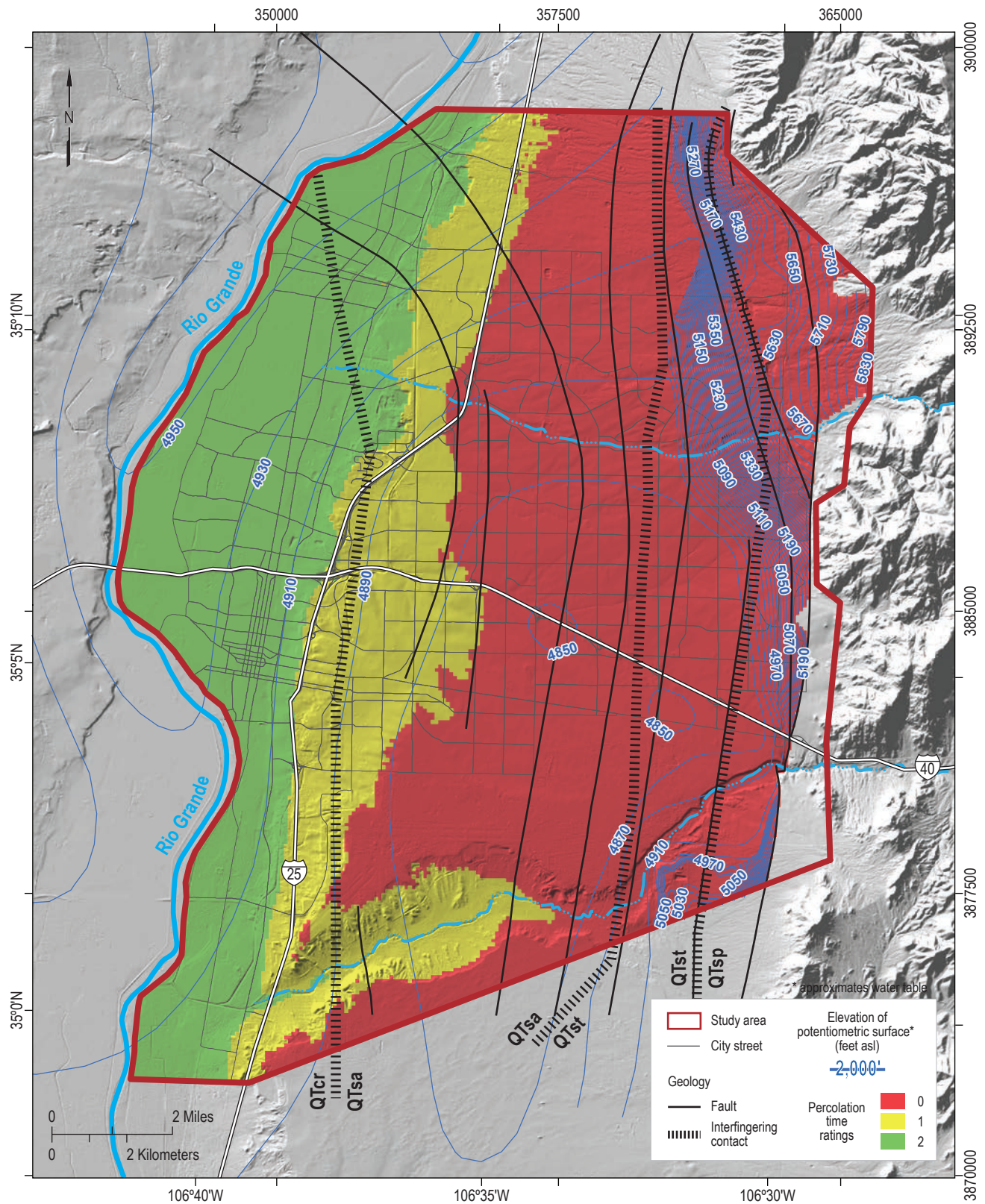


Figure 39. Depth-to-groundwater ratings, reflecting concerns of adverse groundwater mounding. Depths >140 ft are ranked as 2; 30 to 140 ft as 1; and <30 ft as 0 (Fig. 24). Most of the study area has a relatively deep groundwater depth (rated as 2), where potential groundwater mounding is unlikely to be a concern.



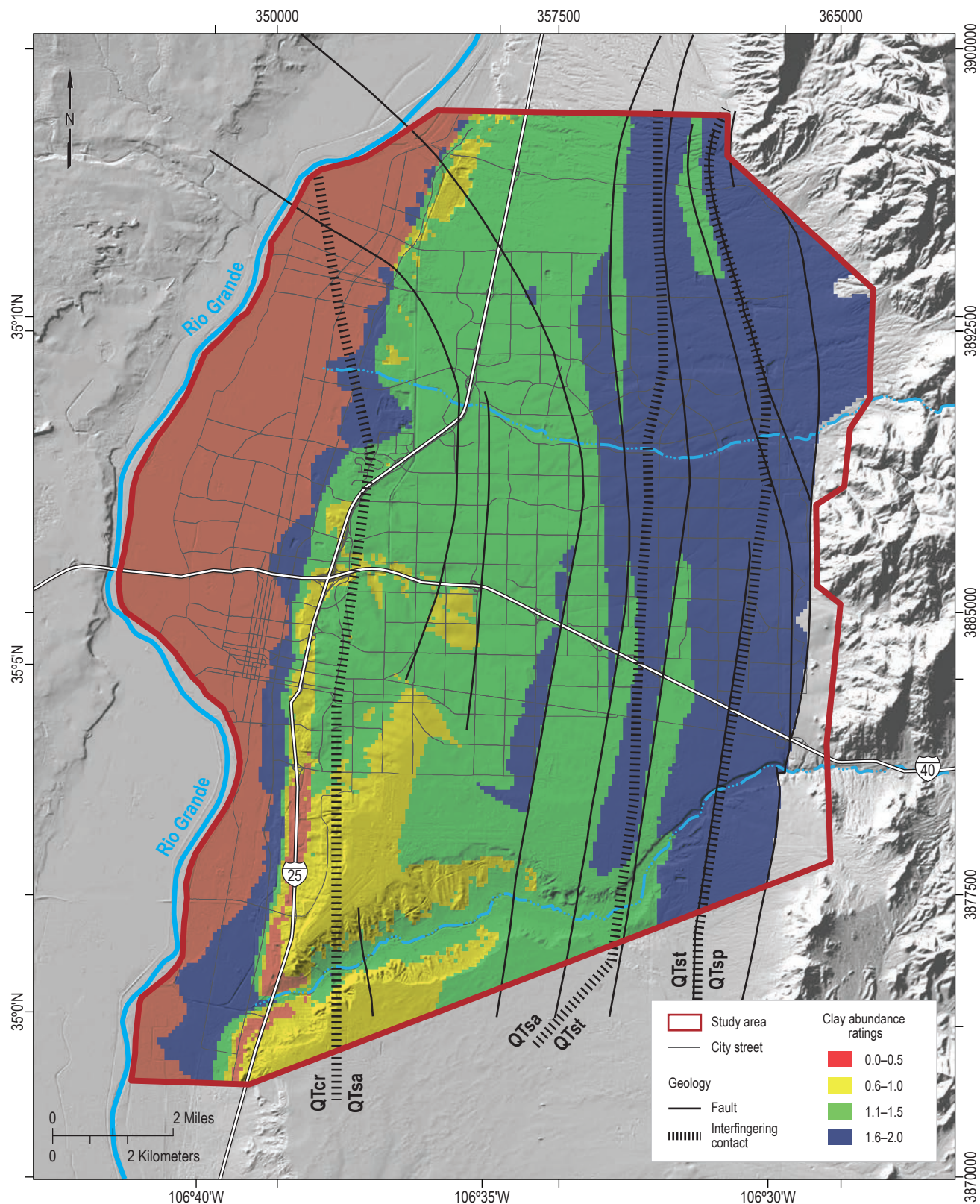


Figure 41. Ratings distribution for clay abundance. Ratings are thickness-weighted and grouped into four bins, with higher values being more favorable for recharge. The geologic units with the least amount of clay are coarse-grained, younger alluvium (Qaya_{cs}) (e.g., where it interfingers with Qaya_{fp} along the eastern side of the modern floodplain) and medial-proximal piedmont deposits (QTsp).

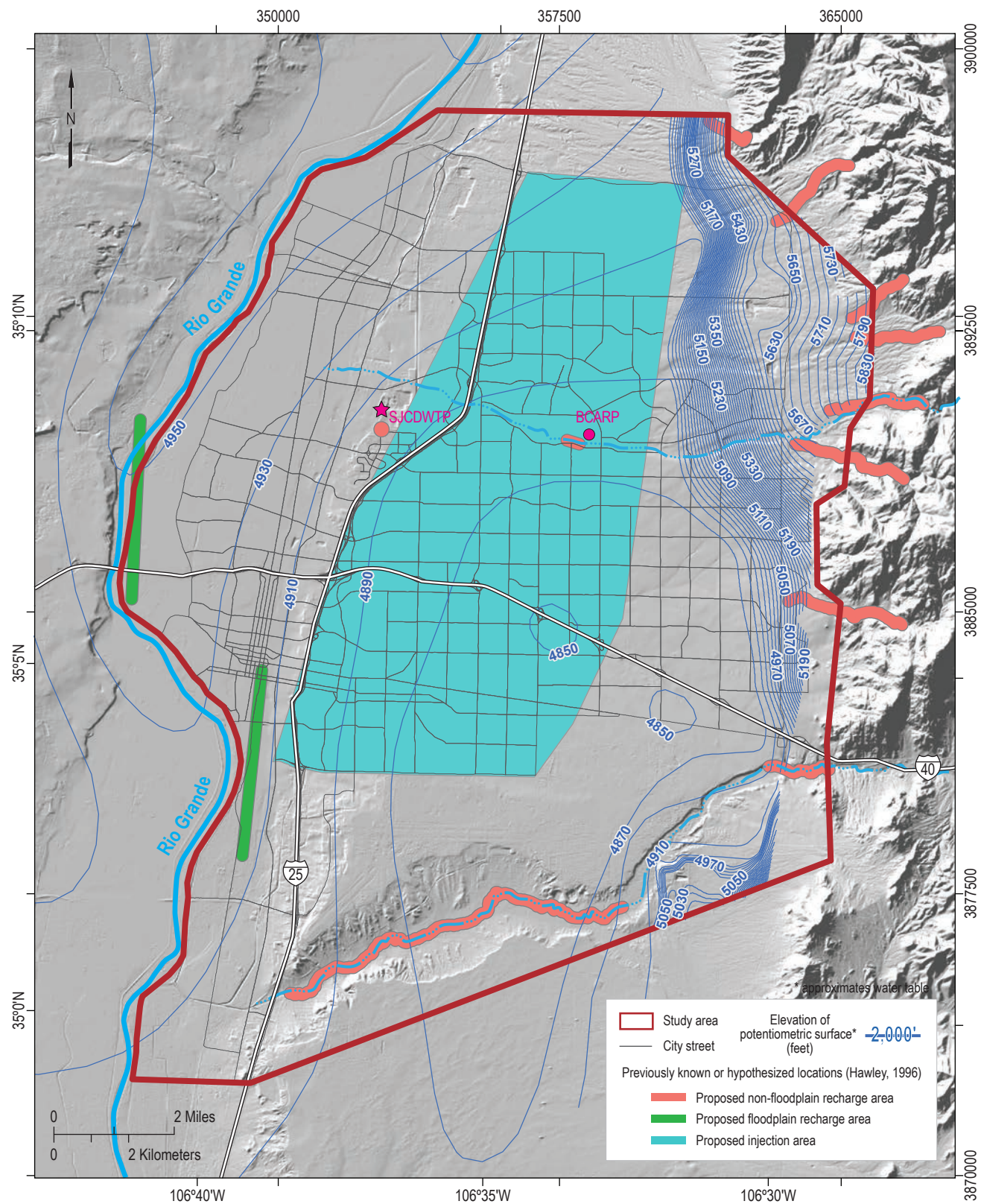


Figure 42. Areas predicted by Hawley (1996) as favorable for various recharge methods. The locations of the San Juan-Chama Drinking Water Treatment Plant (SJCDWTP) and Bear Canyon Arroyo Recharge Project (BCARP) are shown.

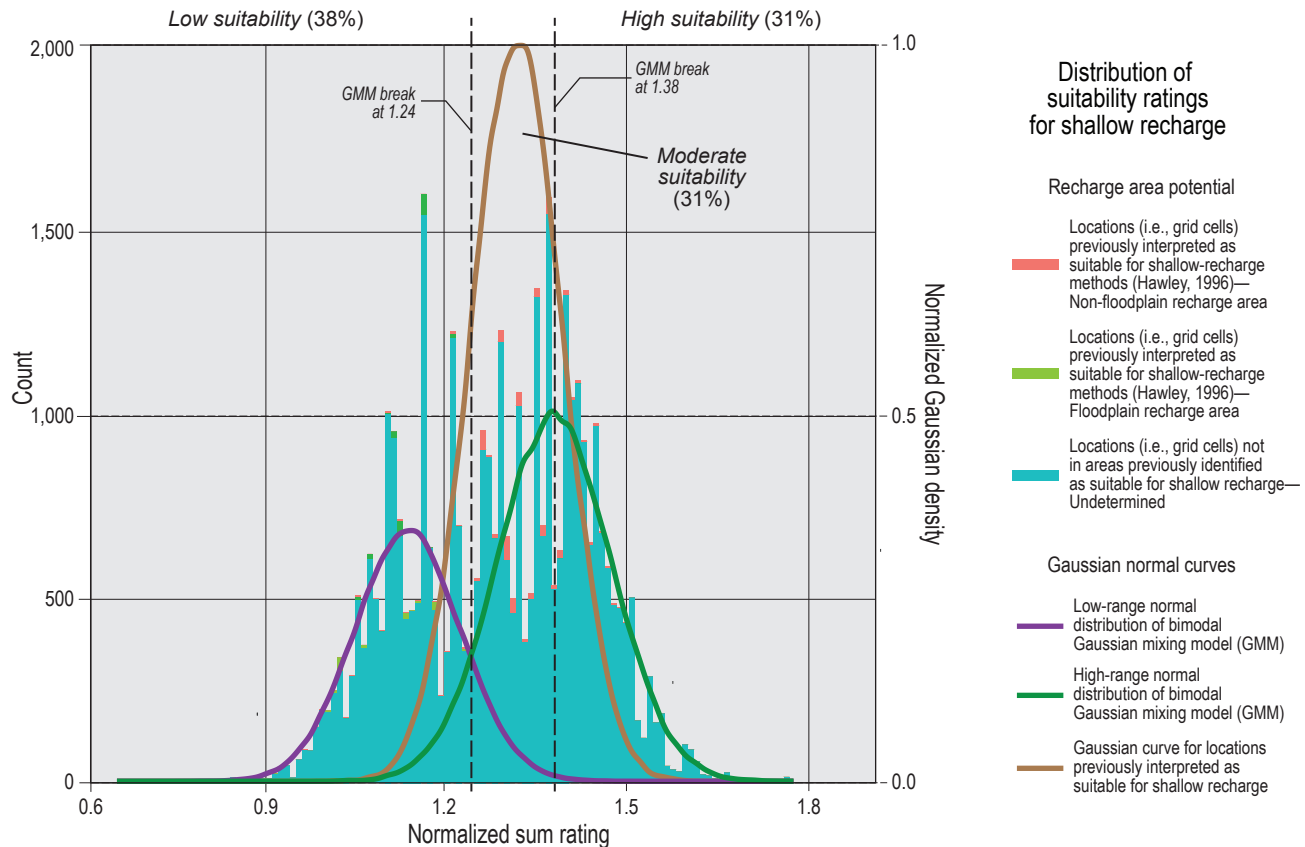


Figure 43. Histogram showing the sum of weighted-ratings values, normalized to 0–2, of all map grid cells for shallow-based MAR. The low-range (purple) and high-range (green) Gaussian normal curves are from bimodal Gaussian mixing models (GMM). Another Gaussian curve (brown) was also fitted for grid cells corresponding to hypothesized recharge areas. Dashed lines show breaks used to separate data into three qualitative bins of low, moderate, and high suitability. The boundaries of bins correspond with the peak of the higher-range GMM peak (1.38) and the trough between the lower-range and higher-range GMM peaks (1.24).

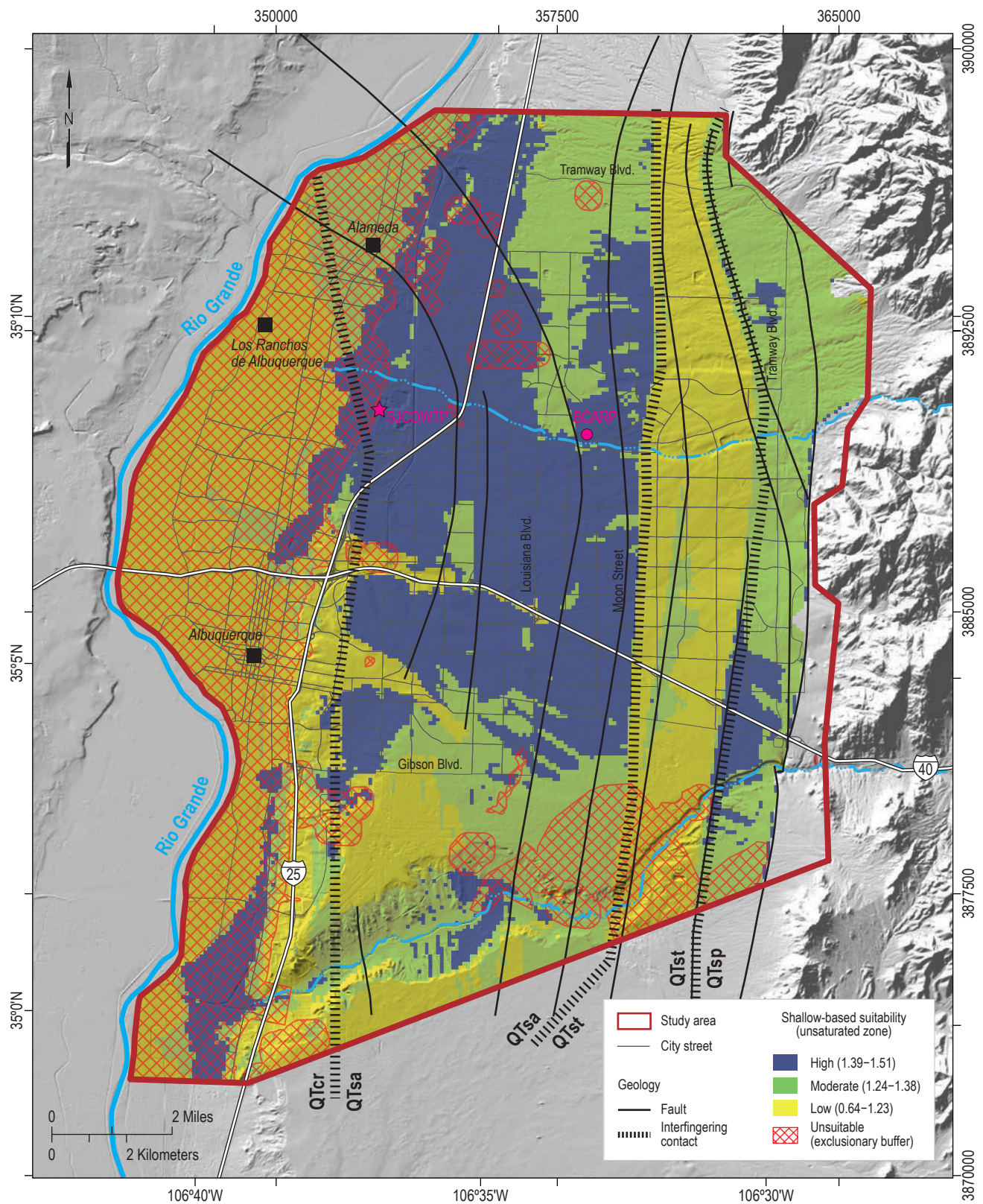


Figure 44. Map showing the final color-coded suitability bins—of unsuitable and low, moderate, and high suitability—that permits qualitative assessment of the efficacy of shallow-based recharge.

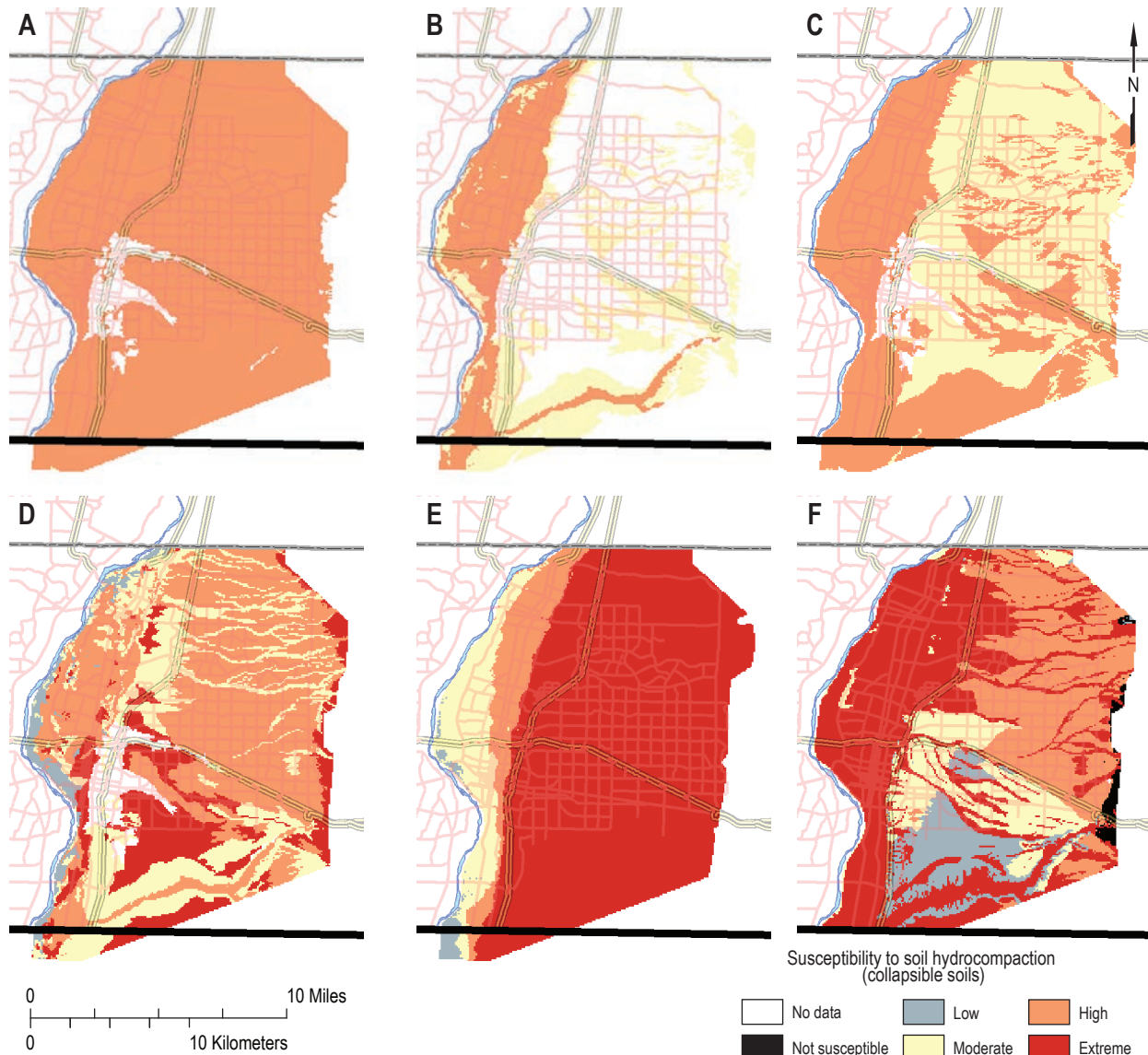


Figure 45. Summary of different susceptibilities for: **A.** soil taxonomic order; **B.** suborder; **C.** great group; **D.** soil texture; **E.** depth-to-groundwater; and **F.** geologic unit. Black line at bottom of each map corresponds to the southern boundary of the geologic map of Connell (2008b).

IX. DISCUSSION

Deep-Injection Recharge

The maps in Figure 35 and Plate 1 provide useful information regarding areas deemed optimal for conducting MAR using deep-injection recharge. The central part of the study area north of Gibson Boulevard is highly suitable for deep-injection MAR; this area extends between about Moon Street and I-25. There, the 1,500 ft of sediment below the land surface is mostly sand-dominated deposits of the axial-river facies of the Sierra Ladrones Formation (QTsa). Near Tijeras Arroyo, the western part of the property belonging to the Kirtland Airforce Base, to the west of the southern projection of Wyoming Boulevard, is predicted to be better for MAR than areas to the east or west. The front of the Sandia Mountains south of Bear Canyon Arroyo (south of Montgomery Boulevard) is also relatively suitable. There are many faults, however, so most of this area is in exclusionary buffers (designated as “unsuitable” in the maps), except for a small window west of Tramway Boulevard and south of Menaul Boulevard.

Areas unfavorable for deep-injection MAR are also depicted in Figure 35 and Plate 1. Most of the modern floodplain of the Rio Grande and a localized area between Eubank and Tramway Boulevards, north of Menaul Boulevard, are of low suitability for deep-injection MAR. The floodplain exhibits low suitability but is already included in an exclusionary buffer (i.e., it was already assumed unsuitable). Between Moon Street and Tramway Boulevard, areas of low to moderate suitability for injection into the saturated zone correspond to the transition between the axial and piedmont facies and to the distal-piedmont facies (QTst). A small area bracketed by Menaul Boulevard, Central Avenue, Eubank Boulevard, and Morris Street, however, appears to be better suited to MAR despite the prevalence of QTst. This may be due to favorable aggregate storage-zone ratings (Fig. 28).

In summary, the deep-recharge map predicts high-suitability areas west of Moon Street and east of about I-25. Near Tramway Boulevard and extending eastward to the mountain front, sandy piedmont sediment may be conducive to deep recharge,

particularly south of Bear Canyon Arroyo. For the study area, care must be exercised to avoid fault zones, where low-permeability damage zones or other cementation may impair injection of water into the saturated zone.

Shallow-Based Recharge

As in the deep-injection map, areas mapped as highly suitable for shallow recharge show a correspondence to the axial-river facies (QTsa) (Fig. 44). The northwestern margin of high suitability, however, extends further, to the area between I-25 and the floodplain. This may reflect optimal water-table elevations that give rise to both moderate percolation times (Fig. 40) and adequate “headspace” to avoid the effects of groundwater mounding (Fig. 39)—combined with favorable transmissivity and storage-zone thickness (Figs. 27–28). For reasons that are not apparent, some areas in the north-central part of the “trough” in the potentiometric surface ranked as moderately suitable rather than highly suitable, even though the subsurface geology contains thick axial sediment (QTsa). The cause for high suitability near I-25 and Tramway Boulevard is also unclear.

There are more areas of low suitability in the shallow-based recharge map than the deep-injection map. At least locally, this may reflect the inclusion of soil characteristics. For example, soil map units correspond to many of the low-suitability areas near the Albuquerque airport and near I-25 between I-40 and Gibson Road (e.g., the artificial fill unit in the soil survey maps). Compared to deep-injection suitability, the lengthened region of low suitability between Tramway Boulevard and Moon Street corresponds to the location of the transitional axial-piedmont and distal-piedmont units (QTst). There, the final summation of weighted scores appears to have been heavily influenced by the extent of this less permeable section in the unsaturated zone.

In summary, application of shallow-based methods for MAR between the modern floodplain and Moon Street is predicted to effectively recharge the aquifer north of Tijeras Arroyo. Soil-related

impedances south of Gibson Road must be considered, which perhaps can be ameliorated by excavation of the surface soil or using vadose-zone wells. Shallow-based infiltration along Tijeras Arroyo west of the downstream projection of Louisiana Boulevard is predicted to achieve recharge of the unsaturated zone, but the valley floor has notable soil hydrocompaction susceptibilities, as discussed below.

Soil Hydrocompaction

High to extreme susceptibility is mapped for most of the Albuquerque region east of the Rio Grande (Plate 3). These high-susceptibility areas should have detailed, site-specific studies before proceeding with shallow, surface-based MAR infiltration projects. Areas mapped herein as highly and extremely susceptible correspond reasonably well to independently reported locations of soil hydrocompaction. These areas include the Tanoan neighborhood, Montessa Park in Tijeras Arroyo, and along Edith Boulevard, where alluvial fans extend out onto lower Rio Grande terraces and the floodplain (Connell et al., 2007; Connell, 2008b). The risk of hydrocompaction is lower near the Rio Grande because groundwater is shallower and the sediment has, therefore, been repeatedly flooded.

Discussion of three areas is warranted. In Tijeras Arroyo region, shallow, surface-based MAR should target older piedmont deposits (Qao) or slopes underlain by axial-river sand of the Sierra Ladrones Formation (QTsa). In contrast, younger valley-floor alluvium (Qaya_{cs}) is highly to extremely susceptible to hydrocompaction, and a case of hydrocompaction has been documented. In the piedmont complex (Qao and Qaya_{cs}) north of I-40, susceptibility is generally high outside of active channels. Sediment in channels

is coarse grained and has been repeatedly saturated, resulting in moderate susceptibility. Alluvial fans (Qaya_{cs}, and where included in Qtr) along the edge of the Rio Grande inner valley should be avoided for shallow, surface-based MAR infiltration. Sufficiently deep vadose-zone wells screened below Holocene deposits (particularly Qaya_{cs}) may compensate for unfavorable soil conditions near the surface.

Limitations

These maps are predictions of areas suitable for managed aquifer recharge (MAR) and areas susceptible to hydrocompaction of soils, the latter of which can compromise recharge operations in areas otherwise considered suitable with respect to the subsurface geology. In general, mapping involved interpolation between data points (generally wells) and extrapolation away from these controls, resulting in errors that are difficult to quantify. Furthermore, mapped MAR suitability would change depending on assignment of weighting values. We usually used “typical” hydrogeologic values for geologic units, but actual values may vary substantially throughout the study area. Actual hydrogeologic conditions in the subsurface may differ from those implied in Plates 1–2. These maps are intended for use at a spatial scale of 1:36,000 for regional planning purposes and to determine where more detailed studies may be warranted.

The map of soil-hydrocompaction susceptibility was developed to provide an overview of this risk at a regional level. None of the proxies are direct measurements of geotechnical parameters, nor has the method been calibrated against such measurements. Rather, the map highlights regions of concern for soil hydrocompaction during infiltration MAR operations.

Acknowledgments

We wish to thank Sean Connell and John Hawley for their advice and critique of this project. We also gratefully acknowledge feedback and assistance from Amy Ewing and Chris Wolf of GeoLogic. This project was funded by ABCWUA, and we had much fruitful interactions with Diane Agnew and Katherine Yuhas about what to incorporate into the project and weighting values.

REFERENCES

- Agarwal, R., Garg, P., and Garg, R., 2013, Remote sensing and GIS based approach for identification of artificial recharge sites: *Water Resources Management*, v. 27, p. 2671–2689.
- Ahini Amineh, Z.B., Hashemian, S.J.A., and Magholi, A., 2017, Integrating spatial multi criteria decision making (SMCDM) with Geographic Information Systems (GIS) for delineation of the most suitable areas for aquifer storage and recovery (ASR): *Journal of Hydrology*, v. 551, p. 577–595.
- American Groundwater Consultants, Inc., 2004, Geohydrology report: Water supply and aquifer performance test of well RG-80337 for McCatharn Estates Subdivision, Bernalillo County, New Mexico: Albuquerque, New Mexico, American Groundwater Consultants, Inc.
- Babcock, H.M., and Cushing, E.M., 1942, Recharge to ground-water from floods in a typical desert wash, Pinal County, Arizona: American Geophysical Union EOS Transactions, v. 23, p. 49–56.
- Beeby-Thompson, A., 1950, Recharging London's water basin: *Timer Review Industry*, p. 20–25.
- Beckwith, G.H., and Hansen, L.A., 1989, Identification and characterization of the collapsing alluvial soils of the western United States, in Kulhawy, F.H., ed., Foundation engineering: Current principles and practices, Volume 1: New York, American Society of Civil Engineers, p. 143–159.
- Bexfield, L.M., and Anderholm, S.K., 2002, Spatial patterns and temporal variability in water quality from City of Albuquerque drinking-water supply wells and piezometer nests, implications for the ground-water flow system: U.S. Geological Survey Water-Resources Investigations Report 01-4224, 101 p.
- Brown, C.J., 2005, Planning decision framework for brackish water aquifer, storage and recovery (ASR) projects [Ph.D. dissertation]: Gainesville, University of Florida, 395 p.
- Brown, C.J., Weiss, R., Verrastro, R., and Schubert, S., 2005, Development of an aquifer, storage, and recovery (ASR) site selection suitability index in support of the comprehensive Everglades restoration project: *Journal of Environmental Hydrology*, v. 13, 13 p.
- Buchen, S., 1955, Artificial replenishment of aquifers: *Institute of Water Journal*, v. 9, p. 111–163.
- Carleton, G.B., 2010, Simulation of groundwater mounding beneath hypothetical stormwater infiltration basins: U.S. Geological Survey Scientific Investigations Report 2010-5102, 64 p.
- Chowdury, A., Jha, M.K., and Chowdary, V.M., 2009, Delineation of groundwater recharge zones and identification of artificial recharge sites in West Medinipur district, West Bengal, using RS, GIS, and MCDM techniques: *Environmental Earth Sciences*, v. 59, p. 1209–1222.
- Connell, S.D., 1997, Geology of the Alameda quadrangle, Bernalillo and Sandoval Counties, New Mexico (revised 2000): New Mexico Bureau of Mines and Mineral Resources Open-File Geologic Map OF-GM-10, scale 1:24,000.
- Connell, S.D., Allen, B.D., Hawley, J.W., and Shroba, R.R., 1998, Geology of the Albuquerque West 7.5-minute quadrangle, Bernalillo County, New Mexico (revised 2000): New Mexico Bureau of Mines and Mineral Resources Open-File Geologic Map OF-GM-17, scale 1:24,000.
- Connell, S.D., 2008a, Refinements to the stratigraphic nomenclature of the Santa Fe Group, northwestern Albuquerque Basin, New Mexico: *New Mexico Geology*, v. 30, p. 14–35.
- Connell, S.D., 2008b, Geologic map of the Albuquerque-Rio Rancho metropolitan area and vicinity, Bernalillo and Sandoval Counties, New Mexico: New Mexico Bureau of Geology and Mineral Resources Geologic Map GM-78, scale 1:50,000.
- Connell, S.D., Allen, B.D., and Hawley, J.W., 1998, Subsurface stratigraphy of the Santa Fe Group from borehole geophysical logs, Albuquerque area, New Mexico: *New Mexico Geology*, v. 20, p. 2–7.
- Connell, S.D., Love, D.W., and Dunbar, N.W., 2007, Geomorphology and stratigraphy of inset fluvial deposits along the Rio Grande valley in the central Albuquerque Basin, New Mexico: *New Mexico Geology*, v. 29, p. 13–31.
- Connell, S.D., Smith, G.A., Geissman, J.W., and McIntosh, W.C., 2013, Climatic controls on nonmarine depositional sequences in the Albuquerque Basin, Rio Grande rift, north-central New Mexico, in Hudson, M.R., and Grauch, V.J.S., eds., *New perspectives on Rio Grande rift basins: From tectonics to groundwater*: Geological Society of America Special Paper 494, p. 383–425.
- Cooper, H., and Jacob, C., 1946, A generalized graphical method for evaluating formation constants and summarizing well-field history: *American Geophysical Union Transactions*, v. 27, p. 526–534.
- Daniel B. Stephens and Associates, 2009, Installation and hydrogeology report, Bear Canyon Recharge Demonstration Project: Prepared for the Albuquerque Bernalillo County Water Utility Authority, June 11, 2009, 22 p., 4 tables, 6 figures, 5 appendices.
- Daniel B. Stephens and Associates, 2010, Data synthesis report, Bear Canyon Recharge Demonstration Project, Underground Storage and Recovery Permit USR-2: Submitted to the New Mexico Office of the State Engineer, April 2, 2010, 22 p., 2 tables, 43 figures, 6 appendices.
- Daniel B. Stephens and Associates, 2014, Application for permit underground storage and recovery, Bear Canyon Recharge Project: Submitted to the New Mexico Office of the State Engineer, March 31, 2014, 9 p., 11 attachments.
- Daniel B. Stephens and Associates, 2018, ASR well installation and testing, DWTP large-scale recharge demonstration project: Prepared for the Albuquerque Bernalillo County Water Utility Authority, March 9, 2018, 32 p., 7 tables, 15 figures, 14 appendices.
- Dar, I., Sankar, K., and Dar, M., 2010, Remote sensing technology and geographic information system modeling: An integrated approach

- towards the mapping of groundwater potential zones in Hardrock terrain, Mamundiyan basin: *Journal of Hydrology*, v. 394, p. 285–295.
- Fisher, A.T., Lozano, S., Beganskas, S., Teo, E., Young, K., Wier, W., and Harmon, R., 2017, Regional managed aquifer recharge and runoff analyses in Santa Cruz and northern Monterey Counties, California: Report to the California State Coastal Conservancy, Project 13-118, 119 p.: <http://www.rcdsantacruz.org/> managed-aquifer-recharge (accessed March, 2019).
- Galusha, T., and Blick, J.C., 1971, Stratigraphy of the Santa Fe Group, New Mexico: American Museum of Natural History Bulletin, v. 144, 127 p.
- Ganapuram, S., Kumar, G.V., Krishna, I.M., Kahya, E., and Demirel, M.C., 2009, Mapping of groundwater potential zones in the Musi basin using remote sensing data and GIS: *Advances on Engineering Software*, v. 40, p. 506–518.
- Gibson, M.T., Campana, M.E., and Nazy, D., 2018, Case report: Estimating aquifer storage and recovery (ASR) region and local suitability: A case study in Washington state, USA: *Hydrology*, v. 5: <https://www.mdpi.com/2306-5338/5/1/7>.
- Gile, L.H., Peterson, F.F., and Grossman, R.B., 1966, Morphological and genetic sequences of carbonate accumulation in desert soils: *Soil Science*, v. 101, p. 347–360.
- Gile, L.H., Hawley, J.W., and Grossman, R.B., 1981, Soils and geomorphology in the Basin and Range area of southern New Mexico—Guidebook to the Desert Project: New Mexico Bureau of Mines and Mineral Resources Memoir 39, 222 p.
- Grauch, V.J.S., and Connell, S.D., 2013, New perspectives on the geometry of the Albuquerque Basin, Rio Grande rift, New Mexico: Insights from geophysical models of rift-fill thickness, in Hudson, M.R., and Grauch, V.J.S., eds., *New perspectives on Rio Grande rift basins: From tectonics to groundwater*: Geological Society of America Special Paper 494, p. 383–425.
- Hantush, M.S., 1967, Growth and decay of groundwater mounds in response to uniform percolation: *Water Resources Research*, v. 3, p. 227–234.
- Hawley, J.W., 1996, Hydrogeologic framework of potential recharge areas in the Albuquerque Basin, central Valencia County, New Mexico, in Hawley, J.W., and Whitworth, T.M., eds., *Hydrogeology of potential recharge areas for the basin- and valley-fill aquifer systems, and hydrogeochemical modelling of proposed artificial recharge of the upper Santa Fe aquifer, northern Albuquerque Basin, New Mexico: New Mexico Bureau of Mines and Mineral Resources Open-File Report 402-D, Chapter 1*, 68 p., 1 appendix.
- Hawley, J.W., and Haase, C.S., 1992, compilers, *Hydrogeologic framework of the northern Albuquerque Basin: New Mexico Bureau of Mines and Mineral Resources Open-File Report 387*, 74 p., 4 tables, 28 figures, 8 appendices, 9 plates.
- Hawley, J.W., McCraw, D.J., Love, D.W., and Connell, S.D., 2005, Map of surficial materials of New Mexico with emphasis on major Quaternary and Pliocene units: *New Mexico Bureau of Geology and Mineral Resources Open-File Report 462*, scale 1:500,000.
- Johnpeer, G.D., Love, D.W., Hawley, J.W., Bobrow, D.J., Hemingway, M.P., and Reimers, R.F., 1985, El Llano and vicinity geotechnical study—Final report: *New Mexico Bureau of Geology and Mineral Resources Open-File Report 226*, variously paginated, 3 tables, 15 figures, 23 appendices.
- Jorgenson, T.L., 1998, Analysis of collapsible soils using statistical and logistical methods [MS thesis]: Salt Lake City, Brigham Young University, 58 p.
- Jury, W.A., and Horton, R., 2004, *Soil Physics*: Hoboken, New Jersey, John Wiley and Sons, 370 p.
- Kelly, V.C., 1977, *Geology of Albuquerque Basin, New Mexico: New Mexico Bureau of Mines and Mineral Resources, Memoir 33*, 60 p.
- Koning, D.J., and Read, A.S., 2010, Geologic map of the Southern Española Basin: *New Mexico Bureau of Geology and Mineral Resources Open-File Report 531*, scale 1:48,000.
- Koning, D.J., Smith, G.A., Lyman, J., and Paul, P., 2004, Lithosome S of the Tesuque Formation: Hydrostratigraphic and tectonic implications of a newly delineated lithosome in the southern Española Basin, New Mexico, in Hudson, M.R., ed., *Geologic and hydrogeologic framework of the Española Basin*, in Proceedings, 3rd Annual Española Basin Workshop, Santa Fe, New Mexico, March 2–3, 2004: U.S. Geological Survey Open-File Report 2004-1093, 17 p.
- Koning, D.J., Grauch, V.J.S., Connell, S.D., Ferguson, J., McIntosh, W., Slate, J.L., Wan, E., and Baldridge, W.S., 2013, Structure and tectonic evolution of the eastern Española Basin, Rio Grande rift, north-central New Mexico, in Hudson, M., and Grauch, V.J.S., eds., *New perspectives on the Rio Grande rift: From tectonics to groundwater: Geological Society of America Special Paper 494*, p. 185–219.
- Lipman, P.W., and Mehnert, H.H., 1975, Late Cenozoic volcanism and development of the Rio Grande depression in the southern Rocky Mountains, in Curtis, B.F., ed., *Cenozoic history of the southern Rocky Mountains: Geological Society of America Memoir 144*, p. 119–154.
- Li, P., Vanapalli, S., and Li, T., 2016, Review of collapse triggering mechanism of collapsible soils due to wetting: *Journal of Rock Mechanics and Geotechnical Engineering*, v. 8, p. 256–274.
- Lowry, C.S., and Anderson, M.P., 2006, An assessment of aquifer storage recovery using ground water flow models: *Groundwater*, v. 44, p. 661–667.
- Lutenegger, A.J., and Saber, R.T., 1988, Determination of collapse potential of soils: *Geotechnical Testing Journal*, v. 11, p. 173–178.
- Machette, M.N., 1978, Geologic map of the San Acacia quadrangle, Socorro County, New Mexico: U.S. Geological Survey Geologic Quadrangle Map GQ-1415, scale 1:24,000.
- Mack, G.H., Salyards, S.L., and James, W.C., 1993, Magnetostratigraphy of the Plio-Pleistocene Camp Rice and Palomas Formations in the Rio Grande rift of southern New Mexico: *American Journal of Science*, v. 293, p. 49–77.
- Mack, G.H., Salyards, S.L., McIntosh, W.C., and Leeder, M.R., 1998, Reversal magnetostratigraphy and radioisotopic geochronology of the Plio-Pleistocene Camp Rice and Palomas Formations, southern Rio Grande rift, in Mack, G.H., Austin, G.S., and Barker, J.M., eds., *Las Cruces country II: New Mexico Geological Society Guidebook 49*, p. 229–236.
- Mack, G.H., Cole, D.R., and Trevino, L., 2000, The distribution and discrimination of shallow, authigenic carbonate in the Plio-Pleistocene Palomas Basin, southern Rio Grande rift, USA: *Geological Society of America Bulletin*, v. 112, p. 643–656.
- Mack, G.H., Leeder, M., and Salyards, S.L., 2002, Temporal and spatial variability of alluvial-fan and axial-fluvial sedimentation in the Plio-Pleistocene Palomas half graben, southern Rio Grande rift, New Mexico, USA, in Renaut, R.W., and Ashley,

- G.M., eds., Sedimentation in continental rifts: Society for Sedimentary Geology Special Publication, p. 165–177.
- Mahmoud, S.H., Alazba, A.A., and Amin, M.T., 2014, Identification of potential sites for groundwater recharge using a GIS-based decision support system in Jazan region-Saudi Arabia: Water Resources Management, v. 28, p. 3319–3340.
- Meinzer, O.E., 1946, General principles of artificial ground-water recharge: Economic Geology, v. 41, p. 191–201.
- Mitchelson, A.T., and Muckel, D.C., 1937, Spreading water for storage underground: Washington, D.C., U.S. Department of Agriculture Technical Bulletin 578, 80 p.
- Momeni, M., Shafiee, A., Heidari, M., Jafari, M.K., and Mahdavifar, M.R., 2012, Evaluation of soil collapse potential in regional scale: Natural Hazards, v. 64, p. 459–479.
- Nasiri, H., Boloorani, A.D., Sabokbar, H.A.F., Jafri, H.R., Hamzeh, M., and Rafi, Y., 2013, Determining the most suitable areas for artificial ground-water recharge via an integrated PROMETHEE II-AHP method in GIS environment (Case study: Garabagan Basin, Iran): Environmental Monitoring and Assessment, v. 185, p. 707–718.
- National Research Council [NRC], 1999, Mitigating losses from land subsidence in the United States: Washington, D.C., National Academy Press, 61 p.
- Peter, K.D., 1987, Ground-water flow and shallow-aquifer properties in the Rio Grande inner valley south of Albuquerque, Bernalillo County, New Mexico: U.S. Geological Survey Water-Resources Investigation Report WRI 87-4015, 29 p.
- Philip, J.R., 1957, The theory of infiltration: 2: The profile at infinity: Soil Science, v. 83, p.435–448.
- Powell, R.I., and McKean, S.E., 2014, Estimated 2012 groundwater potentiometric surface and drawdown from predevelopment to 2012 in the Santa Fe Group aquifer system in the Albuquerque metropolitan area, central New Mexico: U.S. Geological Survey Scientific Investigations Map 3301, scale 1:50,000.
- Pyne, R.D.G., 1995, Groundwater recharge and wells: A guide to aquifer storage and recovery: Boca Raton, Florida, Lewis Publishers, 376 p.
- Rahman, M.A., Rusteberg, B., Gogu, R.C., Lobo Ferreira, J.P., and Sauter, M., 2012, A new spatial multi-criteria decision support tool for site selection for implementation of managed aquifer recharge: Journal of Environmental Management, v. 99, p. 61–75.
- Rawls, W.J., Ahuja, L.R., and Brakensiek, D.L., 1992, Estimating soil hydraulic properties from soils data, in van Genuchten, M.Th., Leij, F.J., and Lund, L.J., eds., Indirect methods for estimating the hydraulic properties of unsaturated soils, Proceedings, International workshop on indirect methods for estimating the hydraulic properties of unsaturated soils, Riverside, California, October 11–13, 1989.
- Rinehart, A.J., Mamer, E., Kludt, T., Felix, B., Pokorny, C., and Timmons, S., 2016, Groundwater level and storage changes in alluvial basins in the Rio Grande basin, New Mexico: New Mexico Water Resources Research Institute Technical Completion Report, 41 p.
- Rinehart, A.J., Cikoski, C.T., Mansell, M.M., and Love D.W., 2017, Collapsible soil susceptibility map for New Mexico (1:750,000) based on multiple proxies: New Mexico Bureau of Geology and Mineral Resources Open-File Report 593, 72 p.
- Rogers, C.D.F., 1995, Types and distribution of collapsible soils, in Derbyshire, E., Dijkstra, T., and Smalley, I.J., eds., Genesis and properties of collapsible soils: Boston, Kluwer Academic Publishers, p. 1–17.
- Russo, T.A., Fisher, A.T., and Lockwood, B.S., 2015, Assessment of managed aquifer recharge site suitability using a GIS and modeling: Groundwater, v. 53, p. 389–400.
- Saaty, T.L., 1977, A scaling method for priorities in hierarchical structures: Journal of Mathematical Psychology, v. 15, p. 234–281.
- Saaty, T.L., 1980, The analytic hierarchy process: New York, McGraw-Hill.
- Saaty, T.L., 1987, The analytic hierarchy process—What it is and how it is used: Mathematical Modelling, vol. 9, p. 161–176.
- Saaty, T.L., 1990, How to make a decision: The analytic hierarchy process: European Journal of Operational Research, v. 48, p. 9–26.
- Saaty, T.L., 2008, Decision making with the analytic hierarchy process: International Journal of Services Sciences, v. 1, p. 83–98.
- Senanayake, I.P., Dissanayake, D.M.D.O.K., Mayadunna, B.B., and Weerasekera, W.L., 2016, An approach to delineate groundwater recharge potential sites in Ambalantota, Sri Lanka, using GIS techniques: Geoscience Frontiers, v. 7, p. 115–124.
- Sigda, J.M., and Wilson, J.L., 2003, Are faults preferential flow paths through semiarid and arid vadose zones?: Water Resources Research, v. 39, 14 p.
- Singh, A., Panda, S., Kumar, K., and Sharma, C., 2013, Artificial groundwater recharge zones mapping using remote sensing and GIS: Environmental Management, v. 52, p. 61–71.
- Smith, A.J., and Pollock, D.W., 2012, Assessment of managed aquifer recharge potential using ensembles of local models: Groundwater, v. 50, p. 133–143.
- Soil Survey Staff, 1992, Keys to soil taxonomy: U.S. Department of Agriculture SMSS Technical Monograph 19 (5th edition), 541 p.
- Soil Survey Staff, 2014, Gridded soil survey geographic (gSSURGO) database for New Mexico: U.S. Natural Resources Conservation Service (NRCS), U.S. Department of Agriculture (USDA) Database Conterminous US Package: <https://gdg.sc.egov.usda.gov/> (accessed April, 2017).
- Soil Science Division Staff, 2017, Soil Survey Manual, in Ditzler, C., Scheffer, K., and Monger, H.C., eds., U.S. Department of Agriculture Handbook 18: Washington, D.C., Government Printing Office: https://www.nrcs.usda.gov/wps/portal/nrcs/detail/soils/ref?cid=nrcs142p2_054262.
- Soil Survey Staff, 2018, Natural Resources Conservation Service (NRCS), U.S. Department of Agriculture (USDA) Web Soil Survey: <https://websoilsurvey.nrcs.usda.gov/> (accessed January, 2019).
- Spiegel, Z., and Baldwin, B., 1963, Geology and Water Resources of the Santa Fe Area, New Mexico: U.S. Geological Survey Water-Supply Paper 1525, 258 p.
- Theis, C., 1935, The relation between the lowering of the piezometric surface and the rate and duration of discharge in a well using groundwater storage: American Geophysical Union Transactions, v. 16, p. 519–524.
- Thomas, C.L., and Thorn, C.R., 2000, Use of air-pressurized slug tests to estimate hydraulic conductivity at selected piezometers completed in the Santa Fe Group aquifer system, Albuquerque area, New Mexico: U.S. Geological Survey Water-Resources Investigations Report WRI 2000-4253, 19 p.
- Thomson, B.M., Hall, G., Stormont, J., and Van Tassell, L., 2000, Evaluation of on-site wastewater treatment and disposal:

- Volume I: Determination of groundwater contamination and demonstration of alternative technologies, final report to Vernalillo County: University of New Mexico, Department of Civil Engineering.
- Thorn, C.R., and Heywood, C.E., 2000, Analytical results of a long-term aquifer test conducted near the Rio Grande, Albuquerque, New Mexico, with section on Piezometric-extensometric test results: U.S. Geological Survey Water-Resources Investigations Report WRI 2000-4291, 19 p.
- Thorn, C.R., McAda, D.P., and Kernodle, J.M., 1993, Geohydrologic framework and hydrologic conditions in the Albuquerque Basin, central New Mexico: U.S. Geological Survey Water-Resources Investigations Report WRI 93-4149, 106 p.
- Todd, D.K., 1959, Annotated bibliography of artificial recharge of groundwater through 1954: U.S. Geological Survey Water Supply Paper 1477, 115 p.
- NRCS [Natural Resources Conservation Service], 2018, Custom soil resource report for Bernalillo County and parts of Sandoval and Valencia Counties, New Mexico: U.S. Department of Agriculture Web Soil Survey, 201 p.
- Wamsley, M.L., 2014, Evidence of ground water contamination by on-site wastewater systems [MS professional project report]: Albuquerque, University of New Mexico, 82 p.: http://digitalrepository.unm.edu/wr_sp/63.
- Ward, J.D., Simmons, C.T., Dillon, P.J., and Pavlic, P., 2009, Integrated assessment of lateral flow, density effects, and dispersion in aquifer storage and recovery: *Journal of Hydrology*, v. 370, p. 83–99.
- Weissmann, G.S., Hartley, A.J., Nichols, G.J., Scuderi, L.A., Olson, M.E., Buehler, H.A., and Massengill, L.C., 2011, Alluvial facies distributions in continental sedimentary basins—Distributive fluvial systems, in North, C., Davidson, S.K., and Leleu, S., eds., *From river to rock record: The preservation of fluvial sediments and their subsequent interpretation:* Society of Sedimentary Geology Special Publication 97, p. 327–355.
- Williams, T., and Rollins, K.M., 1991, Collapsible soil hazard map for the Cedar City, Utah area: Utah Geological Survey Contract Report 91-10.
- Williams, J.R., Ouyang, Y., Chen, J.-S., and Ravi, V., 1998, Estimation of infiltration rate in vadose zone—Volume II: Application of selected mathematical models: Washington, D.C., U.S. Environmental Protection Agency, National Risk Management Research Laboratory, EPA/600/R-97/128b, 44 p., 3 appendices.
- Wilkins, D.W., 1987, Characteristics and properties of basin-fill aquifer determined from three test wells west of Albuquerque, Bernalillo County, New Mexico: U.S. Geological Survey Water-Resources Investigations Report WRI 86-4187, 78 p.
- Yeh, H., Cheng, Y., Lin, H., and Lee, C., 2016, Mapping groundwater recharge potential zone using a GIS approach in Hualian River, Taiwan: *Sustainable Environment Research*, v. 26, p. 33–43.